

Electronic Thesis and Dissertation Repository

8-9-2013 12:00 AM

Electrospinning of Core-shell Collagen Nanofibers


Ying Li, *The University of Western Ontario*

Supervisor: Dr. Wankei Wan, *The University of Western Ontario*

A thesis submitted in partial fulfillment of the requirements for the Master of Engineering Science degree in Chemical and Biochemical Engineering

© Ying Li 2013

Follow this and additional works at: <https://ir.lib.uwo.ca/etd>

 Part of the [Other Biomedical Engineering and Bioengineering Commons](#), [Polymer and Organic Materials Commons](#), [Polymer Science Commons](#), and the [Process Control and Systems Commons](#)

Recommended Citation

Li, Ying, "Electrospinning of Core-shell Collagen Nanofibers" (2013). *Electronic Thesis and Dissertation Repository*. 1499.

<https://ir.lib.uwo.ca/etd/1499>

This Dissertation/Thesis is brought to you for free and open access by Scholarship@Western. It has been accepted for inclusion in Electronic Thesis and Dissertation Repository by an authorized administrator of Scholarship@Western. For more information, please contact wlsadmin@uwo.ca.

Electrospinning of Core-shell Collagen Nanofibers

(Thesis format: Monograph)

by

Ying (Betty) Li

**Graduate Program in Chemical and
Biochemical Engineering**

A thesis submitted in partial fulfillment of the requirements for
the degree of Master in Engineering Science

The School of Graduate and Postdoctoral Studies

The University of Western Ontario

London, Ontario, Canada

© Ying (Betty) Li 2013

Abstract

In tissue engineering, the scaffold plays a critical role in guiding and supporting cells to function and grow optimally. The electrospun nanofibrous scaffold can serve as a near ideal substrate for tissue engineering because it has high surface area and the three-dimensional interconnected porous network can enhance cell attachment and proliferation. Core-shell nanofibrous scaffolds produced with coaxial electrospinning allow bioactive molecule encapsulation to improve cell adhesion, mediate and promote the proper signaling among the cells for their functioning and growth. In the current study, core-shell collagen nanofibers were fabricated via coaxial electrospinning with horizontal and vertical configurations. Core-shell nanofibers with optimum morphology and structure were stabilized with Genipin, a natural crosslinking reagent extracted from the fruits of *Gardenia jasminoides*. The produced crosslinked core-shell collagen fibrous scaffolds have been proven to be cell compatible with improved structure stability and uniformity.

Keywords: Tissue engineering, coaxial electrospinning, collagen, genipin, bovine serum albumin, core-shell nanofibers, crosslinking

Acknowledgments

As with any considerable body of work, there are always a significant number of people to thank for helping make it possible. I would like to start by thanking my supervisor, Dr. Wankei Wan, for taking considerable amount of time and energy to teach me, both with respect to my work and in life. He has always pushed me to work hard and challenged my mind with insightful questions.

I would like to thank all the members in the group as well as everyone else I have had the pleasure to work with. I consider each of you friends and I always love the talks we had, the food we shared, and the challenges we worked through together.

Much of this work would not have been possible without the help and support of Dr. John deBruyn, Dr. Jian Liu, and Helium Mak. I would like to thank Dr. deBruyn for providing me the high speed camera and viscometer; Dr. Jian Liu and Helium Mak for giving me supports and suggestions throughout my work.

I would like to thank Karen Nygard, Dr. Richard Gardiner and everyone at the Biotron for providing me with the technical support.

My gratitude also extends to my advisory committee: Dr. Andrew Hrymak and Dr. Andy Sun. I would like to thank them for giving me helpful advice and suggestions.

Finally, I would like to thank my families, who have supported me unconditionally throughout all these years.

Table of Contents

Abstract.....	ii
Acknowledgments.....	iii
Table of Contents.....	iv
List of Tables	viii
List of Figures.....	ix
List of Abbreviations	xiv
1 Introduction.....	1
2 Background and literature review	4
2.1 Electrospun Nanofibers History	4
2.2 Fundamentals of electrostatically induced jets	4
2.3 Electrostatically induced jets.....	5
2.4 Formation of Bending instability	6
2.5 Parameters effects on nanofiber diameter and morphology.....	9
2.5.1 Jet cross-sectional radius.....	10
2.5.2 Needle collector separation distance on fiber diameter and morphology.....	11
2.5.3 Viscosity.....	11
2.5.4 Concentration.....	12
2.5.5 Conductivity.....	12
2.5.6 Solvent types and vapor pressure.....	13
2.5.7 Electric potential	13
2.5.8 Other parameters.....	14
2.6 Effects of Electrospinning Setup.....	15
2.7 Coaxial electrospinning.....	16
2.8 Coaxial electrospinning setup and process	17

2.9 Processing parameters for coaxial electrospinning	20
2.9.1 Applied voltage	20
2.9.2 Flow rate	20
2.9.3 Solution viscosities	21
2.9.4 Solution concentration	21
2.9.5 Solution conductivity	22
2.9.6 Solution miscibility	22
2.9.7 Solvent vapor pressure	23
2.10 Fiber morphology and alignment	24
2.11 Properties and Applications of Core-shell Nanofibers.....	24
2.12 Collagen as a biomedical material	25
2.13 Crosslinking of electrospun collagen nanofibers	26
2.13.1 Cabodiimides	27
2.13.2 Glutaraldehyde	29
2.13.3 Genipin.....	33
3 Materials and Method	40
3.1 Materials.....	40
3.2 Isolation and purification of Type I Collagen from Rat Tails.....	40
3.3 Core and shell solutions for electrospinning	41
3.3.1 Collagen Shell Solution	41
3.3.2 Protein Core Solution.....	41
3.4 Coaxial Electrospinning	41
3.5 High speed imaging	43
3.6 Genipin crosslinking	43
3.7 Resin Embedding and Ultramicrotoming	44
3.8 Characterization	44

3.8.1 Scanning electron microscopy (SEM)	44
3.8.2 Transmission electron microscopy (TEM).....	44
3.8.3 Laser scanning confocal microscopy (LSCM)	45
3.9 Image processing (Image J)	45
3.10 Cell seeding experiments	45
3.10.1 Cell attachment	46
3.10.2 Cell staining	46
4 Results.....	48
4.1 Optimizing electrospinning process.....	48
4.1.1 Effect of voltage on fiber diameter	51
4.1.2 Effect of other experimental parameters.....	53
4.1.3 Effect of solution parameters	54
4.1.4 Effect of environmental parameters.....	56
4.2 Protein encapsulation of the core-shell collagen nanofibers.....	57
4.3 Core-shell structure of the collagen nanofibers	58
4.4 Optimizing the vertical coaxial electrospinning process	62
4.4.1 Effect of voltage and tip-to-collector distance on fiber morphology..	65
4.4.2 Effect of environmental parameters.....	68
4.5 The core-shell structure of the vertical coaxial electrospun nanofibers.....	68
4.6 Genipin crosslinking on core-shell collagen nanofibers preparation.....	73
4.7 Change in auto-fluorescent before and after crosslinking (LSCM).....	75
4.8 Cell attachment	76
5 Discussion.....	78
6 Summary and Conclusion.....	83
7 Future Work.....	85

References.....	87
Appendix A Isolation of Type I Collagen from Rat Tails	99
Appendix B Low Viscosity Embedding Media (Spurr's Kit)	100
Appendix C TEM on Fiber Breakage	103
Appendix D TEM images on fiber cross-section.....	104
CURRICULAM VITAE.....	111

List of Tables

Table 1: Materials for electrospinning and fiber characterization of core-shell collagen nanofibers	40
Table 2: Horizontal coaxial electrospinning parameters for core-shell collagen nanofibers.....	49
Table 3: Average fiber size vs. applied voltage for horizontal coaxial electrospinning	52
Table 4: Vertical coaxial electrospinning parameters for core-shell collagen nanofibers.....	63
Table 5: Average fiber size for vertical coaxial electrospinning	67
Table 6: Comparison of horizontal and vertical coaxial electrospinning	78

List of Figures

Figure 1: Glycerol jets profile at 0.5mL/min. Left to right: 3.67kV/cm, 4.33kV, 5.0kV/cm (adapted from [18]).....	7
Figure 2: Illustration of the jet bending at the end of the straight segment. (Adapted from [19]).....	7
Figure 3: Horizontal electrospinning setup.....	15
Figure 4: a: shaft type vertical electrospinning. b: converse type vertical electrospinning.....	15
Figure 5: Coaxial electrospinning.....	18
Figure 6: Compound jet formation a: a compound droplet formed at the tip of the spinneret, b: shell solution elongates and stretches due to charge-charge repulsion, c: stream ejected from the Taylor cone.....	18
Figure 7: Voltage dependence of the core-shell fiber formation. A: voltage below optimal range (subcritical voltage), B: optimal voltage (critical voltage), C: voltage above optimal range (super critical voltage).....	20
Figure 8: Crosslinking of collagen with EDC and NHS.....	28
Figure 9: Possible structure of glutaraldehyde (GA) in aqueous solutions	30
Figure 10: a: Schiff base formation obtained by crosslinking of lysine residues from two protein molecules by monomeric glutaraldehyde. b: Suggested end product obtained from the reaction between the polymeric glutaraldehyde with lysine residues from the crosslinked proteins under alkaline conditions. c: Suggested end product obtained from the reaction between the polymeric glutaraldehyde with lysine residues from the crosslinked proteins under acidic conditions	31
Figure 11: Aldol condensation of monomeric glutaraldehyde to form polymeric glutaraldehyde.....	32

Figure 12: The two reaction mechanisms between genipin and a primary amine group, proposed by Butler et al. [96]	34
Figure 13: Schematic illustration of the intramolecular crosslinking structure of genipin crosslinks [97].....	35
Figure 14: Formation of intermolecular chains with genipin	36
Figure 15: Reaction mechanism of genipin crosslinked collagen proposed by Zhu et al. [100].....	37
Figure 16: Genipin crosslinking mechanism proposed by Muzzareli [101].....	38
Figure 17: Humidity controlled chamber for electrospinning	42
Figure 18: Horizontal coaxial electrospinning configuration.....	42
Figure 19: Vertical coaxial electrospinning setup configuration.....	43
Figure 20: Redlake MotionScope M high speed camera captured stable Taylor cone formed at the tip of the needle (Horizontal configuration).....	50
Figure 21: Distorted Taylor cone due to gravitational force and extended coaxial electrospinning.....	51
Figure 22: SEM image of horizontal coaxial electrospun collagen nanofibers at 22kV, 7cm	51
Figure 23: Histogram of horizontal coaxial electrospun collagen nanofiber size distribution obtained at six applied voltages with 7cm tip-to-collector distance.	52
Figure 24: Average fiber size at applied voltage between 19kV to 25kV with a tip-to-collector distance of 7cm	53
Figure 25: Coaxial electrospun collagen nanofibers with increased flow rate (OFR:0.3mL/hr, IFR: 0.1mL/hr) and yielded beads-on-string morphology fiber.....	54
Figure 26: Flattened ribbon-like collagen nanofibers were collected with PEG core concentration of 200mg/mL	55

Figure 27: Distorted Taylor cone during electrospinning with increased temperature (a: 22 °C, b: 29 °C, c: 34 °C).....	56
Figure 28: At 34 °C, fiber ejected out brokenly from the Taylor cone. a: suspended droplet with no applied electric field, b,c,d: with applied electric field, droplet distorted due to both electrostatic force and gravitational force, e,f: fiber shooting out from tip of the distorted Taylor cone, g: after solution being carried out by the fiber, droplet size reduced and electrospinning process stopped. Same process would continue with increasing droplet size due to continuous solution pumping (the series images were screen captured from a high speed video, the spinning process from first to last image took about 0.2s).....	57
Figure 29: Confocal images of as-prepared electrospun core-shell BSA-PEG/collagen nanofibers: a) auto-fluorescence of collagen; b) fluorescent-labelled BSA-Alexa Fluoro 594 in the core material; c) overlaid image of collagen and BSA-Alexa Fluoro 594 fluorescence	58
Figure 30: TEM on core-shell collagen nanofibers. The dark core and light shell in some of the fibers indicates the difference in electron transmission ability with the core shell material.....	59
Figure 31: TEM on core-shell collagen nanofibers. There are fibers with dark core light shell and fibers with dark shell light core.....	59
Figure 32: Non-uniform distribution of core-shell material along the nanofiber. The fiber showed dark core light shell at the left side of the image while evolving into dark shell lighter core as moving to the right side.....	60
Figure 33: Three possible types of resultant fiber structure:(a)core-shell structure, (b)separate core fibers and shell fibers, and (c) composite fibers from blended mixture	61

Figure 34: Non-uniform distribution of cross-section of core-shell material from horizontal coaxial electrospinning, both the edge and centre of the fiber display dark regions62

Figure 35: Electrostatic force and gravitational force act together to pull out extra solution from the increased-size droplet to form Taylor cone (Captured with AOS-QPRI camera) a: solution accumulated at the tip of the needle, b: Taylor cone distorted due to applied electric field, c,d: stream ejecting from the apex of the Taylor cone, e: Taylor cone size reduced to stable Taylor cone64

Figure 36: Stable Taylor cone with continuous fiber drawing, no solution dripping, no change in Taylor cone size and shape a: focus on the fibers (Captured with Olympus I-speed 3 camera) b: focus on the Taylor cone65

Figure 37: SEM image on vertical coaxial electrospinning at 7cm, not much fiber can be collected with solution mostly dripped onto the substrate.....65

Figure 38: Coaxial electrospinning with droplets formation66

Figure 39: Coaxial electrospinning produced combination of fiber and droplets66

Figure 40: Stable coaxial electrospinning result smooth nanofibers with no droplet or beads67

Figure 41: Histogram of fiber size distribution collected with optimum range using vertical coaxial electrospinning (fitted with normal function)67

Figure 42: For vertical coaxial electrospinning, nanofibers whipped upward with fumehood air and stuck to the needle. (Image was captured with AOS Q-PRI camera)68

Figure 43: Dark core structure close to the surface of the fiber, thick fiber breakage allows observation of the core-shell structure69

Figure 44: Looking at the core-shell structure via two directions. Direction 1: dark core at the centre, direction 2: dark core close to the surface.....70

Figure 45: TEM images on the cross-section of the vertical coaxial electrospinning nanofibers	71
Figure 46: Microtoming directionality determines the resultant cross-section shape. a: round fiber cross-section. b: ellipse shape cross-section	71
Figure 47: Cross-section of the genipin-crosslinked core-shell nanofibers with BSA encapsulation	72
Figure 48: Cross-section of the uranyl acetate stained nanofibers	72
Figure 49: SEM images on Left: The as spun electrospun core-shell BSA-PEG/collagen nanofibers . Right: Electrospun core-shell BSA-PEG/collagen nanofibers immersed in water for 5 seconds.	73
Figure 50: Left: As-spun core-shell core-shell BSA-PEG/collagen nanofibers on aluminum foil. Right: Crosslinked core-shell core-shell BSA-PEG/collagen nanofibers turned blue	74
Figure 51: Left: Crosslinked collagen core-shell nanofibers. Right: Crosslinked collagen core-shell nanofibers immersed in water for 7 days	74
Figure 52: Confocal images of crosslinked electrospun core-shell BSA-PEG/collagen nanofibers: genipin crosslinked nanofibers fluorescence overwhelmed other fluorescence signals	75
Figure 53: Fluorescence images of primary human fibroblasts cultured on crosslinked BSA-PEG/collagen core-shell nanofibers (3D) a: cell nucleus; b: filamentous actin; c:crosslinked-nanofibers; d: overlaid image (scale bar = 20μm).....	76
Figure 54: Fluorescence images of primary human fibroblasts cultured on crosslinked BSA-PEG/collagen core-shell nanofibers (3D). Blue: cell nucleus, green: actin filament, red: genipin-crosslinked core-shell collagen nanofibers. Side bars represent the side view of the scaffold.....	77

List of Abbreviations

BSA	bovine serum albumin
DHT	dehydrothermal
DMF	dimethylformamide
ECM	extracellular matrix
EDC	1-ethyl-3-(3-dimethyl aminopropyl) carbodiimide
FBS	fetal bovine serum
GA	glutaraldehyde
HA	hyaluronan
HFIP	hexafluoroisopropanol
IFR	inner solution flow rate
LSCM	laser scanning confocal microscopy
NHS	n-hydroxysuccinimide
OFR	outer solution flow rate
PBS	phosphate buffered saline
PDT	poly(dodecylthiophene)
PEG	poly(ethylene glycol)
PEO	poly(ethylene oxide)
PVA	poly(vinyl alcohol)
SEM	scanning electron microscopy
TEM	transmission electron microscopy
THF	tetrahydrofuran

1 Introduction

Disease, injury and trauma can cause damage and degeneration of tissues and organs in the human body. Treatments are needed to facilitate their repair, replacement or regeneration. These treatments typically involve the use of autografts or allografts [1]. However, tissue availability from the patient may be limited and in the case of allografts, immune rejection and donor availability place limits to their use [2]. Alternatively, an approach using tissue engineering to regenerate the damaged tissues by implanting biological substitutes that restore, sustain or improve tissue function was applied. In this technique, cells from the patient's body are isolated, expanded, and cultured on a three-dimensional porous supporting structure called scaffold for implantation [3]. It is assumed that the cells will adhere to the scaffold, proliferate and produce the natural tissue replacement [4].

In tissue engineering, the scaffold plays a critical role as it provides mechanical support for the cells to function and grow optimally. Several design criteria have been proposed for an ideal scaffold [5]:

- 1) the scaffold surface should allow cell adhesion, growth and differentiation;
- 2) the material used to construct the scaffold should be biocompatible, degradable and its degradation by-products should not provoke inflammation or cytotoxicity
- 3) the scaffold structure should be highly porous to allow cell growth and extracellular matrix (ECM) regeneration, nutrients diffusion and waste-product removal from the cells
- 4) the porous structure of the scaffold should permit uniform cell distribution throughout the scaffold to form a homogeneous tissue
- 6) the scaffold should be mechanically strong to stimulate cell growth.

Electrospinning has emerged as a method to produce such scaffold with simplicity

and the cost effectiveness. In this technique, charged polymer solution was flowing out of a capillary at a high drawing ratio. With strong electrostatic field, the obtained nanofibers form a nonwoven scaffold. A typical electrospinning setup operates by applying an electrostatic potential between the spinneret and a collector, with fluid slowly pumping through the spinneret. Both the spinneret and collector are electrically conducting and separated by a distance of 5 ~30 cm in between. While the jet stream travels from the conducting spinneret to the collector, the collector can be covered with a removable substrate for easier harvesting of the deposited scaffold. Electrospinning has been performed with either horizontal or vertical configuration to produce solid nanofibers with different fiber diameters and morphologies.

Coaxial electrospinning has emerged as a branch of electrospinning and the resulting nanofibers possess a core-shell structure [6]. In contrast with the solid electrospun fibers, core-shell nanofibers provide a feasible route for controlled release of embedded bioactives that are required for stimulating cell growth, proliferation and migration. Although electrospinning was performed in both horizontal and vertical configurations, all the reported coaxial electrospinning studies were performed with vertical configuration only. The effects of different configurations on coaxial electrospinning process and resultant fibers quality have not been studied.

Collagen, a major component of the extracellular matrix (ECM) and the most common structural protein in the human body, is one of the most promising candidates for tissue regeneration scaffold applications [7]. Electrospinning has been utilized to create nonwoven nanofibrous solid collagen scaffolds. However, electrospinning does not reproduce the structure of native collagen fiber. These fibers possess poor mechanical properties and are unstable in aqueous environment [8, 9]. Crosslinking is required to stabilize the electrospun collagen nanofibers. Studies have been done to stabilize electrospun collagen nanofibers, and showed the biocompatibility of the resultant crosslinked collagen nanofibers [9]. But no attempts

have been made on fabrication and stabilization of core-shell collagen nanofibers with bioactive molecule encapsulation. The objectives of the current research are to

- (1) Utilize coaxial electrospinning to prepare core-shell collagen nanofibers to encapsulate a model protein (i.e. bovine serum albumin (BSA))
- (2) Stabilize the core-shell collagen nanofiber with genipin crosslinking reagent, and
- (3) Demonstrate the stability and biocompatibility of the core-shell collagen nanofibers

2 Background and literature review

Electrospinning is one way to directly engineer nanofibers with diameter of tens to hundreds of nm. Nanostructures which are made via electrospinning have nonwoven structure with interconnected pores and large surface-to-volume ratio. These features enable such nanofibrous scaffolds to have many biomedical and industrial applications. The processing flexibility in tailoring scaffold properties, such as fiber diameters, scaffold size, porosity, and texture, offers the possibility to design electrospun scaffolds that can meet the demands of numerous practical applications. The stability of the nonwoven structures, which depends on the chemical composition and processing procedure, can be further improved by post processing.

2.1 Electrospun Nanofibers History

The process of using electrostatic forces to form synthetic fibers has been known for over 100 years. This process, known as electrospinning, was first observed by Rayleigh in 1897 who utilized high voltage source to inject charge of a certain polarity into a polymer solution, which is then accelerated toward a collector of opposite polarity. In 1914, Zeleny studied the process in detail on electro spraying where the solution came out as droplets instead of fibers [10] and the process was patented by Formhals [11] in 1934. The theoretical and experimental work by Taylor and others on electrically driven jets has laid the groundwork for electrospinning [12]. Taylor produced useful experimental evidence, and calculated the conical shape of the protrusion where a jet leaves the surface of a liquid [13].

2.2 Fundamentals of electrostatically induced jets

When an external electrostatic field is applied to a conducting fluid, a suspended conical droplet, whereby the surface tension of the droplet is in equilibrium with the applied electric field, is formed. As the applied electrostatic field is strong enough to

overcome the surface tension of the liquid, the liquid droplet at the tip of the spinneret then becomes unstable, and the liquid jet is ejected from the surface of the droplet. As the jet travels and whips in air, the solvent evaporates and is collected on a grounded target.

The charged liquid jet, consisting of sufficiently long-chain molecules and without breakup due to the Rayleigh instability, can elongate into a single fiber of considerable length with an extremely small diameter. The small fiber diameter is also responsible for the high specific surface area to volume ratio which is important for many biomedical and industrial applications. The high degree of molecular alignment is caused by the very large effective spin draw ratio and results in unique mechanical properties of the nanofibers.

2.3 Electrostatically induced jets

The surface of the fluid droplet held by its own surface tension at the spinneret tip gets electrostatically charged. Excess charges in the solution tend to move toward the part of this shape that protrudes the most with highest curvature. The subsequent charge accumulation causes the shape to distort and extend more to eventually form a conical shape. The interactions of the electric charges in the polymeric fluid with the external electric field cause the droplet to form a conical shape called Taylor cone [12, 14]. Accumulation of the charge at the tip of the cone increases the charge density in that region even further. The electrode shape and spinneret diameter are designed to yield a high electric field strength with an appropriate field gradient at the tip of the cone, so a fluid jet stream can be ejected out by overcoming the surface tension. Subsequently, the surface tension causes the droplet shape to relax again, but the liquid jet continues to be ejected in a steady fashion, namely, steady-state electrospinning.

The travelling liquid jet stream is subject to a variety of forces with opposing effects

[15]. Electrostatic repulsion of the charges in the jet tends to increase its surface area, thus reduce fiber diameter for fibrous structure. The effect of electrostatic repulsion is similar to that of stretching by mechanical drawing in conventional fiber spinning. If the liquid is a solution and the solvent gradually evaporates, the concentration and the viscosity of the liquid would change and the electrostatic repulsion effect would be enhanced.

In any liquid, the surface tension tends to reduce the total surface of the jet, but not by keeping the fiber diameter large. Rather, what usually occurs is an instability that causes the jet to break up into droplets, each with a surface-minimizing spherical shape. This effect is known as Rayleigh instability [16]. If the viscosity of the fluid is sufficiently high and the fluid contains long-chain molecules, the fluid jet stream diameter will continuously shrink to very small value until the essentially dried filament is eventually deposited onto the collector, and at the same time, the solvent is evaporated along the jet stream pathway. This is the desired situation for electrospinning.

If Rayleigh instability occurs for long-chain molecules that cannot be easily broken up into discrete droplets, a “pearls-on-a-string” morphology, also known as “beading”, can be formed. The occurrence of beading depends on the processing variables [17], especially the viscosity and the surface tension.

The strong repulsion due to high surface charges may, in principle, also be utilized to initiate a bifurcation process in which the jet stream is spatially separated into subfibers, known as splaying or branching.

2.4 Formation of Bending instability

During the electrospinning of an aqueous solution of high molecular weight polymer, a straight jet was formed as a consequence of electrical forces (Fig 1) [18]. On the

surface of a pendent drop of solution the electrically charged jet traveled for a few centimeters in a straight line. At the end of this straight segment, a diaphanous shape, also conical, with its vertex at the end of the straight segment was seen when proper illumination was provided [19]. This cone is the envelope, in space, of the complicated set of paths taken by a jet during the observation time. Baumgarten and Warner [20, 18] using appropriate illumination to observe and track the travelling path of the jet indicated that the jet was continuously bending for as far as it could be followed after it entered the envelope cone (Fig 2).



Figure 1: Glycerol jets profile at 0.5mL/min. Left to right: 3.67kV/cm, 4.33kV, 5.0kV/cm (adapted from [18])

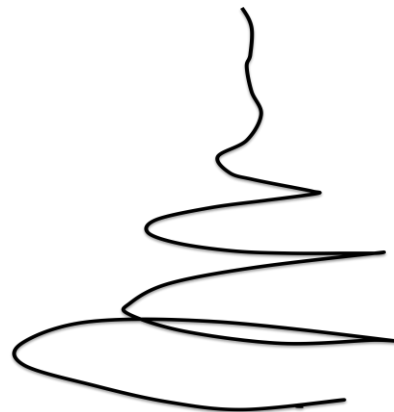


Figure 2: Illustration of the jet bending at the end of the straight segment. (Adapted from [19])
 After traveling linearly for a certain fraction of its path, solvent continuously evaporating and jet stream thinning its diameter by stretching, the ejected liquid usually experiences instability in the jet propagation. It is shown that the longitudinal

stress caused by the external electric field acting on the charge carried by the jet stabilized the straight jet for some distance. Then a lateral perturbation grew in response to the repulsive forces between adjacent elements of charge carried by the jet. The motion of segments of the jet grew rapidly into an electrically driven bending instability [21]. This instability appears to be splaying in the form of repeated bifurcations, the initial single jet stream lead into multiple jet streams. However, subsequent experiment gathered with high speed cameras and theoretical models suggested that the apparent splaying was an optical illusion in the form of a very fast whipping motion of the jet [14]. Reneker and coworkers [19, 21] explained the observed whipping motion by a bending instability. The bending instability often causes the whipping jet to assume a spiraling loop conformation (Fig 2).

Shin et al. [13] developed a theory for electrified fluid jets to describe the electrospinning process using operating diagrams of electric field versus flow rate to define regions of stable fiber formation. By assuming the fluid is Newtonian and incompressible, electrohydrodynamic equations were developed for conservation of mass, conservation of charge and differential momentum balance. The steady state jet profiles can then be calculated numerically. Based on their previous work [22], their systematic experimental and theoretical analysis suggests that three different types of instability can be predicted: two axisymmetric modes and one non-axisymmetric mode. Whereas the first axisymmetric mode is associated with the classical Rayleigh instability, which is dominated by surface tension and resulted in the nearly straight region in the jet path. The other two modes are electrically driven, and it is the competition between the two conducting modes that is of importance at the high-applied fields. Their results showed good agreement between experiments and theory, but they also indicated that a third operating parameter, the electric current, is also crucial but not an independent parameter in the experimental process. The charge density carried by the jet not only depends on the manner in which charge is induced in the fluid, but also fluid parameters and equipment configuration.

Reneker et al. [21] used a theoretical model of the electrospinning process to calculate the three-dimensional paths of continuous jets, both in the nearly straight region where the instability grew slowly and in the region where the bending dominated the path of the jet. The mathematical model provides a reasonable representation of the experimental data, particularly of the jet paths determined from high speed videographic observations. The theory accounts for the nonlinear effects that are characteristic of finite perturbations, as well as for the rheological behavior of viscoelastic liquids.

Although mathematical model and experimental data did show good agreement, in many ways, mathematical models are oversimplification because they ignore couplings among parameters for real materials.

2.5 Parameters effects on nanofiber diameter and morphology

The fiber diameter and morphology can be controlled by various parameters, such as applied electric field strength which is tailored by applied voltage between spinneret and collector; distance between the spinneret and the collecting substrate; temperature; feeding flow rate; humidity; air velocity; and properties of the solution, including polymer type, molecular weight, surface tension, conductivity, and viscosity. Moreover, solution properties such as surface tension, conductivity, and viscosity, depend not only on temperature but also concentration. Other variables which are not stated are dependent on one or more other variables such as solution concentration, solvent quality, additives and temperature-dependent behavior of these parameters.

At the same time, jet formation also depends on the electrode design and electric field strength at the tip of the spinneret, whereas fiber formation from the jet stream also depends on the fluid flow rate and the solution evaporation rate [23]. In some cases, to control and to promote solvent evaporation, additional gas flow at the elevated temperature can be introduced. This causes reductions in solution viscosity,

concentration and surface tension [6].

The properties of the electrospun scaffold can also be modified by post-spun process such as annealing, stretching or crosslinking, which can improve their mechanical properties or/and degradation behavior.

Thompson et al. [23] studied the effects of experimental parameters on nanofiber diameter based on electrospinning model. The model indicates which parameters have the greatest influence on the fiber diameters. Among the 13 material and operating parameters studied in the paper, researchers evaluated the parameters on a relative basis to determine a strong-moderate-minor rating for the influence on the nanofiber diameter [24]. The result showed that volumetric charge density, distance from nozzle to collector, initial jet radius, relaxation time, and viscosity are the five parameters having the most significant effect on the jet radius. Initial polymer concentration, solution density, electric potential, perturbation frequency, and solvent vapor pressure have moderate effects on the fiber diameters. While parameters such as relative humidity, surface tension, and vapor diffusivity have minor effects on the resulting jet radius [23]. Although the study hasn't considered the effect of temperature, temperature does factor indirectly into the calculations through changes in solution density, vapor diffusivity, viscosity, relaxation time, etc. In addition, other potential factors such as solution pH, charge polarity and pressure were not included in the model for studying [23].

2.5.1 Jet cross-sectional radius

By normalizing the results from other research literature to the model in the paper, Thompson et al. [23] predicted that the jet cross-sectional radius starting at the nozzle is directly related to needle size based on the single paper on electrospun poly(lactide-co-glycolide), which is corresponding to the final fiber radius. However, this result is only based on one single paper and other papers have identified the initial

jet diameter at the tip of the Taylor cone is significantly affected by the applied voltage, jet cross-sectional radius cannot be treated as a fully independent parameter when the applied voltage changes.

2.5.2 Needle collector separation distance on fiber diameter and morphology

The electrospinning literature reports different separation distances between the needle and collector separation distance in the experimental setups. Although not all research articles report the effects of separation distance on final cross-sectional fiber diameter, in several experiments, it was reported that a decrease in fiber diameter with increase in collector distance when smooth fibers were produced [25]. On the contrary, with beaded fibers present, the beads tend to grow larger as distance increased probably due to the capillary instability, which have more time to develop [26]. Although Still et al. pointed that beaded morphologies only occur when the distance between the needle and collector is too short [27].

2.5.3 Viscosity

Viscosity plays an important role in governing electrospinning, it is directly controlled by the molecular weight and solution concentration [28, 29]. Most viscosity values were measured at zero-shear values. The experimental data showed a strong dependence on viscosity for fiber morphology [30, 31]. An increase in viscosity, beyond minimum necessary, increases visco-elastic force which opposes columbic force and leads to an increase in fiber diameter [6]. Increasing zero-shear viscosity will increase the resulting fiber radius, however, if the solution viscosity is above a critical value, the shear between the solution and the spinneret wall would prevent the formation of stream ejection [32].

2.5.4 Concentration

The basic requirement for fiber formation is sufficient inter-chain entanglements, so polymer concentration, which affects both viscosity and surface tension of the solution, plays a crucial role in electrospinning process. If the solution concentration is too low, the as spun fiber will break up into droplets due to the effects of surface tension, whereas a concentrated solution enables high viscosity making jet initialization extremely difficult. In most experiment, the effect of concentration was not studied; the initial polymer concentration was maintained constant for other variables. A report on Nylon-6 showed increased fiber diameters with increasing initial polymer concentration [26]. It was also reported that as the polymer concentration increase, the as spun structure changed from highly beaded fiber to uniform morphology and eventually to a ribbon-like structure [33]. Similar studies on electrospun collagen nanofibers also indicated that only concentrations above a threshold (5wt%) will allow fiber formation [9].

2.5.5 Conductivity

Fluids with high conductivity have high surface charge density. Under a given electric field, this results in an increase in the elongation force on jet, which is caused by the self-repulsion of the excess charges on the surface [23]. This inhibits the Rayleigh instability, enhances whipping and leads to finer fibers [6]. Since most synthetic polymers do not carry charge, it is preferred to increase solution conductivity by adding extra salts or polyelectrolytes in the solution [34]. Solution with higher conductivity undergoes a greater tensile stretch caused by self-repulsion of the excess charges distributing on the surface. It also prevents axisymmetric instability and creates thinner fibers to some extent [21]. Thus, with increasing solution conductivity, fiber diameter would decrease [27].

2.5.6 Solvent types and vapor pressure

Several studies reported on the effect of various solvents and their effect on the electrospinning process [35, 36]. Discussions in these works indicated that low vapor pressure solvents tend to inhibit solution flow which prevents a fully developed Taylor cone to be maintained due to low charge density or high viscosity. High vapor pressure solvent may bring about irregular multiple jets emerging from the droplet [32]. Megelski et al. [37] examined the polystyrene fibers fabricated from solutions containing various ratios of dimethylformamide (DMF) and tetrahydrofuran (THF). 100% THF as solvent gives rise to many deep pores embedded in fibers, whereas smooth fibers with complete loss of microtexture yielded from 100% DMF solvent. Between these two extremes, pore gradually became enlarged and shallowed as the solvent volatility decreased with decreased THF percentage [37]. As most of the information on vapor pressure is related to morphological changes due to conductivity, viscosity or surface tension, and considering various solvents, it is difficult to make true comparison due to the variation of other solvent properties and lack of data on the vapor pressure effect [23].

2.5.7 Electric potential

Katti et al. [5] reported an initial decrease in diameter of poly(lactide-*co*-glycolide) fibers with an increase in electric potential from 8-10 kV, but no significant correlation with subsequent increases. No such results have been reported by other researchers and one research showed no significant change in fiber diameter for solution with different initial polymer concentration at different applied voltage [38]. Still et al. [27] studied the effect of applied voltage on fiber morphology and concluded that the fiber diameter would decrease within optimal voltage range.

2.5.8 Other parameters

No literature research has been reported on vapor diffusivity while the effect of humidity on fibers was dealt with the development of porous fibers [39]. Moreover, the effects of relative humidity are strongly coupled to other parameters and operating conditions, so the coupled effects cannot be directly identified [23]. For surface tension, it was shown that the effect of the surface tension is negligibly small when electrospinning solutions retain their viscoelasticity, indeed, Thompson et al. indicated that the viscoelastic forces completely dominate the surface tension [23]. With low molecular weight polymers or when polymer concentrations are significantly reduced, the viscoelastic forces dramatically diminish and surface tension then plays a strong role in the morphology of the resulting fibers. In these cases, beaded fibers tend to form for higher surface tension solvents, low viscosity and low conductivity/charge density systems. Polymer feed rate has influence on fiber morphology as well as scaffold porosity [32]. It maintained the Taylor cone by keeping a mass balance between the feed solution and ejected stream. It has been reported that fiber diameter and pore sizes increase as flow rate increases until formation of ribbon-like structure [33] and beaded morphologies occur if the flow rate is too high [27].

Air velocity also has an effect on the morphology of the fibers. According to the model adapted by Thompson et al. these effects are not linear and do not necessarily mean that the quality of the product is maintained but give a general idea about the trends [23].

The electrospinning process is complex and it is difficult (or in some cases, impossible) to experimentally vary one parameter while others are kept constant. The reports on varying one parameter at a time give insight into the electrospinning process and suggest that to better control the process one must control the parameters with the strongest effect. For each polymer type and solvent system, there is usually a

relatively narrow set of manufacturing conditions that provide optimum results. Moreover, most of parameters effect investigations were done on solid fibers. With coaxial electrospinning, which is the current spinning system, no work has been reported to systematically investigate the effect of these parameters.

2.6 Effects of Electrospinning Setup

The arrangement for electrospinning could be horizontal or vertical according to the geometrical arrangements of the spinning needle and collector, where vertical type includes shaft type and converse type (Fig 3, 4).

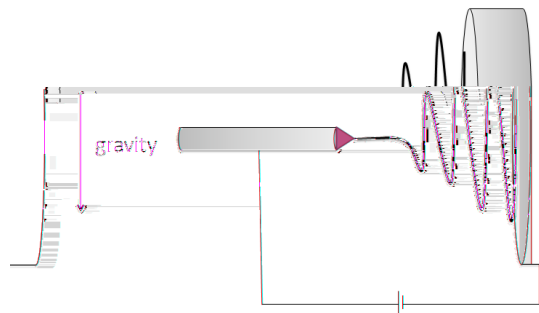


Figure 3: Horizontal electrospinning setup

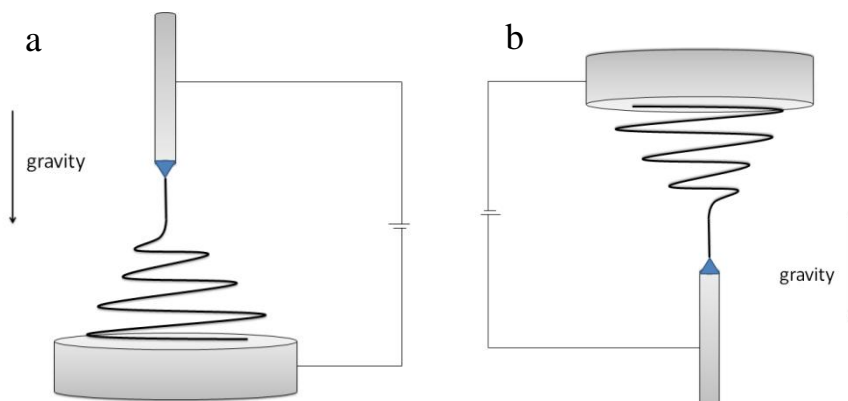


Figure 4: a: shaft type vertical electrospinning. b: converse type vertical electrospinning

Using different electrospinning system configurations, the obtained fiber properties could be quite different. The vertical setup allows solution flow to be inline or against

gravity. Yang et al. [40] studied the differences of fibers diameters and fibers mats morphology between the three electrospinning systems. The results showed that in the shaft type system, the electrospinning fibers were the thinnest as the gravitational force strengthen the effect of electric field to maximize fiber extension. While this setup results in the broadest fiber diameter distribution. In the converse type system, the average fiber diameter was the largest and the fiber diameter distribution was the narrowest. The horizontal type system resulted in average fiber diameter and size distribution between shaft and converse types [40].

In another study, Rodoplu and Mutlu [41] indicated that the effect of gravitational force on electrospinning process is negligible with respect to the electric field forces. However, they also found that gravity has an effect on the shape of the polymer droplet and the Taylor cone. This results in a difference in electrospinning parameters used in horizontal and vertical systems.

These studies were all based on electrospinning setup used for producing solid nanofibers, the effect of electrospinning configuration on coaxial electrospinning has not been reported.

2.7 Coaxial electrospinning

Coaxial electrospinning has emerged as a branch of electrospinning, the resulting nanofibers possess a core-shell structure. Similar to electrospinning, coaxial electrospinning employs electric forces acting on polymer solutions in DC electric fields and resulting in significant stretching of polymer jets due to a direct pulling and growth of the electrically driven bending perturbations [42, 43]. Comparing to electro spraying, where the jets should be rapidly atomized into tiny core-shell droplets, with no viscoelasticity or jet bending involved; coaxial electrospinning produces jet which stays intact and become core-shell nanofibers [44].

A novel idea in developing scaffolds is to use core-shell structure with two different polymers that degrade at different rates. Such spinning was first demonstrated by King et al. [9] using bicomponent carpet fiber melt-spinning technology to spin resorbable materials. The idea of coaxial electrospaying for encapsulation of liquid droplets was also introduced by Loscertales et al. [45] and the same principle has been successfully applied to electrospinning of composite and hollow fibers by several groups [46, 47, 48].

2.8 Coaxial electrospinning setup and process

Coaxial electrospinning is an important method used to form bicomponent continuous nanofibers through spinning solutions of two dissimilar polymers within a concentric needle. This results in an end product that comprises the two polymers in a distinct shell and core form [32]. Coaxial electrospinning setup adopted by most researchers is quite similar to that used for electrospinning of solid fibers. A smaller (inner) capillary that fits concentrically inside the bigger (outer) capillary makes the coaxial spinneret (Fig 5). The two compartments containing different polymer solutions or a polymer solution in the shell and a non-polymeric Newtonian liquid or even a powder in the core are used to initiate a core-shell jet.

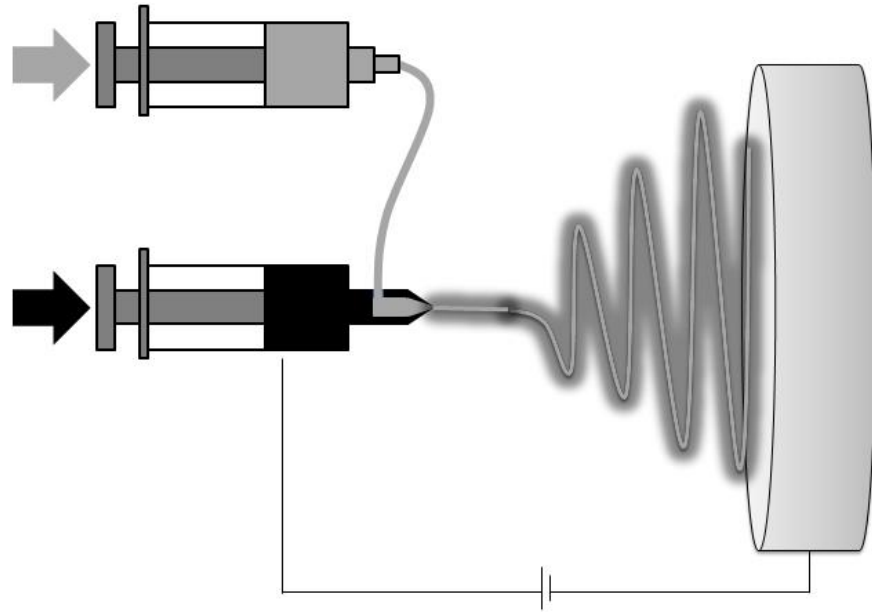


Figure 5: Coaxial electrospinning

Two polymers solutions are held in separate syringes and fed independently through the concentric needle. At the exit of the coaxial needle appears a core-shell droplet, when electric field is applied, the charge accumulation occurs predominantly on the surface of the shell liquid coming out of the outer coaxial needle (Fig 6a) [49].

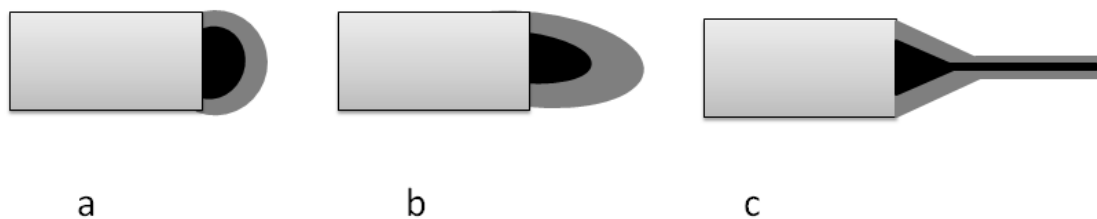


Figure 6: Compound jet formation a: a compound droplet formed at the tip of the spinneret, b: shell solution elongates and stretches due to charge-charge repulsion, c: stream ejected from the Taylor cone

The pendant droplet of the shell solution elongates and stretches due to the charge-charge repulsion to form a conical shape (Fig 6b) and once the charge accumulation reaches the threshold value due to the increased applied potential, the

stream is ejected from the cone (Fig 6c). The stress generated in the shell solution causes shearing of the core solution via "viscous dragging" and "contact friction" [50]. This causes the core liquid to deform into the conical shape with the shell solution and a compound coaxial jet develops at the tip of the cone. Liquid in the compound cone, being subjected to a sufficiently strong electric field, forms a compound jet, which undergoes the electrically driven bending instability [46, 51, 52]. Strong jet stretching resulting from the bending instability is accompanied by enormous jet thinning and fast solvent evaporation. As long as the process becomes stable, the as-spun fibers undergo bending instability for stretch and the resultant core-shell jet solidifies and depositing on the counter-electrode. This technique has found broad applications, especially for polymers that are difficult to be spun alone [6]. Coaxial electrospinning improves the properties of a nonwoven fibrous mat, such as creating controlled degradation rate, controlling mechanical properties [53], or serving as a scaffold for tissue engineering where a less-biocompatible polymer is surrounded by a biocompatible material so that the overall structural integrity of the scaffold can be maintained with the structural support of the inner component [54].

As the shell and core solutions are in contact and undergo the same bending instability and whipping motion, the degree of dissimilarity between the two solutions, in terms of composition, physical and rheological properties, plays an important role in the formation of the composite fibers [6].

Moghe et al. claimed electrospinnable shell solution was a fundamental requirement to ensure continuous fiber formation [6]. A stable Taylor cone created by shell solution would spontaneously cooperate with core solution by interfacial viscous drag to form a coaxial jet. However, several studies used liquids such as mineral or olive oil as core material and obtained hollow fibers [50, 55]. Indeed, electrospinnable shell solutions work as templates greatly expand inner material selections [32].

2.9 Processing parameters for coaxial electrospinning

2.9.1 Applied voltage

As most studies only used one voltage value for specific compound cone stabilization, no systematic investigation of this parameter has been done. For a given pair of polymer systems and flow rates, it was found that there exists a narrow range of applied voltage in which a stable compound Taylor cone can be formed (Fig 7b). Below this optimal range, both or any one liquid cannot be driven out and results in discontinuous dripping (Fig 7a) [6]. Due to the increased size of the cone, mixing of the two solutions tended to occur [56]. Voltage above the critical range caused the strength of the electric field to exceed that required for the material and the processing conditions used. Instead of the coaxial jet, separate jets formed from the shell and core solutions (Fig 7c).

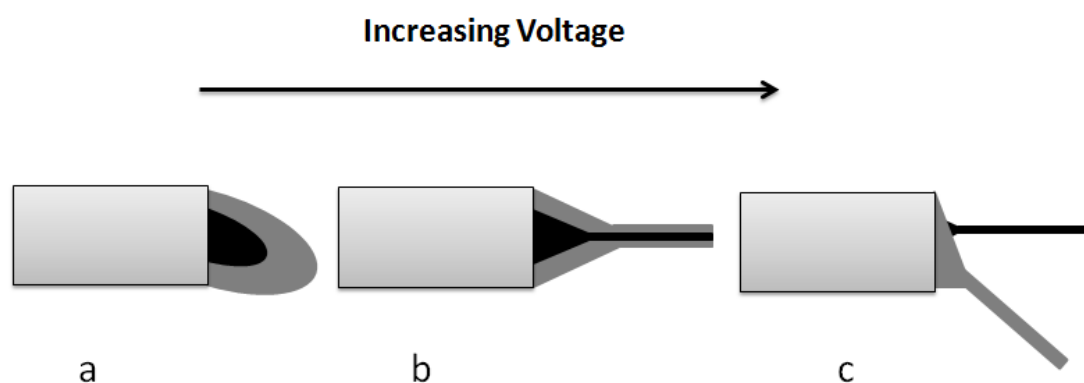


Figure 7: Voltage dependence of the core-shell fiber formation. A: voltage below optimal range (subcritical voltage), B: optimal voltage (critical voltage), C: voltage above optimal range (super critical voltage)

2.9.2 Flow rate

Flow rate of the two solutions are crucial to the structure of the core-shell fiber, especially the thickness of the two layers [33]. Several groups found the core and shell layer thickness can be tailored by keeping one flow rate constant while changing

the other one [57, 58]. By keeping the shell flow rate constant while change the core solution flow rate, several groups found the volume expansion of the overall droplet. Eventually, with increasing in core flow rate while keeping the shell flow rate constant, the shell solution may fail to appropriately encapsulate the inner liquid, and cause a disrupted process. Typically, the core flow rate is lower than the shell flow rate, however, insufficient delivery of core material may lead to discontinuous segments in the fibers [59].

2.9.3 Solution viscosities

The electrospinnable shell solution drove the inner liquid, dominating the fiber formation process. The viscosity of the shell solution is required to be such that the viscous stress imparted on the core is sufficient to overcome the interfacial tension between the two solutions and allows the formation of a compound Taylor cone [59]. Viscosity of the shell solution is critical and the shell polymer solution should be electrospinnable by itself to lead the core-shell structure formation. It appears that the requirements for the spinnability of the core solution by itself are not as critical as they are for the shell material [6].

2.9.4 Solution concentration

The polymer concentration determines the spinnability of a solution, the solution must have a high enough concentration for chain entanglements to occur. An increasing solution concentration would increase fiber diameter for conventional single fluid electrospinning, similar effect has been observed in coaxial electrospinning. Zhang et al. [60] reported increased core diameters and overall fiber diameters by increasing core solution concentration while keeping the shell concentration constant. It was found that the ratio of outer layer thickness to that of inner one decreased at the same time [60].

He et al. on the other hand, inversed Zhang's process by using shell solutions with different concentrations to create nanofibrous drug release systems. They found that as the shell solution concentration increases, the fiber diameters increase as well [61].

2.9.5 Solution conductivity

The difference in conductivity between the shell and core solutions has a great impact on charge accumulation, which determines the origin of the jet. Yu et al. [62] found discontinuity in the core-shell structure occurs if the conductivity of the core solution is higher and is being pulled at a higher rate. On the other hand, higher shell conductivity imposes higher shear stress on the inner material, which induces a thinner core structure [33]. Even non-conductive or less conductive liquids can be incorporated into a higher conducting shell to form core-shell structure [6].

2.9.6 Solution miscibility

The interaction between the core and shell solutions governs the resultant fiber structure, the interfacial tension between the shell and core solution should be as low as possible for the generation of the stabilized compound Taylor cone [59]. However, some researchers reported that if the core and shell solutions are miscible, mutual diffusion starts as soon as the two fluids encounter at the tip. It might last at the order of 1 second before forming a compound cone [6]. Li [50] and Kurban [63] revealed that fiber morphologies strongly depend on degree of miscibility of the two solutions. Fibers electrospun from immiscible solutions had a distinctive core-shell structure, whereas fibers embedded with dense through-pores were created in semi-miscible systems. Miscible systems failed to form fibers although the shell solution was electrospinnable on its own. The fast diffusion may perturb Taylor cone formation or make shell material permeate into core solution, disrupting the electrospinning process [6].

Sun et al. [46] insisted that the characteristic time of diffusion spreading of a boundary between two miscible solutions was much greater than that of whipping instability, thus no mixing took place. Distinguishable core-shell structure of poly(dodecylthiophene) (PDT, core) and poly(ethylene oxide) (PEO, shell) in chloroform was derived from his system demonstrated that extensive mixing did not take place.

Diverse results reported for the use of miscible core/shell polymer solutions were based on observations on limited work. This indicates that further research is needed for a clearer understanding of the condition that would restrict mixing when miscible core-shell polymer solutions are used.

2.9.7 Solvent vapor pressure

The type of solvent used for core and shell solutions can have effects on the resulting morphology of the core shell structure. Li et al. [48] reported that when high vapor pressure solvents (e.g. chloroform, acetone etc.) were used in the core, a thin layer of the core material formed at the interface of the shell and the core due to rapid evaporation of core solvent. This layer traps the interior solvent that diffuses out more slowly due to the newly created barrier. When the core solvent fully leaves the structure, it creates a vacuum. This vacuum in the core causes the core structure collapse and form ribbon-like fibers under atmospheric pressure [48]. Moghe et al. also found a collapsed core structure when chloroform was used as a solvent for the core polymer [56]. In their experiment, the shell solution used was poly(vinyl alcohol) (PVA) in water and the core was poly(ethylene oxide) (PEO) dissolved in chloroform.

Since the stabilized compound Taylor cone and the initial jet are required for the coaxial electrospinning, high vapor pressure solvents should not be used as they may produce unstable Taylor cones [64].

2.10 Fiber morphology and alignment

If the collector in the electrospinning process is a plate, the deposited nanofibers typically assume a completely isotropic orientation. However, for many applications, it is desired to control the alignment of the fibers. For example, aligned nanofibers can enhance cell attachment and proliferation [65]. To introduce uniaxial alignment into the nanofiber deposited, the fibers should be collected on a rotating drum with the rotation speed matching the extremely high speed of the whipping motion caused by the bending instability. However, the achievable degrees of alignment obtained by this method are limited [6].

Several groups have studied different collector configuration to control the orientation of electrospun fibers. As Xia and coworkers [66, 67] showed, using a paired electrode with a gap in between, uniaxial alignment of the deposited nanofibers can be obtained. The fibers span across the gap from hundreds of micrometers to several centimeters. Using geometric configurations consisting of multiple pairs of electrodes and sequentially activates pairs of electrodes, one can guide the nanofiber alignment and generate more complicated aligned nanofiber fabrics [67, 68].

2.11 Properties and Applications of Core-shell Nanofibers

Coaxial electrospinning rapidly became popular and is used by many research groups for different purposes. In particular, coaxial electrospinning allows encapsulation in the core or wrapping as a shell for non-spinnable polymers, or non-polymeric materials like powders, nanoparticle suspensions, catalysts, and proteins [52, 69].

One of the possible motivations for applying coaxial electrospinning is to modify wetting properties of nanofiber surface [59, 70]. Some groups work with applying coaxial electrospinning for encapsulation of drugs or biologically active objects in the fiber core [51, 71, 72, 73]. In this way, the release rate can be controlled and the

biologically active agents in the core can be protected from harsh solvents with the spinnable polymer solution in the shell.

2.12 Collagen as a biomedical material

Natural biopolymers are often of interest as they simulate a biomimetic environment for tissue regeneration. Chitosan, hyaluronan (HA), heparin, collagen are examples of natural polymers that have been extensively used in biomedical applications.

Collagen is one of the most promising candidates for tissue engineering applications. It is the major component of the ECM and the most common structural protein in the human body. It serves for the maintenance of the structural integrity of tissues and organs and is involved in the interaction with specific receptors that define cellular adhesion, differentiation, growth and survival [74]. Most of collagen molecules self-assemble into insoluble, triple-helical structures that are packed together into the staggered patterns called fibril and act as the major stress-bearing component of connective tissues and of the fibrous matrices of skin and blood vessels. Over the last 20 years, increased interest has emerged in the use of collagen and collagen-containing tissues in medical devices. Purified collagen obtained from animal tissue can be processed to generate collagen containing products that find applications not only in the medical field, but also in manufacturing of cosmetics, water treatment and nanofluidics [75]. The individual polypeptide chains of collagen contain 20 different amino acids and the precise composition varies among different tissues. There are over twenty genetically different types collagen molecules located in many diverse tissues within the human body given by the variation in specific amino acid sequence. Collagen type I and III are the most abundant types and they form the long-recognized characteristic fiber bundles seen in tissues [7]. Type I collagen is found within skin, ligaments, tendons and bone while type II is found in blood vessel. Collagen type I consists of triple helical fibrils made of polypeptide

chains with carboxyl groups, interconnected by covalent and hydrogen bonds. The triple helical structure protects the collagen fiber from being broken down by proteases and is important for cell adhesion and the assembly of the ECM.

2.13 Crosslinking of electrospun collagen nanofibers

The electrospinning process allows the production of fibers with diameters down to the tens of nanometer range. Using this method, 3-D scaffolds made from collagen fibers with interconnected pores can be generated. The porous structure enables cells and blood vessels to infiltrate into the construct in vivo [3, 7]. It is desirable to have a 3D structure of organized collagen fibers to better mimic native tissue environments to guide the tissue regeneration process [76]. However, electrospinning produces only collagen fibers that are unstable in aqueous environments. Post processing techniques such as crosslinking treatment is therefore necessary to stabilize these fibers to be useful for our purposes.

Crosslinking is essential to stabilize the electrospun nanofibers by targeting intramolecular covalent bonds. It is accomplished by the reaction of functional groups on the surface of collagen fiber that can bridge and link to construct an interpenetrating and water-resistant network. Furthermore, crosslinking can tailor the rate of biodegradation, providing collagen networks the specific rate to degrade into bioresorbable components as cells produce their own ECM [77]. A number of cross-linking methods have been shown to successfully improve the stability and mechanical properties of collagen-based scaffolds [78, 79, 80]. These methods can be categorized into chemical, physical or biophysical crosslinking. Although physical methods can avoid introduction of potentially toxic residuals, the degree of crosslinking achievable is limited. Therefore, chemical crosslinking treatment is the preferred choice [81]. Performance of the resulting scaffolds were studied by evaluating the degree of crosslinking, degree of swelling, rate of degradation,

mechanical properties, their biocompatibility and cell compatibility of the nanofibers [82, 83]. The common chemical crosslinking treatment of protein in general and collagen in particular involves the use of a carbodiimide, glutaraldehyde and genipin.

2.13.1 Carbodiimides

Carbodiimide treatments are used to form crosslinks between different functional groups within the collagen molecules, without itself being incorporated. They can be used to establish an isopeptide bond between the carboxyl and amino groups from amino acid residues; the only byproduct of this reaction is water-soluble urea which can be easily removed [84].

Two different carbodiimides have been used to crosslink collagen: cyanamide or 1-ethyl-3-(3-dimethyl aminopropyl) carbodiimide (EDC) [80], while EDC is more commonly studied.

EDC contributes no components to the final crosslinked product, and the two crosslinking residues must be in direct contact in situ, hence the crosslinks formed are referred to as “zero length” crosslinks. EDC has been used to enhance the biostability of collagen scaffolds in the presences of N-Hydroxysuccinimide (NHS), which helps to prevent the formation of side products and to increase the reaction rate. For electrospun fibers, solvents which can preserve fiber morphologies are needed. Possible solvents for EDC crosslinking are proposed, including pure ethanol and acetone/water mixture [85].

The chemical reactions of EDC/NHS crosslinking on collagen are outlined in Figure 8. Crosslinking of the collagen material can be controlled by varying the EDC/NHS concentration. By comparing EDC crosslinked dermal sheep collagen to GA crosslinked collagen, a higher shrinkage temperature and enzymatic resistance were obtained with the EDC crosslinked samples [84]. Subsequent rat subdermal

implantation studies showed the EDC/NHS crosslinked collagen samples had low tendency to calcify with good biocompatibility [84]. The formed amide crosslinks may be beneficial in terms of anticalcification due to the reduction in calcium binding sites [85]. Lee et al. [86] crosslinked bovine pericardium with EDC/NHS, the resulting materials had comparable in-vitro stability as GA crosslinked pericardium.

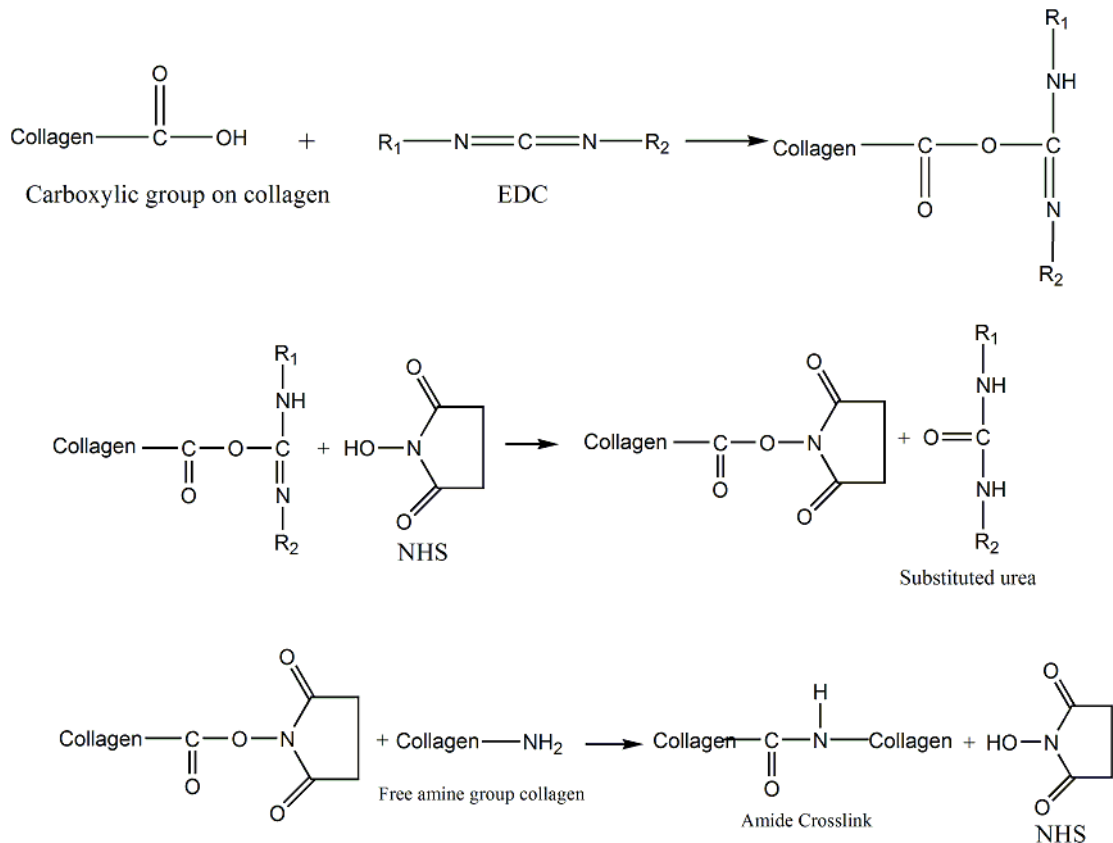


Figure 8: Crosslinking of collagen with EDC and NHS.

Haugh et al. [80] crosslinked collagen/glycosaminoglycan scaffolds using EDC, glutaraldehyde (GA) and dehydrothermal (DHT) and investigated the effect of crosslinking on compressive modulus and cellular attachment, proliferation and migration of the scaffold. They demonstrated that a wide range of scaffold compressive moduli that can be attained by varying the crosslinking treatment parameters and claimed that EDC and GA produced the stiffest scaffold with enhanced cellular activities.

Barnes et al. [87] carried out a systematic study on crosslinking of type II collagen fibers for the purpose of cartilage tissue engineering. Different crosslinking conditions were used to compare the effect of the EDC crosslinking method (i.e. EDC concentration, presence of NHS) with glutaraldehyde crosslinking. Ultimate tensile strength tests were performed on as-spun dry samples and crosslinked electrospun collagen fibers in hydrated state. A statistically significant difference in mechanical properties had been proven to exist between the dry sample and all the crosslinked fibers. Although Barnes et al. [87] claimed all the other crosslinked samples had displayed a fibrous texture, SEM images showed samples display a mixture of fibrous and gel characteristics. The significant fiber swelling and gelling would reduce the level of porosities and prevent the samples from being used for biological applications.

2.13.2 Glutaraldehyde

Glutaraldehyde (GA) ($\text{CH}_2(\text{CH}_2\text{CHO})_2$) is an organic compound commonly used as a chemical preservative and disinfectant. At low concentrations, GA produces intramolecular crosslinks in collagen; while at higher concentration, GA forms long polymeric chains which produce intermolecular crosslinks. While other “zero length” crosslinks are limited to crosslinking collagen molecules that are directly adjacent to each other (1nm), GA can crosslink molecules that are separated by a distance [78]. The long polymeric chains have potential to link residues that are spaced far apart and thereby enhance the extent of crosslink formation [88]. Thus, GA gives materials with the highest degree of crosslinking when compared with other known methods [89]. The reactions involved during GA crosslinking had been extensively studied, but the reaction mechanism is very complex and still not completely understood. Aqueous solutions of GA contain a mixture of free aldehyde and mono- and dihydrated glutaraldehyde and monomeric and polymeric hemiacetals (Fig. 9).

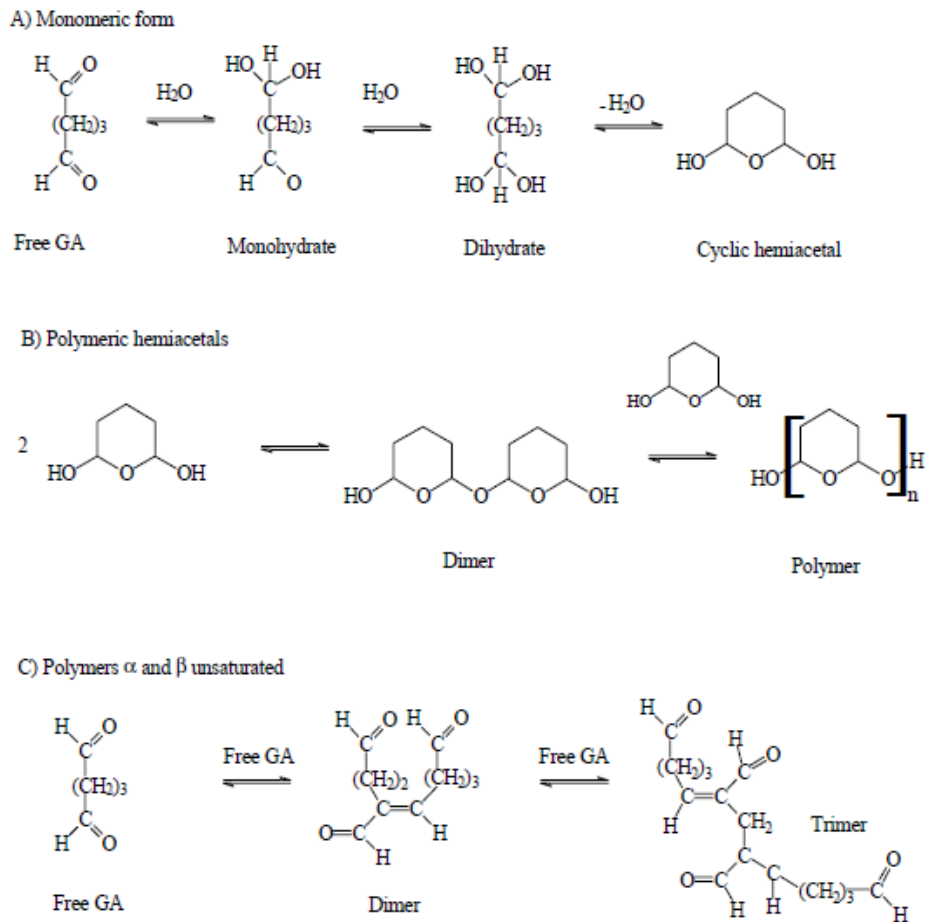
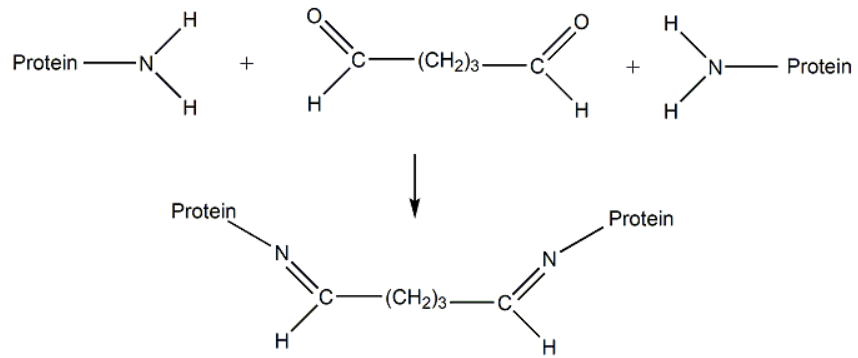


Figure 9: Possible structure of glutaraldehyde (GA) in aqueous solutions

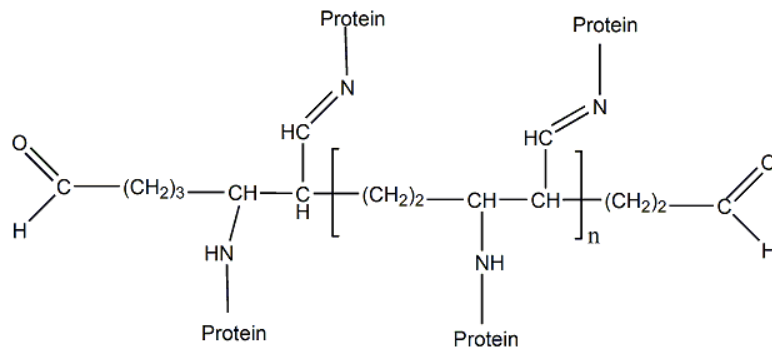
Due to the complexity of the reaction solutions, many reactions can occur during crosslinking [90]. Studies showed that glutaraldehyde or its polymerization products may react with several functional groups presenting on the protein surface, for example, amines, thiols, phenols, and imidazoles, although its crosslinking effect is dominated by reactions with the ϵ -amino groups of lysine residues [82, 91]. Proposed mechanisms for the crosslinking reaction of the monomeric form of glutaraldehyde with these ϵ -amine groups, involving nucleophilic attack on the aldehyde groups to yield a non-conjugated Schiff base (Fig 10a), were considered to be unstable under acidic conditions [91]. Several alternative mechanisms have been proposed involving the aldol condensation of the active monomeric glutaraldehyde species into polymeric forms (Fig 11) and reacting with proteins under alkaline or acidic conditions (Fig 10 b,c) [91, 92]. The monomeric GA results in "zero length" crosslinks, whereas the

polymeric forms crosslinks residues that are separated far apart.

a



b



c

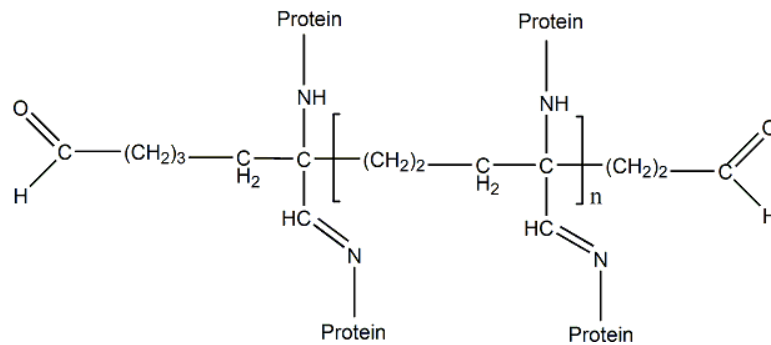


Figure 10: a: Schiff base formation obtained by crosslinking of lysine residues from two protein molecules by monomeric glutaraldehyde. b: Suggested end product obtained from the reaction between the polymeric glutaraldehyde with lysine residues from the crosslinked proteins under alkaline conditions. c: Suggested end product obtained from the reaction between the polymeric glutaraldehyde with lysine residues from the crosslinked proteins under acidic conditions

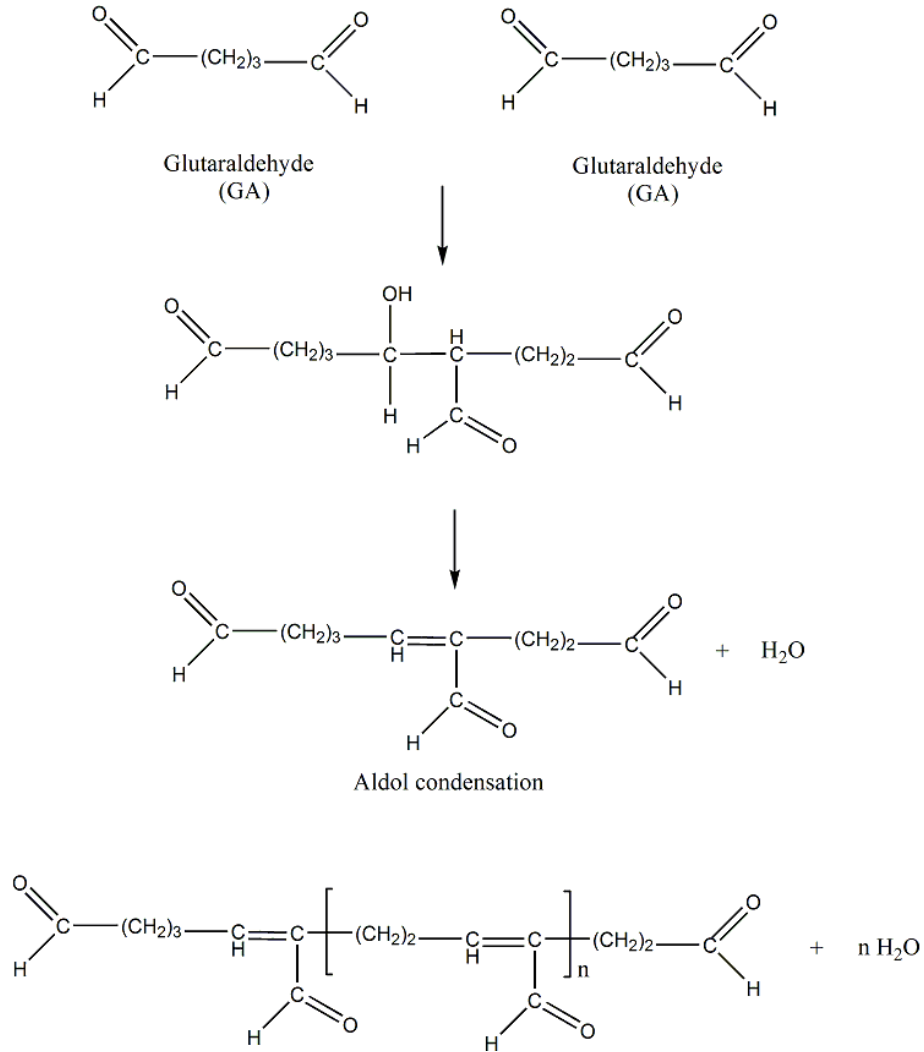


Figure 11: Aldol condensation of monomeric glutaraldehyde to form polymeric glutaraldehyde

Since collagen scaffold produced from purified soluble collagen degrades immediately as it is exposed to wet condition, to avoid its disintegration during the crosslinking process, GA crosslinking was performed in the vapor phase by placing the collagen scaffold in a sealed container filled with glutaraldehyde (GA) vapor.

Yang et al. [93] used GA vapor to crosslink electrospun collagen fibers and showed that fibers preserve their fibrous structure even after immersion in aqueous solutions. Nanomechanical tests were also performed on these electrospun collagen fibers and it was shown the bending modulus increased significantly due to crosslinking.

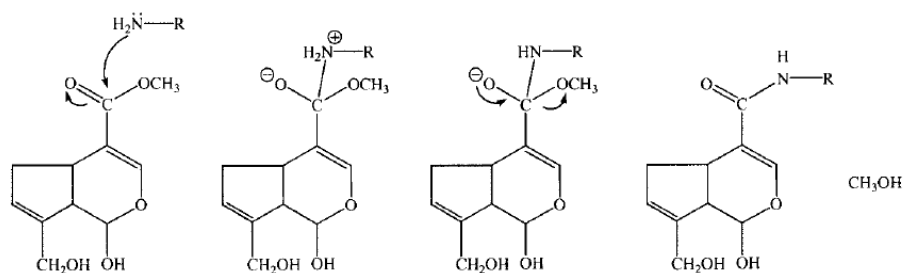
Crosslinking using GA introduces cytotoxic aldehyde groups into the scaffold [94]. These aldehyde groups remain non-specifically bound to the matrix even after exhaustive rinsing and these molecules will be released as the matrix degrades over time [94]. Moreover, heterogeneous crosslinking is often observed through the scaffold structure.

2.13.3 Genipin

Genipin is a natural crosslinking agent which is derived from geniposide found in the fruits of *Gardenia jasminoides* Ellis [9]. The geniposide is hydrolyzed with β -glucosidase to produce genipin and when genipin reacts with primary amine groups, it produces blue pigments [95]. Prior to using genipin as a crosslinking agent, it was used as a food dye.

Various groups studied the crosslinking mechanism involving genipin, Butler et al. [96] used ultraviolet-visible spectroscopy, C-NMR, protein-transfer reaction mass spectroscopy, photon correlation spectroscopy and rheology to characterize the genipin crosslinking mechanisms (Fig 12). Two crosslinking reactions that involve different sites in the genipin molecule were proposed. The first reaction involves an S_N2 nucleophilic substitution reaction that involves the replacement of the ester group on the genipin molecule by a secondary amide linkage. The second reaction results a monomer which later referred in other reports as "genipin-amino-group monomer". The free amine group initiates a nucleophilic attack on the olefinic carbon at C-3 of genipin, resulting in the opening of the dihydropyran ring and the formation of an intermediate aldehyde group. Then the genipin-amino-group monomer is formed through the new covalent bonds between the aldehyde group and the secondary amine. Butler et al. admitted that other more complex reactions also took place in order to form blue pigments, however, the polymerization reaction which leads to the blue coloration was not studied.

reaction scheme 1



reaction scheme 2

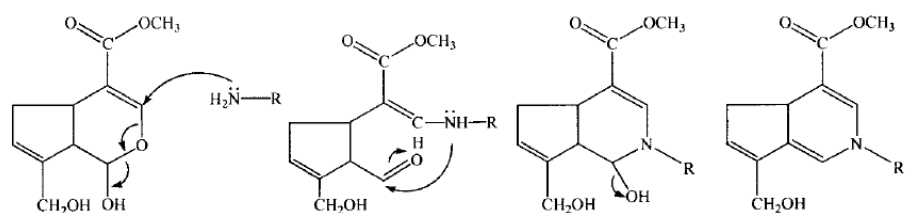


Figure 12: The two reaction mechanisms between genipin and a primary amine group, proposed by Butler et al. [96]

Chang et al. [97] crosslinked bovine jugular vein graft with genipin and they also proposed the reaction mechanism of genipin-amino-group monomer formation similar to Butler et al. based on studies by Touyama and colleagues [98]. Moreover, they proposed that dimerization occurs at the second stage by means of radical reaction. The blue-pigment polymers were presumably formed through monomer polymerization. Polymerization occurred among genipin molecules which had already reacted with free amino groups in collagen and then inter-molecular covalent bonds were formed among protein molecules (Fig 13). Finally, inter-molecular and intra-molecular crosslinks with cyclic structure were formed.

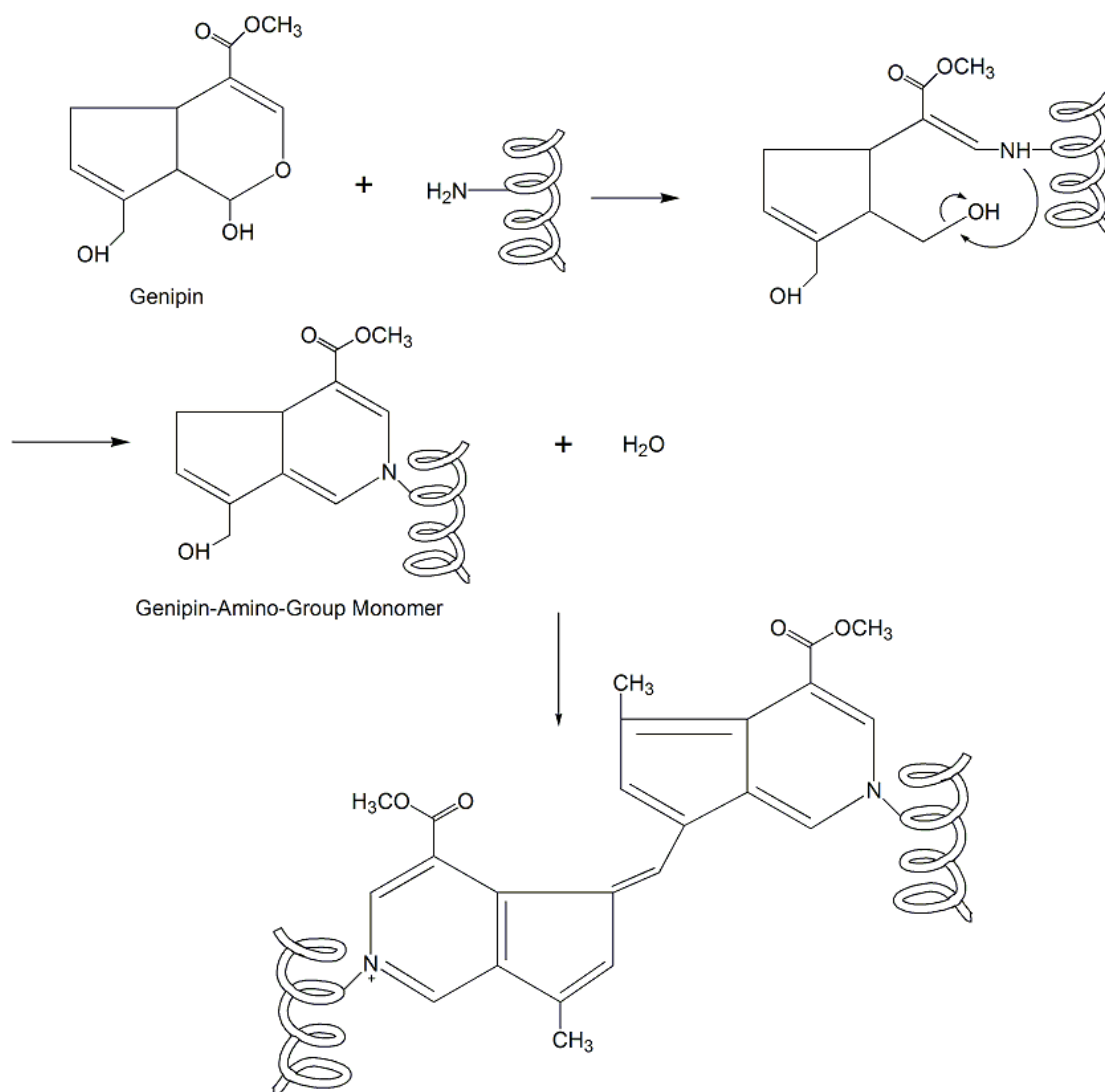


Figure 13: Schematic illustration of the intramolecular crosslinking structure of genipin crosslinks [97]

Wang et al. [99] crosslinked silk fibroin films with genipin, with formation of genipin-amino-group monomer, they proposed the blue-pigment formation through monomer polymerization at another location of the ring structure (Fig 14).

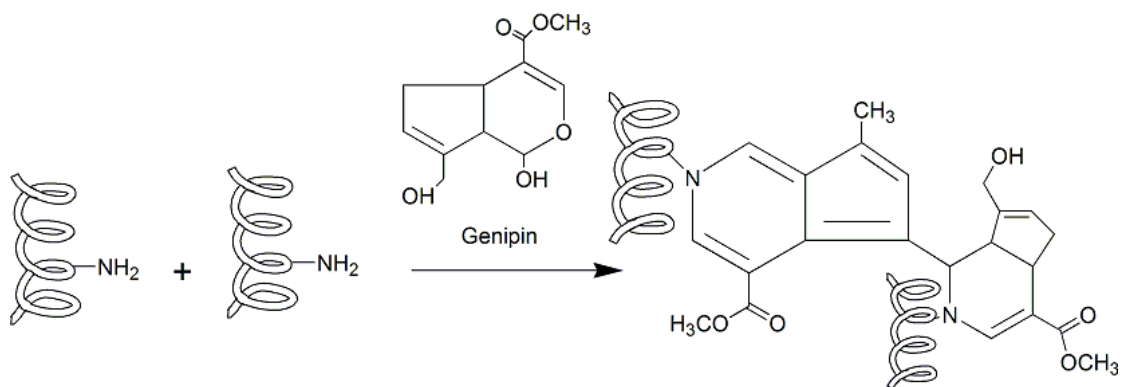


Figure 14: Formation of intermolecular chains with genipin

While most of the proposed reaction mechanism involving polymerization of the genipin-amino-group monomers, Zhu et al. [100] illustrated a reaction mechanism without monomer formation (Fig 15). Using genipin as crosslinker, covalent bonding between genipin and one amino group can be formed as illustrated in Figure 12, scheme 2. An unstable intermediate is then formed and collapses to form a tautomeric aldehyde. The resultant aldehyde group will be subsequently attacked by another amine group from collagen.

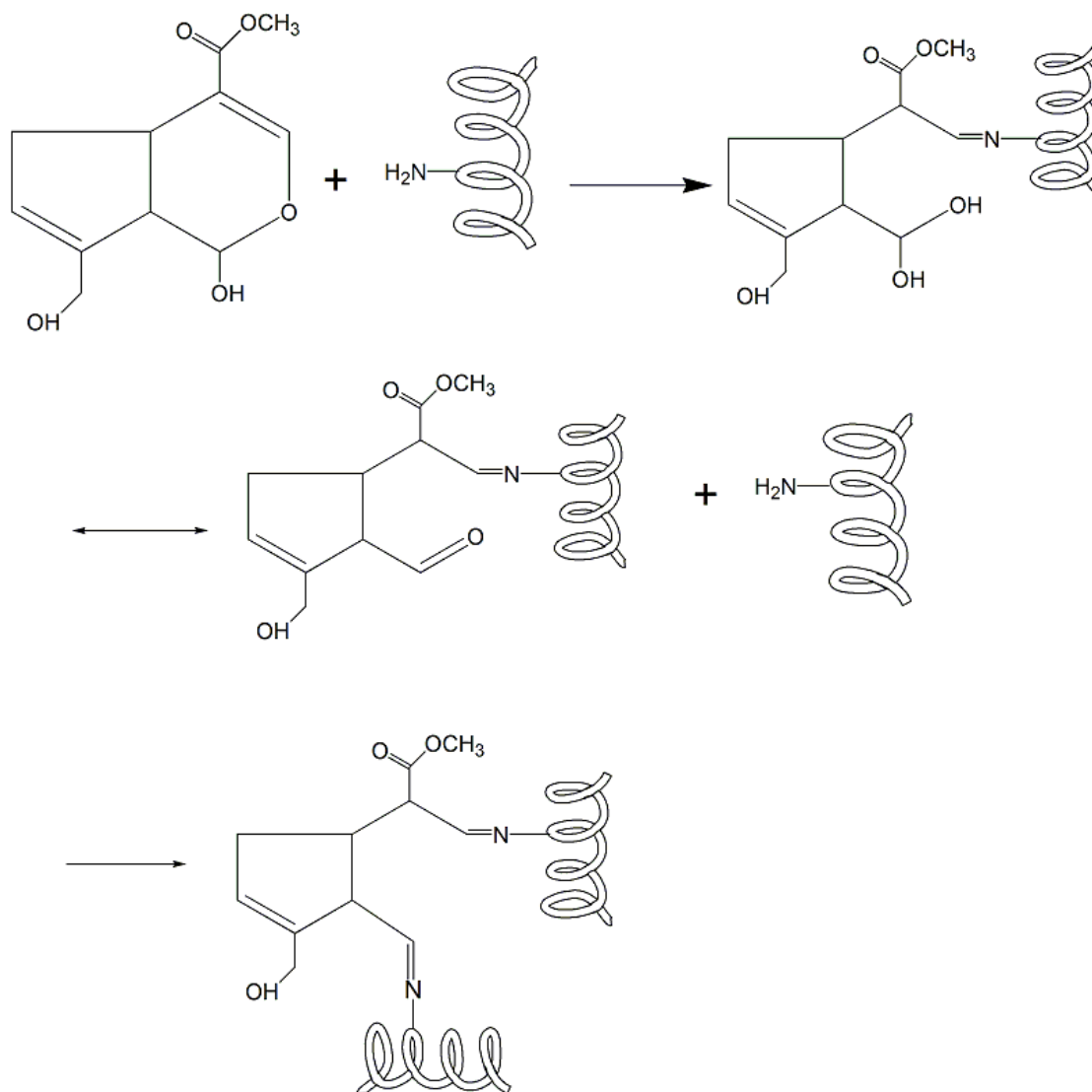


Figure 15: Reaction mechanism of genipin crosslinked collagen proposed by Zhu et al. [100]

Muzzarelli suggested that genipin reacts with chitosan to yield two main crosslinking reactions within the genipin monomer (Fig 16) [101]. Further reaction will be the homopolymerization of genipin to form polymeric genipin unit and then crosslink the chitosan along the genipin polymer. Butler et al. [96] found that the fast reaction is a nucleophilic attack of an amino group to carbon 3 of genipin and the subsequent slower reaction is a nucleophilic substitution of the ester group. Whereas Muzzarelli indicated that the crosslinking reaction mechanism for chitosan are pH controlled. Under acidic and neutral conditions, the nucleophilic attack by the amino groups of chitosan on the olefinic carbon atom at C3 occurs while under basic conditions, the

terminal aldehyde group on the polymerized genipin undergoes a Schiff reaction with the amino group on chitosan to form crosslinked networks.

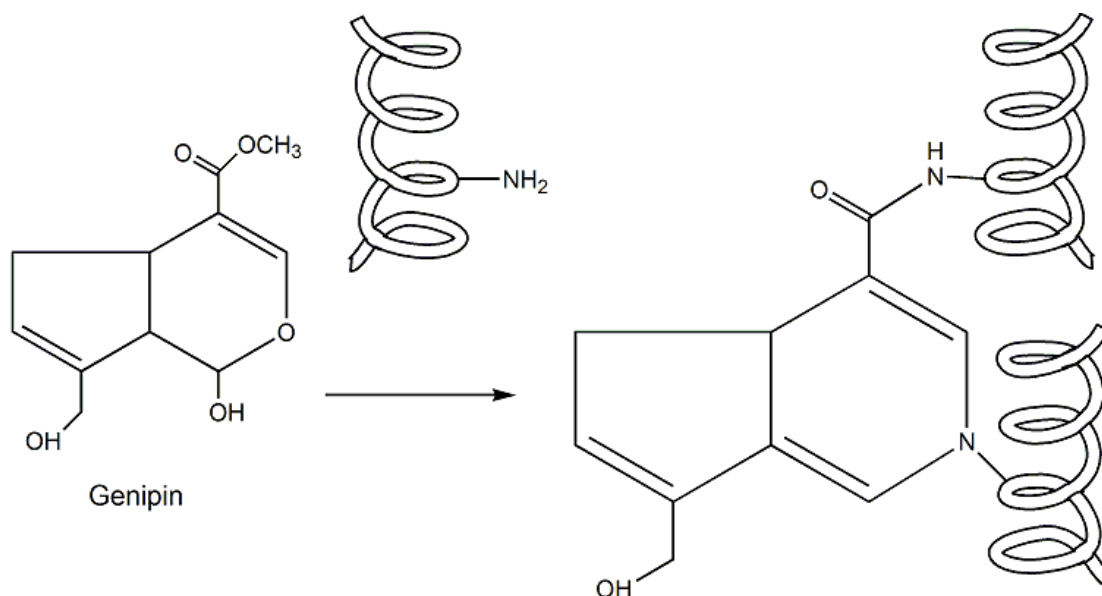


Figure 16: Genipin crosslinking mechanism proposed by Muzzareli [101]

Although various groups studied the crosslinking mechanism, it has not been understood in detail yet due to the complexity of the reaction.

Nevertheless, genipin has been shown to possess anti-inflammatory, anti-oxidative, anti-apoptotic, and anti-carcinogenic traits. And it has been shown to be approximately 10000 times less cytotoxic than GA and induced ~5000 times greater cell proliferation of mouse embryo cell line (BALB/3T3 C1A31-1-1) compared to GA [9].

Genipin crosslinking of collagen and collagen/chitosan biomimetic scaffolds showed remarkable change in morphologies and pore sizes while the swelling ratio of the scaffolds could be tailored by adjusting crosslinking treatment [9, 81].

Mekhail et al. [9] crosslinked electrospun collagen fibers with genipin under a range of experimental conditions, all fibers maintained fibrous morphologies upon exposure

to aqueous environment. By using four different conditions, scaffold porosity and fiber morphologies were all maintained, but all samples were swelled to some degree. The different degree of swelling can be achieved by changing crosslinking conditions thus further control fiber properties. Compared to fibers crosslinked by other methods, genipin crosslinked fibers possess reduced and controlled degrees of swelling.

3 Materials and Method

3.1 Materials

Type I collagen from the rat tail was isolated and purified according to the procedure developed previously (see Appendix A). Other materials are listed in Table 1.

Table 1: Materials for electrospinning and fiber characterization of core-shell collagen nanofibers

Materials	Supplier
Hexafluoroisopropanol (HFIP) (105228, 1,1,1,3,3,3-hexafluoroisopropanol)	Sigma Aldrich, Oakville, ON, Canada
Poly (ethylene glycol) (PEG) (309028, 10 kDa)	Sigma Aldrich, Oakville, ON, Canada
Alexa Fluor® 594 Albumin Bovine Serum conjugate (A13101)	Invitrogen Canada Inc, Burlington, ON, Canada
Alexa 488 Phalloidin SelectFX Nuclear Labelling Kit	Invitrogen Canada Inc, Burlington, ON, Canada
Prolong Gold Antifade Reagent	Invitrogen Canada Inc, Burlington, ON, Canada
Genipin (MW = 226.23g/mol)	Challenge Bioproduct Co
Anhydrous Ethyl Alcohol	Commercial Alcohols, Brampton, ON, Canada
Glacial acetic acid	Caledon Labs, Georgetown, ON, Canada

3.2 Isolation and purification of Type I Collagen from Rat Tails

The procedure for the isolation of type I collagen from rat tails is detailed in Appendix A. Frozen rat tails were thawed in 70% ethanol for at least 30 minutes, scapular and

forceps were used to dissect the rat tail skin and expose the white collagen fibers. The collagen fibers were removed and placed in a sterile dish. The collagen fibers were weighed and washed in 70% ethanol for 30 minutes, dried in a sterile Petri dish and UVC sterilized over night. Collagen fibers were then dissolved in 0.0175M acetic acid at 4 °C for 7 days. The solution was centrifuged at 11,000 rpm for 2 hours and the supernatant was collected. The collagen solution was stored at 4 °C or frozen at -20 °C to be lyophilized for collagen powder.

3.3 Core and shell solutions for electrospinning

3.3.1 Collagen Shell Solution

5wt% Type I collagen solution was prepared by adding 84.2 mg of lyophilized rat tail collagen into 1mL of HFIP, and vortex to dissolve the collagen.

3.3.2 Protein Core Solution

The core solution was made by first dissolving PEG into 80% ethanol to yield a final concentration of 200mg/mL. BSA-Alexa Fluor® 594 was added to the PEG-ethanol solution to obtain a final concentration of 10mg/mL. The solution was then wrapped in aluminum foil and store at 4 °C to preserve fluorescence.

3.4 Coaxial Electrospinning

Coaxial electrospinning was performed at room temperature in a custom designed humidity-controlled chamber (Fig 17). By feeding two solutions into a needle concentrically, the flow rate of each solution was controlled independently with a dual syringe pump (Model 33, Harvard Apparatus). An electric field of 0~30 kV was created by connecting a high voltage source to the custom designed stationary metal collector and the tip of the metal needle. Using an initial set of fiber spinning condition, a standard set of fiber spinning parameters was established for continuous

fibers production. For 5 wt% collagen and 10mg/mL BSA in PEG solution, an inner flow rate of 0.06 mL/hr and outer flow rate of 0.18mL/hr was used for the coaxial electrospinning system.

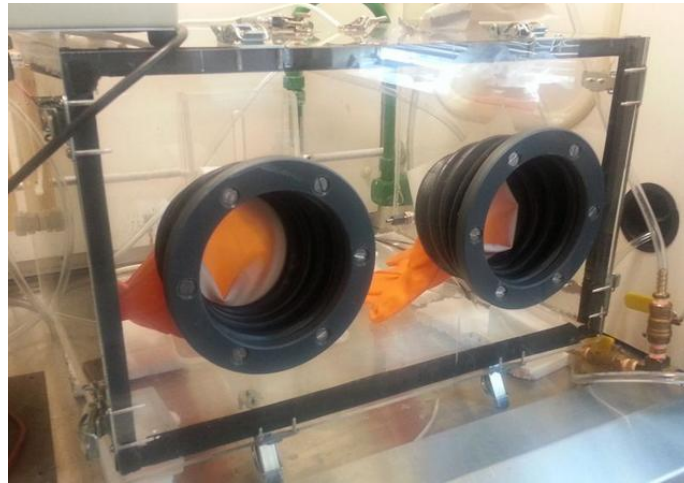


Figure 17: Humidity controlled chamber for electrospinning

Two coaxial electrospinning configurations were used to generate the nanofibers. In the horizontal electrospinning setup, the needle was placed parallel to the floor and the collector was placed perpendicular to the floor, across the needle of syringe (Fig 18). For horizontal electrospinning, the spinning distance and voltage which generates continuous fibers were 7 cm and 23 kV, respectively.



Figure 18: Horizontal coaxial electrospinning configuration

In the vertical coaxial electrospinning configuration the collector was placed 6.5cm below the needle tip with a voltage of 22kV to produce core-shell fibers (Fig 19). In both configurations the collector was chosen to be an aluminum plate.

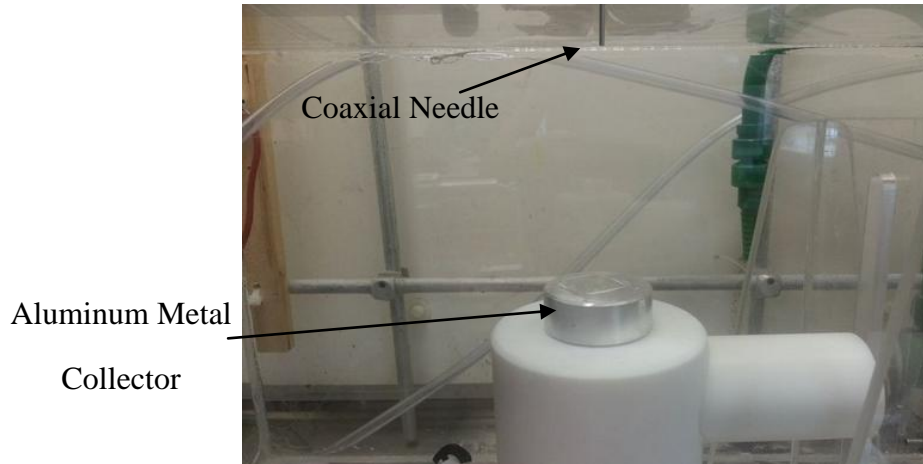


Figure 19: Vertical coaxial electrospinning setup configuration

3.5 High speed imaging

The process of electrospinning was captured and recorded with a high speed camera. Due to the differences in camera availability and quality, three different cameras were used, they were: Redlake MotionScope M with frame rate of 60 frames/second to 1000 frames/second, AOS Q-PRI camera with frame rate up to 2000 frames/second and Olympus I-speed 3 camera with a frame up to 2000 frames/second.

3.6 Genipin crosslinking

Genipin crosslinking was carried out based on the experimental procedures previously established in our lab [9]. In general, the crosslinking solution was prepared by adding genipin into 3% and 5% water in ethanol solution to reach a genipin concentration of 0.03M (~11.3 mg of genipin per mg of collagen) [102]

3.7 Resin Embedding and Ultramicrotoming

In order to characterize the cross-section of the obtained fibers, ultramicrotoming was performed to slice the fibers in to 70nm thick sections. For optimum trimming condition, the Spurr's Low Viscosity embedding mixture was chosen for its excellent penetration qualities. The hardness of the block was adjusted to "firm standard" so the blocks have good trimming and sectioning qualities. The detailed introduction and preparation instruction on the embedding media is given in Appendix B.

The crosslinked core-shell nanofibers were embedded in Spurs resin and cured at 60° C for 48 hours. The blocks were then sliced using an ultrafine diamond knife microtome. The thickness of the each slide was approximately 70nm. After collecting approximately 30 to 40 slides, a TEM grid was used to pickup these slides and the slides could then be scanned with TEM to examine the cross-section of the core-shell structure.

3.8 Characterization

3.8.1 Scanning electron microscopy (SEM)

A Leo 1530 scanning electron microscope was used to obtain images for fiber morphology and size distributions of the electrospun fibers. An accelerating voltage of 2~ 5 kV was used to generate high resolution images without damaging the samples.

3.8.2 Transmission electron microscopy (TEM)

A Philips CM 10 transmission electron microscope with a digital camera was used to obtain images of core-shell collagen fibers structure. For the side view of core-shell nanofibers' structure, collagen core-shell fibers were directly electrospun onto a TEM grid. Later, TEM was also used to image the cross-section of the core-shell nanofibers to study and verify the core-shell structure. An accelerating voltage of 60 ~80kV was

used to characterize the nanofibers.

3.8.3 Laser scanning confocal microscopy (LSCM)

A Carl Zeiss laser scanning confocal microscope (LSM-410) equipped with an Argon/He/Ne laser was used to image encapsulated fluorescent proteins and detect the auto-fluorescence of collagen to characterize the fiber structure. The excitation and emission wavelengths of Alexa Fluor ® 594 are 590 nm and 620 nm, respectively. Whereas the auto-fluorescence of collagen has an excitation wavelength around 490 and emission wavelength around 520 nm.

3.9 Image processing (Image J)

ImageJ was used to determine fiber diameter. The scale bar on the image was first measured in pixels and calibrated into actual length/pixel. The fiber diameters were then measured in pixels and converted into nanometers. For each sample, three images were acquired for each sample and forty fibers were randomly selected for each image for measurement. To measure the fiber diameter, a line was drawn on the fiber perpendicular to its axis. The length of the line was automatically converted into micrometers by the software.

3.10 Cell seeding experiments

To demonstrate the biocompatibility of the resultant core-shell PEG-BSA/collagen nanofibers and their stability in cell growth media, primary human fibroblasts were acquired and seeded on the genipin crosslinked core-shell nanofibrous scaffold. The scaffolds were first sterilized in ethanol for 30 mins, then washed thoroughly with PBS three times.

3.10.1 Cell attachment

The cell culture media in culture plates which contains fibroblasts was aspirated and the cells were washed three times with phosphate buffered saline (PBS) to remove growth factor and other nutrients that may stick to trypsin. 2mL of trypsin was added to each plate and incubate for 5 to 10 mins at 37 °C to detach cells from the bottom of the petri dish. 2mL of growth media (α MEM supplemented with 10% fetal bovine serum (FBS), glutamine and 2mM of antibacterial) was added to the plate to deactivate the trypsin. The solution containing cells was collected in a centrifuge tube and spun at 2000 rpm for 5 mins so the cells were aggregate at the bottom of the tube. All the medium was aspirated to leave all the cells at the bottom. 1 mL of growth media was added to the pellicle and pipetted up and down until a uniform solution of cells was formed. A cell count was then performed using a hemocytometer and the solution was diluted to acquire the desired cell concentration.

1mL of diluted cell solution was added into the plate and incubated at 37 °C for 72 hours. Samples were seeded with 1.2×10^5 cells/well. After 72 hours of cell seeding, growth media was sucked out and samples were rinsed with PBS by placing them on a shaker for five minutes. 1mL of 4% paraformaldehyde was added to each well and incubated for 10 mins to fix the cells.

3.10.2 Cell staining

Phalloidin staining reagent was prepared by adding 1.5mL of methanol into 300 units of Alexa 488 phalloidin. The reagent was stored in the dark to avoid photo bleaching.

Samples were washed twice with PBS and permeablized with 0.1% Triton x-100 in PBS for 5 minutes. After rinsing three times in PBS, SNIPER block background was added to the samples and incubated for 5 mins. By rinsing the samples in PBS for 2-3 mins, phalloidin mix was then used to stain the actin filament of the cytoskeleton for

15 mins. After two washes with PBS, 70 μ L of 1:300 dilute DAPI stain was used to stain the cell nucleus for 2mins in the dark. Finally, two washes with PBS were carried out and the samples were mounted onto slides with Prolong gold mounting media. All samples were left to dry overnight before imaging.

4 Results

Although the purpose of this study is to prepare electrospun core-shell BSA-PEG/collagen nanofibers that are stable in aqueous environments, it is essential to first establish the feasibility of coaxial electrospinning process and then optimize the conditions for good quality nanofibers production. Aside from a study of the process parameters such as voltage, flow rate and tip to collector distance, coaxial electrospinning was also performed in both the horizontal and vertical configuration to determine the method for best quality fiber production. For coaxial electrospinning, quality of the product was not only based on fiber diameters or morphologies, but also the uniformity in the core-shell structure.

This chapter starts with horizontal coaxial electrospinning collagen nanofibers. The parameters were adjusted to optimize the fiber morphology (Section 4.1). After the fibers were characterized with LSCM (Section 4.2) and TEM (Section 4.3), it was found that the obtained fibers did not have uniform core-shell structure. As an alternative, vertical coaxial electrospinning was performed (Section 4.4), the resultant fibers were again evaluated with TEM (Section 4.5). As the fibers collected with vertical coaxial electrospinning showed better core-shell structure, further characterization were carried out with vertical coaxial electrospun nanofibers. These fibers were crosslinked with genipin (Section 4.6) and characterized under LSCM(Section 4.7). Finally, the biocompatibility of the crosslinked nanofibers was assessed using primary human skin fibroblasts (Section 4.8).

4.1 Optimizing electrospinning process

Coaxial electrospinning setup was assembled as previously established [103]. The process was performed as shown in Fig 10, with a dual syringe pump (Harvard Apparatus, Model 33) to control the flow rate of the core and shell solution

independently. The two solutions were fed concentrically into a single metal needle tip with an 18 gauge outer needle and a 22 gauge inner needle.

During coaxial electrospinning process, experimental, environmental and solution parameters would all affect the final quality of the nanofibers, only a specific narrow range conditions allow fiber formation. The controlled variables are divided into three groups and the values which allow coaxial electrospinning in the current study are summarized in Table 2.

Table 2: Horizontal coaxial electrospinning parameters for core-shell collagen nanofibers

Parameters		Value
Solution	Concentration of collagen shell solution	5wt%
	Composition of PEG solvent	80v/v%
	Concentration of PEG solution	250mg/mL
Experimental	Flow Rate	OFT*:0.18mL/hr, IFR*:0.06mL/hr
	Voltage	19~24kV
	Needle to Collector Distance	7cm
Environmental	Humidity	~20RH%
	Temperature	~22° C

*OFR: outer shell solution flow rate. IFR: inner core solution flow rate

There are other parameters which belong to these categories that could affect the fiber formation, morphology and sizes such as solution conductivity, evaporation rate, vapor pressure, viscosity and surface tension. Some of the parameters are strongly

correlated with each other and cannot be considered as an independent parameter. For example, increasing in polymer concentration would likely increase solution viscosity, surface tension depends on ambient temperature, and humidity would affect solution evaporation rate. Due to the complication of the coaxial electrospinning process and time constraint, not all parameters can be examined, but if possible, the effect of these parameters should be considered.

The experimental parameters listed in Table 1 were varied so that no solution dripping at the tip of the needle occurred during the spinning process and the shape of the Taylor cone which was formed at the tip of the needle was maintained over time. To help to observe the Taylor cone formation and fiber movement at the tip of the needle, Redlake MotionScope M high speed camera was used to capture the Taylor cone formation and its stability. With a constant core-shell solution flow rate, the tip to collector distance and applied voltage were varied to obtain the stable Taylor cone. Figure 20 shows an image of stable Taylor cone formed at the tip of the needle.

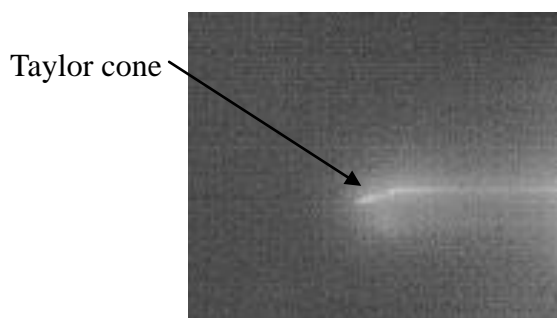


Figure 20: Redlake MotionScope M high speed camera captured stable Taylor cone formed at the tip of the needle (Horizontal configuration).

Optical images were first used to examine beadings in the fibers, then the fiber diameters were examined with scanning electron microscope (SEM).

It was found that in some cases, even if a stable Taylor cone was formed the Taylor cone would increase in size and became distorted due to gravitational force (Fig . 21a).

Even with the distorted Taylor cone, nanofibers can still be formed (Fig 21 b).

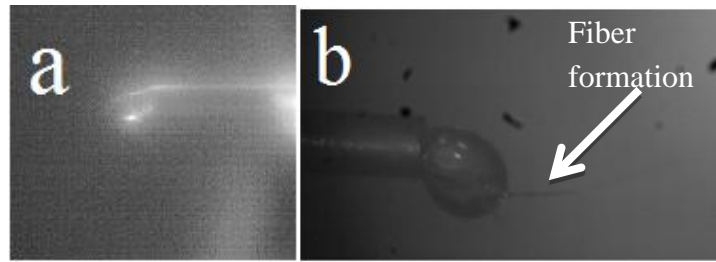


Figure 21: Distorted Taylor cone due to gravitational force and extended coaxial electrospinning

4.1.1 Effect of voltage on fiber diameter

Coaxial electrospun collagen nanofibers were collected with conditions listed in Table 1. The average diameters of the nanofibers are plotted in Figure 23. The fibers have a non-woven structure with smooth morphology (Fig 22). The potentials which allow fiber formation ranged from 19kV to 24 kV, lower voltage resulted in droplet dripping, while higher voltage resulted in unstable coaxial electrospinning process.

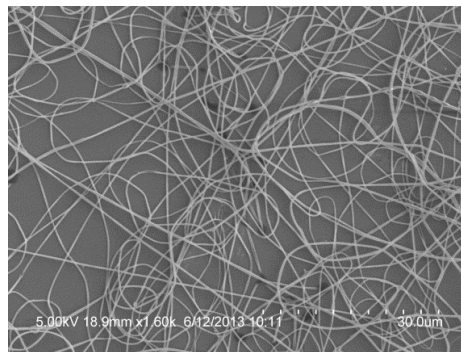
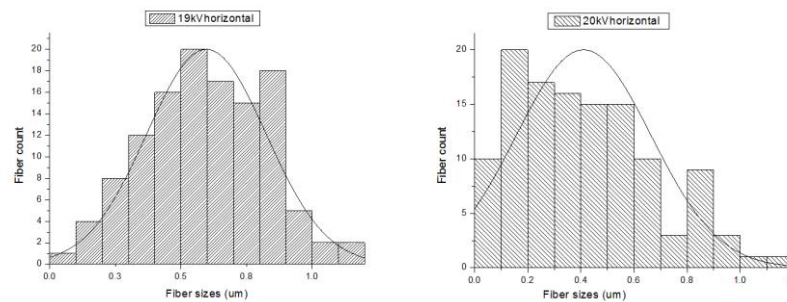


Figure 22: SEM image of horizontal coaxial electrospun collagen nanofibers at 22kV, 7cm



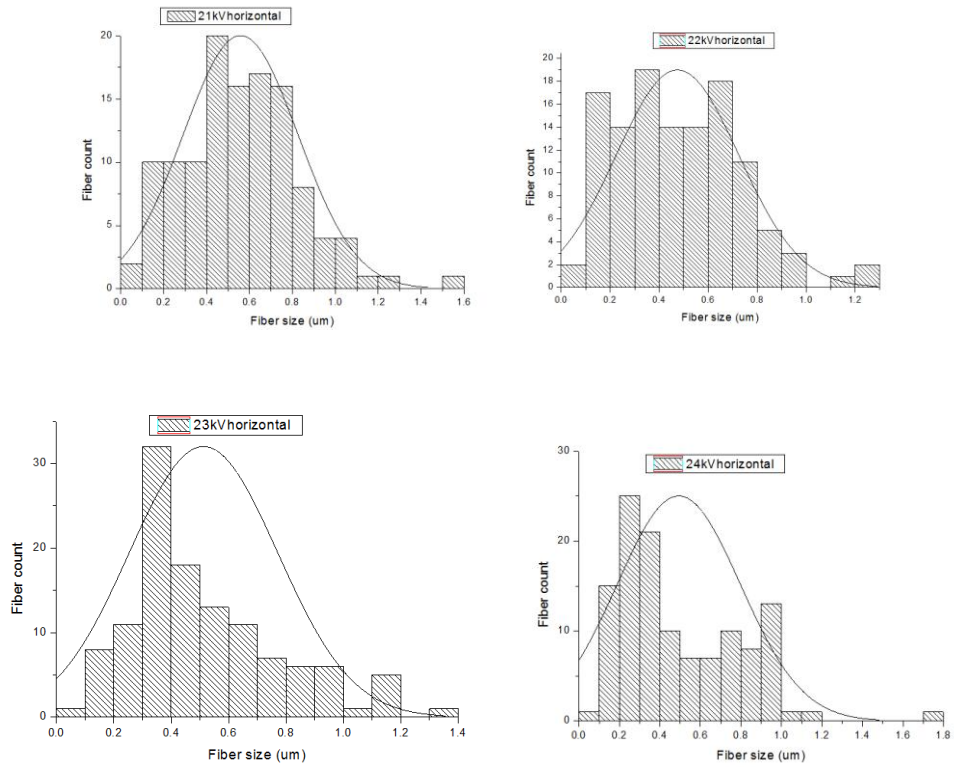


Figure 23: Histogram of horizontal coaxial electrospun collagen nanofiber size distribution obtained at six applied voltages with 7cm tip-to-collector distance.

The fibers had diameters ranged from 20nm to $\sim 1.2\mu\text{m}$ in most samples at 19kV to 24kV (Fig 23). The average fiber diameter was determined from three samples obtained at each condition, 40 fibers were randomly measured in each sample (Table 3). With a normal function fit, most of the histograms do not fit to the normal distribution. Figure 24 shows the average fiber size vs. applied voltage, no specific correlation can be obtained between fiber diameter and applied voltages .

Table 3: Average fiber size vs. applied voltage for horizontal coaxial electrospinning

Applied Voltage (kV)	Average Fiber Size (nm)	Standard Deviation (nm)
19	555.2	113.7
20	508.9	136.6
21	555.5	128.5

22	471.2	126.1
23	501.9	135.6
24	547.9	159.8

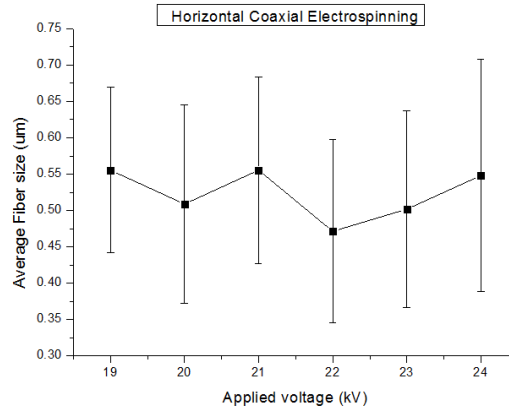


Figure 24: Average fiber size at applied voltage between 19kV to 25kV with a tip-to-collector distance of 7cm

4.1.2 Effect of other experimental parameters

The tip-to-collector distance determines the flight time of the fiber in the whipping process. A longer distance extends the flight time of the fibers and the greater stretch of the polymeric jet would result in thinner fibers. Therefore, a smaller fiber diameter is expected at increase tip-to-collector distance. As we were aiming to make nanofibers with small diameter, the tip-to-collector distance was increased. However, with a 0.5cm increase in tip-to-collector distance, the minimum applied voltage which allows the droplet deforming into Taylor cone starts at ~24kV. Further increase in tip-to-collector distance would further increase the potential for fiber formation. Since the maximum voltage that the power supply can achieve is 30kV, no systematic study on the effect of tip-to-collector distance on fiber diameter can be acquired.

The OFR and IFR used in this study were based on the previous research on core-shell collagen nanofibers [103]. The 1:3 ratio of core-shell solution flow rate

worked well for making nanofibers, slight deviation of this ratio also allowed fiber formation (e.g. OFR:0.175~0.185 mL/hr, IFR: 0.055~0.06mL/hr), further change in flow rate ratio or rate resulted in solution dripping or electrospaying of collagen beads. Faster core-shell solution flow rate were tried out with the 3:1 OFR:IFR ratio (e.g. OFR:0.3mL/hr, IFR: 0.1mL/hr), but fibers showed beads-on-string morphology (Fig. 25). Thus, all the experiments were done at a constant flow rate with 3:1 OFR:IFR ratio.

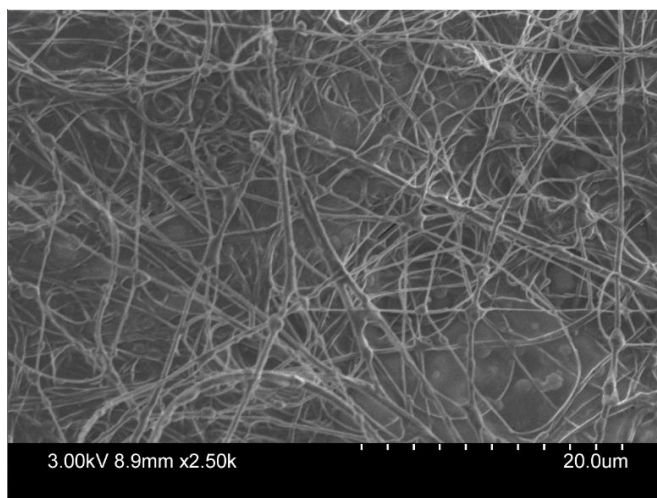


Figure 25: Coaxial electrospun collagen nanofibers with increased flow rate (OFR:0.3mL/hr, IFR: 0.1mL/hr) and yielded beads-on-string morphology fiber

4.1.3 Effect of solution parameters

The concentration and molecular weight of the polymer solution play an important role in the resulting fiber formation and size distribution. The 5wt% collagen shell concentration, which allows fiber formation, was established previously [103]. Study on collagen nanofibers also indicated that reduced collagen solution concentration would produce beaded fibers or fiber breakup [9]. Due to the scarcity of rat tail collagen, the minimum collagen concentration which allows smooth fiber formation (i.e. 5wt%) was used.

Poly(ethylene) glycol (PEG) solution was used as a carrier for the BSA protein, to

ensure rapid solvent evaporation so that dry fibers could be formed, ethanol-water mixture was used. However, with an ethanol concentration above 90v/v%, not all PEG can be completely dissolved, while reducing ethanol concentration may decrease solvent evaporation rate. 80v/v% ethanol was chosen to dissolve PEG while ensuring fast solvent evaporation.

PEG solutions with different concentrations were prepared for coaxial electrospinning. PEG concentration of 200mg/mL was established previously [103], decreasing the concentration prevented fiber formation, while increasing the PEG concentration to 300mg/mL interrupted the fiber spinning process. 200mg/mL and 250mg/mL PEG concentration produced stable Taylor cone; however, some samples collected with 200mg/mL PEG concentration showed flattened ribbon-like morphology rather than round smooth fibers (Fig 26). Therefore, fiber collected in this study had the fluorescently tagged protein suspended in a core PEG solution with a concentration of 250mg/mL.

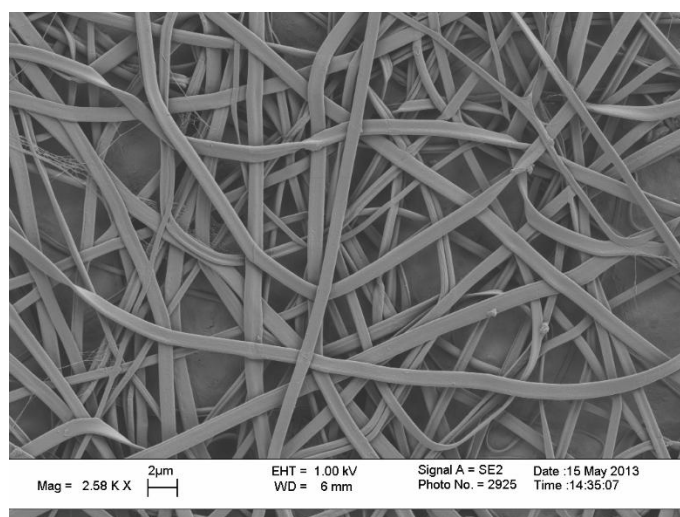


Figure 26: Flattened ribbon-like collagen nanofibers were collected with PEG core concentration of 200mg/mL

4.1.4 Effect of environmental parameters

The solvent in the whipping jet must be fully evaporated during the flight time between the tip to collector. To ensure the fiber is completely dried when it reaches the collector, not only a high vapor pressure is needed for the solution, the ambient humidity must be relatively low. At room temperature ($\sim 22\text{ }^{\circ}\text{C}$), a humidity chamber was used to control the relative humidity in the electrospinning environment at $\sim 20\%$. It was found that collagen fibers can only be formed with RH% less than 30%, high RH% either resulted in solution dripping or unstable coaxial electrospinning.

In order to better observe the stable Taylor cone, halogen lamps were used to light up the humidity control chamber for high speed image capture. However, it was found that with the heat generated from halogen lamps, the temperature inside the humidity controlled chamber would increase rapidly and dramatically ($\sim 1\text{ }^{\circ}\text{C}$ per 30 seconds). The increased temperature not only changed the relative humidity level in the chamber, but also the surface tension of the droplet at the tip of the needle (Fig 27). As a result, the Taylor cone distorted severely due to gravitational force and changes in surface tension.

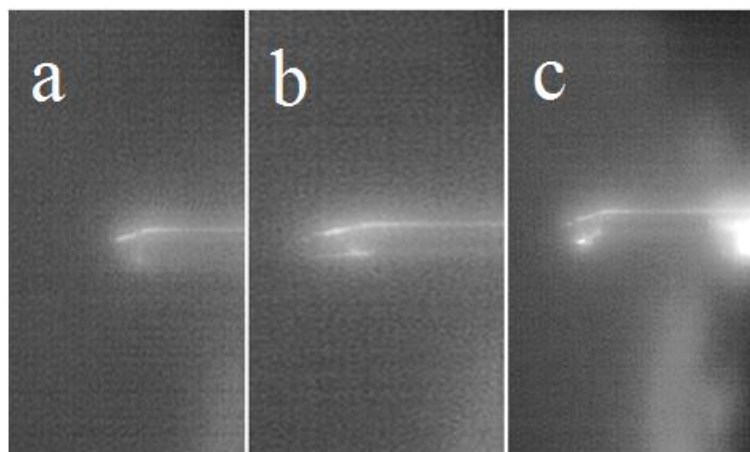


Figure 27: Distorted Taylor cone during electrospinning with increased temperature (a: 22°C , b: 29°C , c: 34°C)

The increased temperature caused Taylor cone distortion and the electrospinning

process was interrupted with fibers ejected intermittently (Fig 28). The fibers would eject out when there is sufficient solution accumulated at the tip of the needle. After the droplet size reduced with ejected stream, the coaxial electrospinning process would stop. The ejecting process would start again when enough solution is accumulated at the tip of the needle. To ensure all the samples were collected in a controlled environment, fibers were collected by turning off the halogen lamp and waiting until the temperature dropped back to $\sim 22\text{ }^{\circ}\text{C}$. Later, the halogen lamp were only switched on during the 2 seconds of high speed recording to minimize the heating radiation from the lamp.

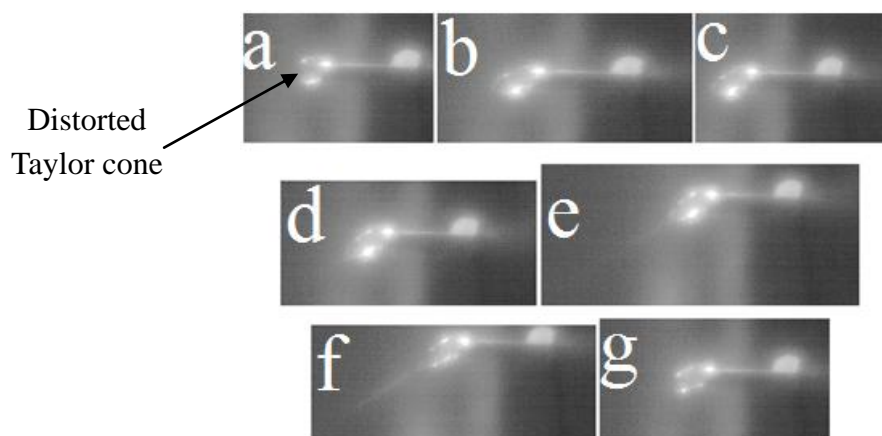


Figure 28: At 34°C , fiber ejected out brokenly from the Taylor cone. a: suspended droplet with no applied electric field, b,c,d: with applied electric field, droplet distorted due to both electrostatic force and gravitational force, e,f: fiber shooting out from tip of the distorted Taylor cone, g: after solution being carried out by the fiber, droplet size reduced and electrospinning process stopped. Same process would continue with increasing droplet size due to continuous solution pumping (the series images were screen captured from a high speed video, the spinning process from first to last image took about 0.2s)

4.2 Protein encapsulation of the core-shell collagen nanofibers

Samples prepared using optimized preparation conditions were imaged using LSCM to verify the encapsulation of the fluorescently tagged protein. Results are shown in Figure 29.

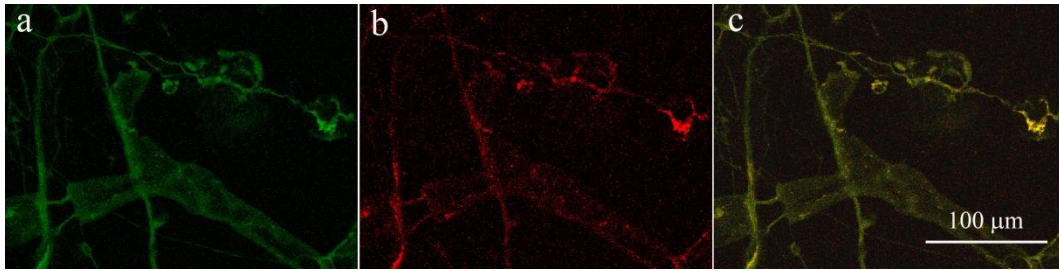


Figure 29: Confocal images of as-prepared electrospun core-shell BSA-PEG/collagen nanofibers: a) auto-fluorescence of collagen; b) fluorescent-labelled BSA-Alexa Fluoro 594 in the core material; c) overlaid image of collagen and BSA-Alexa Fluoro 594 fluorescence

The as-spun collagen nanofibers auto-fluorescence green (Fig 29a), BSA tagged with Alexa Fluoro 594 which fluoresces in red was chosen to avoid the auto-fluorescent emission range of collagen, so the signal of the core protein can be differentiated. Although Figure 29b does indicate presence of the core protein in the fiber, the detailed structure of the core and shell boundary cannot be distinguished. Another important observation was that core protein signal was really dim, probably caused by the presence of the shell layer that scattered the light emitted by the core protein. TEM images were then taken to study the core-shell structure. Figure 29c is the overlay of 29a and 29b which indicates the co-localization of both collagen fiber and fluorescent-tagged BSA.

4.3 Core-shell structure of the collagen nanofibers

The TEM images on the smooth core-shell PEG-BSA/collagen nanofibers produced under optimized conditions revealed an apparent core-shell structure in some of the fibers (Fig 30).

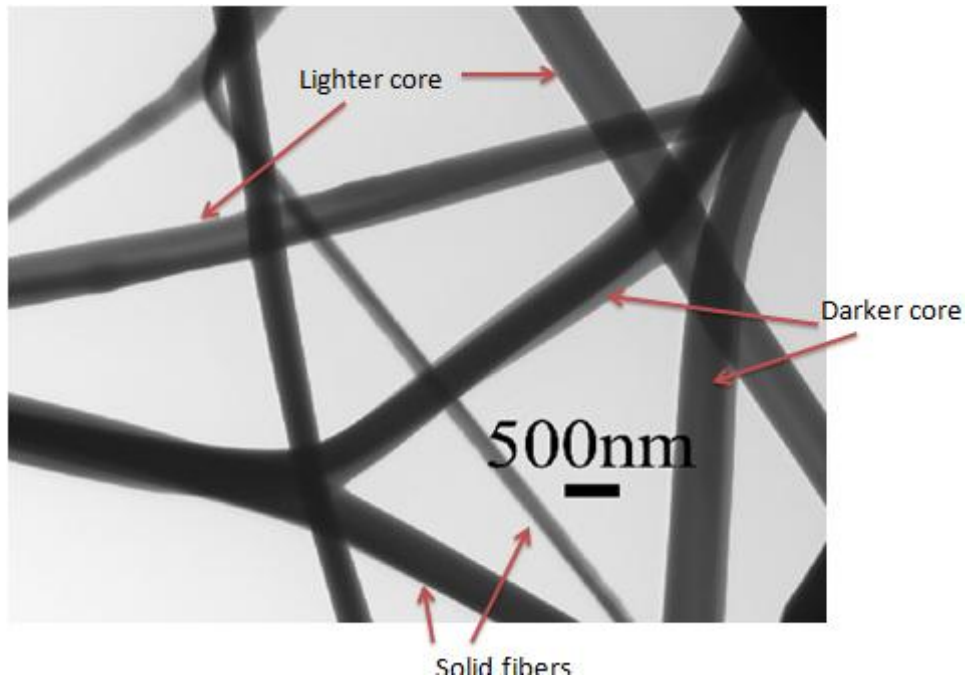


Figure 30: TEM on core-shell collagen nanofibers. The dark core and light shell in some of the fibers indicates the difference in electron transmission ability with the core shell material

However, if the dark core represents one material and lighter shell represents the other, there are cases where the dark centre and light edge reversed into dark edge and light centre fibers (Fig 31, 32). The reverse contrast of the dark and light region suggested that the fiber core-shell structure was not uniform throughout the sample.

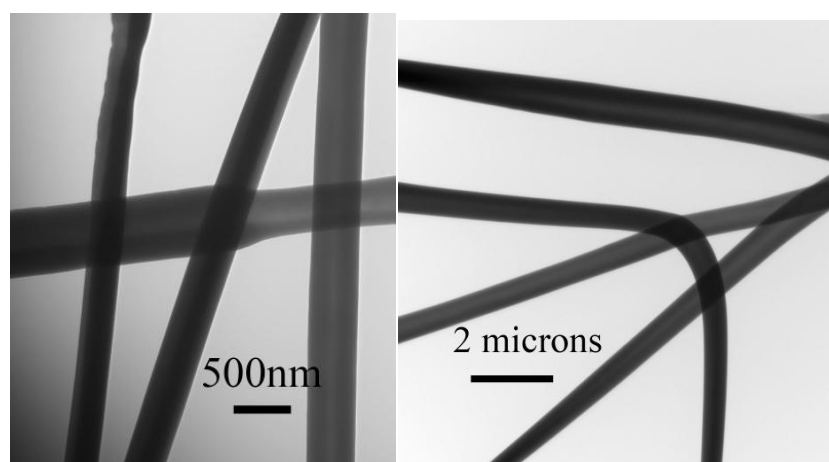


Figure 31: TEM on core-shell collagen nanofibers. There are fibers with dark core light shell and fibers with dark shell light core

In some cases, by looking along the fiber, the structure of the fiber would transformed from one to another. In Figure 32, the fiber across the centre of the image had darker core lighter shell structure at the left side, as moving along the fiber to the right, the fiber showed darker shell and lighter core. The interchange of fiber core-shell structure indicated possible materials mixing and diffusion during the electrospinning process.

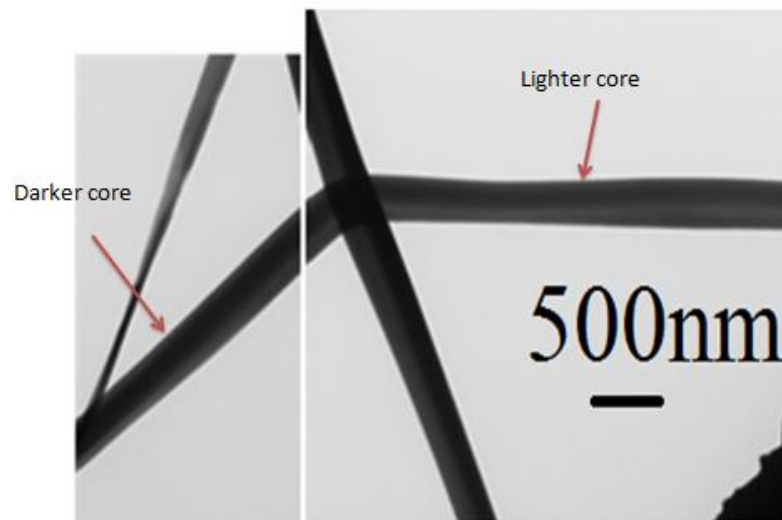


Figure 32: Non-uniform distribution of core-shell material along the nanofiber. The fiber showed dark core light shell at the left side of the image while evolving into dark shell lighter core as moving to the right side

Hypothetically, three types of structures are possible when using two types solutions in electrospinning (Fig 33): core-shell structures which is expected from the process; solid fibers formed by either the core or shell solution; or composite fibers resulting from mixture of the core-shell solutions.

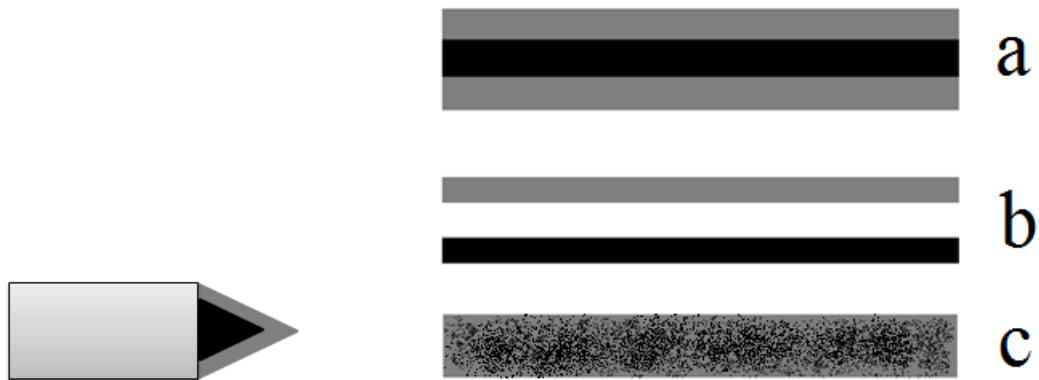


Figure 33: Three possible types of resultant fiber structure:(a)core-shell structure, (b)separate core fibers and shell fibers, and (c) composite fibers from blended mixture

If the fibers can be cut open to look at its cross-section, then the difference in core-shell contrast should be more pronounced. However, the as-spun collagen nanofibers were extremely unstable and disintegrated immediately in aqueous environment, so the fibers were first crosslinked with genipin and then embedded in Spurr's resin for ultra-microtoming. The cross-section of the nanofibers were imaged with TEM.

In Figure 34, by observing the cross-section of these core-shell nanofibers, both the shell edge and centre present dark intense regions. The difference between the dark and light region reflect the difference in electron transmission ability, if the dark region represents one material and the light region represents the other, there is a high degree of material mixing in the structure. This uneven mixing can explain the non-uniform distribution of core-shell structure in the horizontal coaxial electrospinning nanofibers.

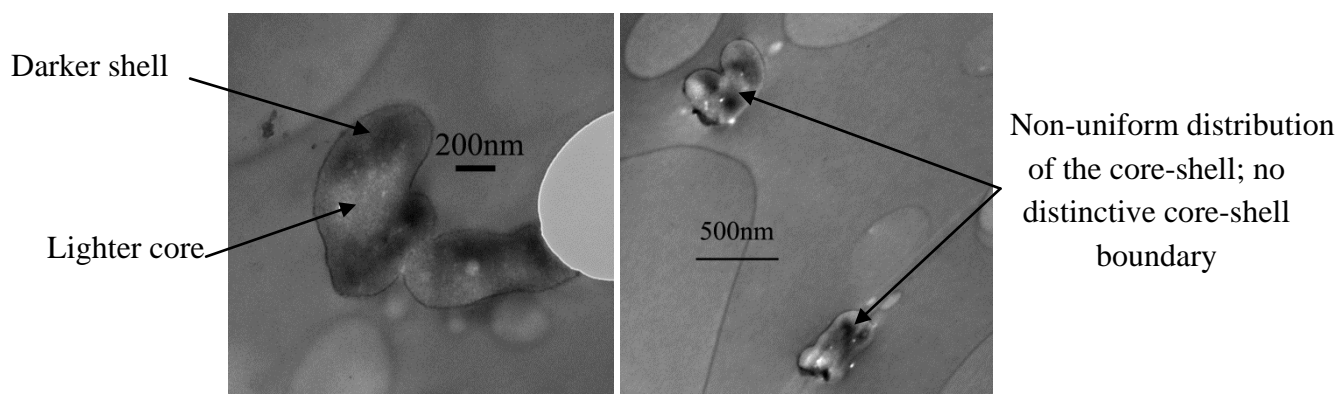


Figure 34: Non-uniform distribution of cross-section of core-shell material from horizontal coaxial electrospinning, both the edge and centre of the fiber display dark regions

These results indicated that the current coaxial electrospinning was not performed at a steady state. Sun et al. [46] claimed that no diffusion should take place between the core and shell solution as the electrospinning process was so fast and fiber drawing ratio was high enough to prevent core-shell material diffusion. From current study, there is some degree of core-shell diffusion and mixing resulting non-uniform material distribution.

Since coaxial electrospinning has been widely studied over the past a few years, a further review of the literature [6, 51, 73, 53] revealed that most of the coaxial electrospinning was performed in a vertical configuration. This could allow the compound core-shell droplet formed above the collecting electrode and the fibers, which were ejected from the Taylor cone, whipped and travelled along the direction of gravitational force. In this way, the droplet distortion due to gravity can be eliminated.

With this reasoning, we proceeded to investigate core-shell fiber preparation by electrospinning in the vertical configuration.

4.4 Optimizing the vertical coaxial electrospinning process

With the switch to vertical coaxial electrospinning, all the experimental parameters

must be readjusted to optimize the fiber morphology. As the custom-designed humidity controlled chamber was only compatible with horizontal coaxial electrospinning configuration, vertical coaxial electrospinning was carried out in fumehood. In comparison with horizontal coaxial electrospinning, the humidity cannot be precisely controlled and the air flow velocity in the fumehood should also be considered as an environmental parameter. The solution parameters were exactly the same in horizontal and vertical coaxial electrospinning. For the purpose of comparison, other coaxial electrospinning parameters were adjusted based on the values used in horizontal coaxial electrospinning. The parameters for vertical coaxial electrospinning collagen nanofibers are summarized in Table 4.

High speed cameras were also used to capture the deformation of Taylor cone and due to high speed camera's availability, AOS Q-PRI and Olympus I-speed 3 were used for vertical coaxial electrospinning imaging.

Table 4: Vertical coaxial electrospinning parameters for core-shell collagen nanofibers

Parameters		Value
Solution	Concentration of collagen shell solution	5wt%
	Composition of PEG solvent	80v/v%
	Concentration of PEG solution	250mg/mL
Experimental	Flow Rate	OFT*:0.18mL/hr, IFR*:0.06mL/hr
	Voltage	22~23kV
	Needle to Collector Distance	6.5cm

Environmental	Humidity	~30 RH%
	Temperature	~22° C
	Air velocity (100fpm)	0.508m/s

OFT: outer shell solution flow rate; IFT: inner core solution flow rate

For vertical electrospinning, the gravitational force act along the fiber drawing direction. Even if there was solution accumulated at the tip of the needle, the gravitational force would reinforce the electrostatic force to pull the extra solution out until the size of the droplet is reduced (Fig 35). For steady state condition, the overall shape of the droplet and Taylor cone would not change over time (Fig 36). The Taylor cone was easily obtained with vertical coaxial electrospinning and there was barely any change in droplet shape during vertical coaxial electrospinning process.

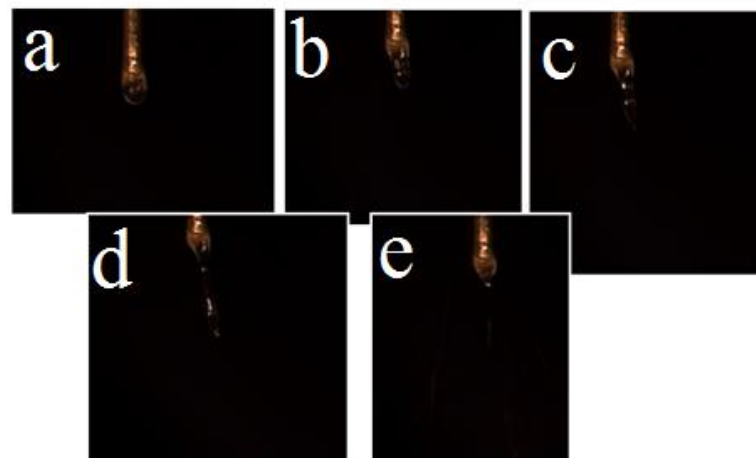


Figure 35: Electrostatic force and gravitational force act together to pull out extra solution from the increased-size droplet to form Taylor cone (Captured with AOS-QPRI camera) a: solution accumulated at the tip of the needle, b: Taylor cone distorted due to applied electric field, c,d: stream ejecting from the apex of the Taylor cone, e: Taylor cone size reduced to stable Taylor cone

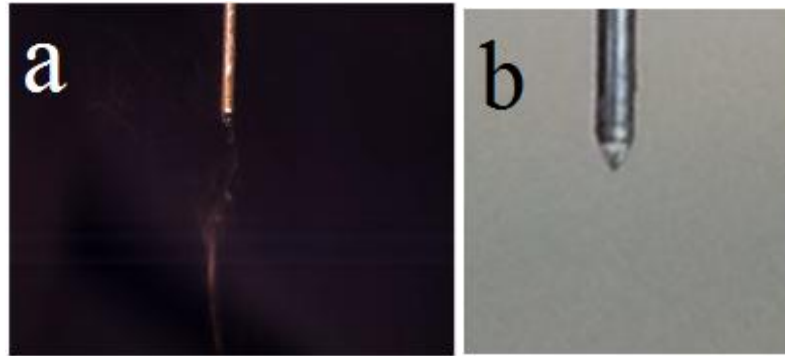


Figure 36: Stable Taylor cone with continuous fiber drawing, no solution dripping, no change in Taylor cone size and shape a: focus on the fibers (Captured with Olympus I-speed 3 camera) b: focus on the Taylor cone

4.4.1 Effect of voltage and tip-to-collector distance on fiber morphology

The tip-to-collector distance was first kept at 7cm to be consistent with horizontal coaxial electrospinning. The voltages were also varied between 19 to 24 kV; however, even with the formation of stable Taylor cone, dripping and beading in fibers still occurred. At 19kV, even though the Taylor cone seemed to be stable, only droplets with scattered fibers were formed. With an increase in voltage, there were slightly more fibers forming, but the coaxial electrospinning process was rather difficult and a lot of collagen droplets were collected on the substrate (Fig 37).

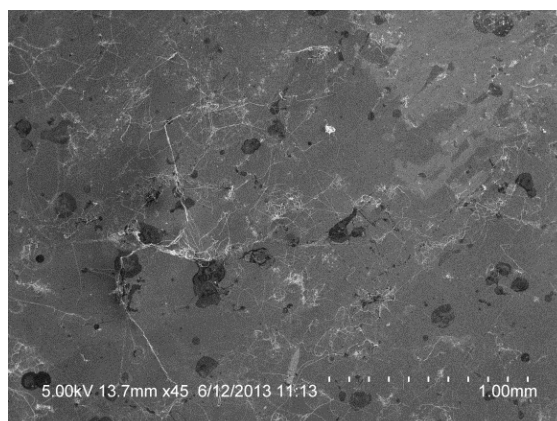


Figure 37: SEM image on vertical coaxial electrospinning at 7cm, not much fiber can be collected with solution mostly dripped onto the substrate.

None of the samples obtained at 7cm had "free of droplet" conditions and the tip-to-collector distance was then adjusted until smooth fibers were produced.

The optimum condition for making nanofibers with vertical configuration was at 6.5cm, 22~23kV. After collecting droplets at 20~20.5 kV (Fig 38) and fiber/droplet mixture at 21~21.5kV (Fig 39), no beading fibers were collected at around 22~23kV (Fig 40). Droplet at the tip of the needle kept increasing in size without formation of fibers when voltage was at or below 19.5kV, while at voltage above 24kV Taylor cone cannot be formed.

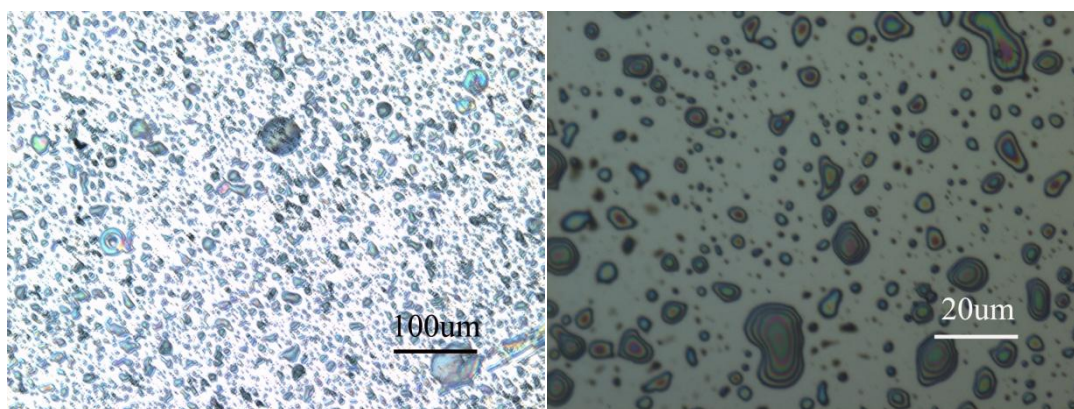


Figure 38: Coaxial electrospaying with droplets formation

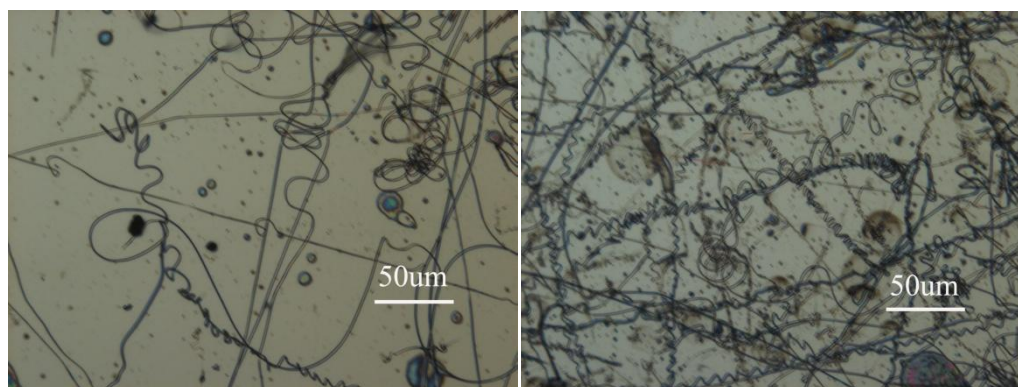


Figure 39: Coaxial electrospinning produced combination of fiber and droplets

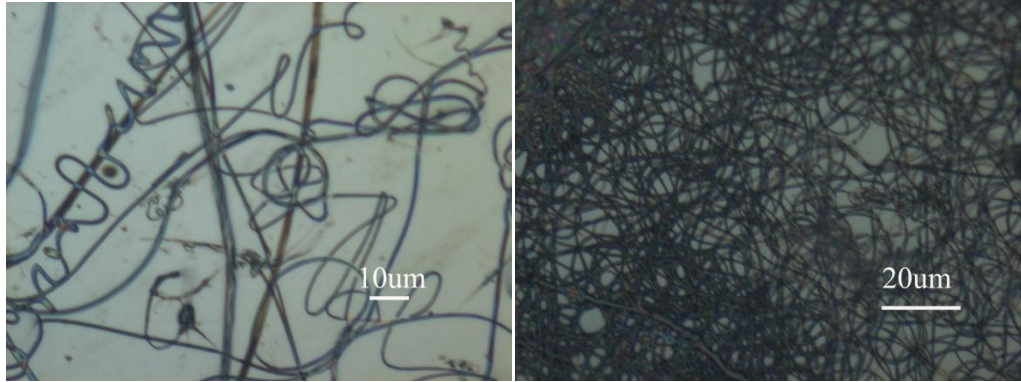


Figure 40: Stable coaxial electrospinning result smooth nanofibers with no droplet or beads
 The smooth nanofibers with no droplet or beads were used for further characterization.
 The fiber diameter distributions under optimal conditions are plotted in Figure 41.

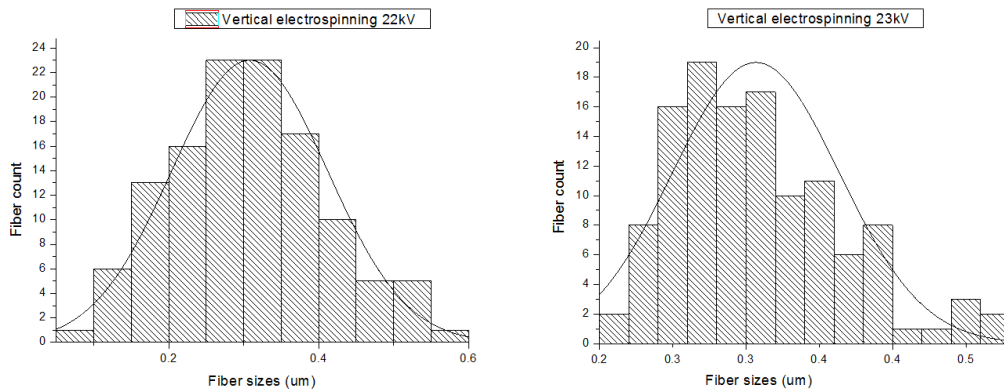


Figure 41: Histogram of fiber size distribution collected with optimum range using vertical coaxial electrospinning (fitted with normal function)

Table 5: Average fiber size for vertical coaxial electrospinning

Voltage (kV)	Average Fiber Size (nm)	Standard Deviation (nm)
22	306.52	96.01
23	291.53	56.90

Although the applied voltage which allowed fiber formation falls into a narrow range, the nanofibers collected with the optimum conditions also had narrow size

distribution with smaller average fiber diameter (Table 5).

4.4.2 Effect of environmental parameters

By placing the vertical coaxial electrospinning setup in the fumehood, the humidity control chamber can no longer be used. Without the control of humidity, nanofibers were collected only when the humidity level was low. An important observation was when the relative humidity was above 30% or the temperature was above 24 °C, the vertical coaxial electrospinning process became unstable. Also, the fumehood, where the coaxial electrospinning setup was located, has a face velocity of 100 fpm. With the upward air flow, the nanofibers would sometime whipped upward and deposited on the needle (Fig. 42). This upward whipping motion of the fibers was not observed for horizontal coaxial electrospinning.

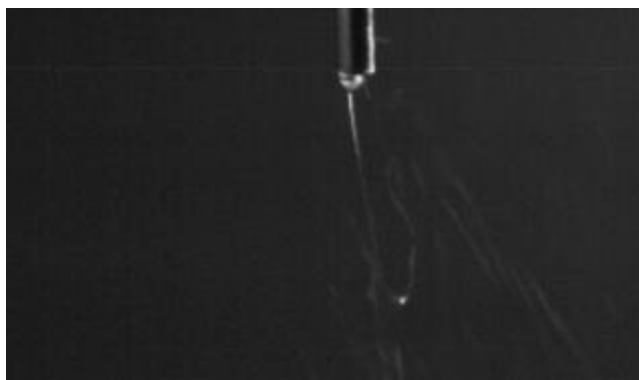


Figure 42: For vertical coaxial electrospinning, nanofibers whipped upward with fumehood air and stuck to the needle. (Image was captured with AOS Q-PRI camera)

4.5 The core-shell structure of the vertical coaxial electrospun nanofibers

The TEM images on the smooth core-shell PEG-BSA/collagen nanofibers produced with optimized conditions via vertical coaxial electrospinning are shown in Figure 36. Compared to the TEM images obtained from horizontal coaxial electrospinning, vertical coaxial electrospinning produced fibers with higher percentage of core-shell

structure and more uniform structure.

Among the fibers characterized under TEM, ~ 60% fibers resembled core-shell structure along the fiber line. The rest of fibers' structure could not be identified, either because the fibers were too thick for electron penetration or fibers were immediately damaged with high energy electrons. The sharp boundaries in the TEM images essentially reflected the difference of electron transmission ability between the core and shell materials. However, there were also cases of non-uniform distribution of the inner component just as what had been seen in horizontal coaxial electrospinning (Fig 43). The dark core was not always at the center, rather it moved along the fiber close to the surface.

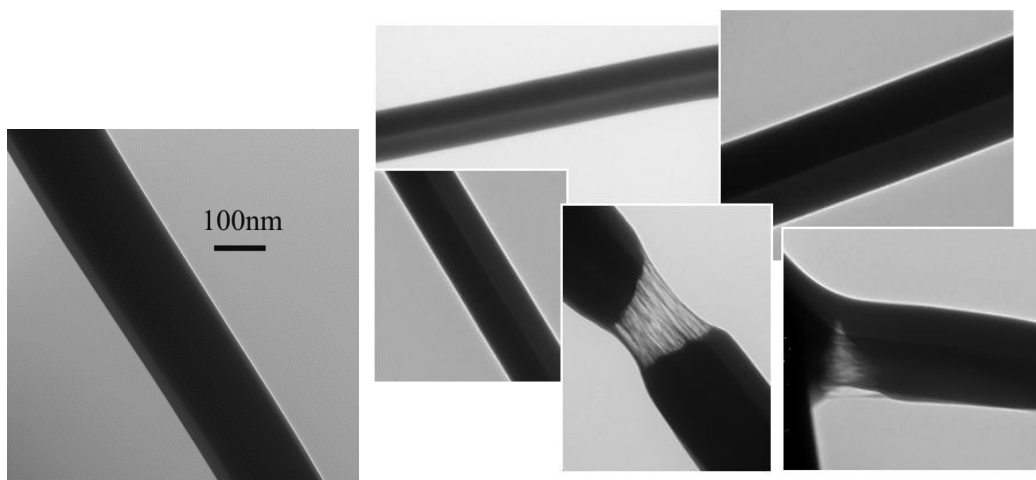


Figure 43: Dark core structure close to the surface of the fiber, thick fiber breakage allows observation of the core-shell structure

Indeed, the core-shell structure might not be perfectly concentric, probably due to the whipping motion of the nanofibers. If the core structure touches the shell surface, by viewing the structure via two directions as illustrated in Figure 44, two structures can be obtained. Dark core is located at the centre of the structure by viewing through direction 1 and the core structure touching the surface can be imaged via direction 2.

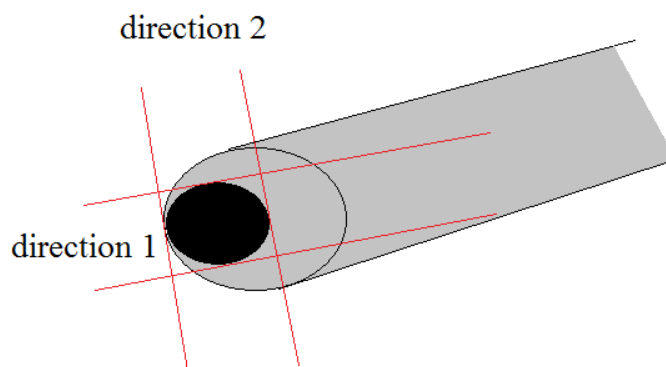


Figure 44: Looking at the core-shell structure via two directions. Direction 1: dark core at the centre, direction 2: dark core close to the surface

Even with the nanofibers which their core-shell structure could be observed under TEM, the thickness of the shell structure could not be accurately determined. It was interesting to find that for fibers which were damaged by electrons, the core-shell structure was even more evidently shown (Fig 43). Fibers which were too thick for electron penetration, their core-shell structure could be observed at the location of fiber breakage. Thus the core-shell structure of the thick fibers could be observed under TEM. Cross-section of the core-shell nanofibers might give more information of the core-shell structure of the vertical coaxial electrospun fibers (Fig 45). Again, since the as-spun nanofibers were unstable in embedding resin, the nanofibers were first crosslinked, followed by resin embedding and microtoming.

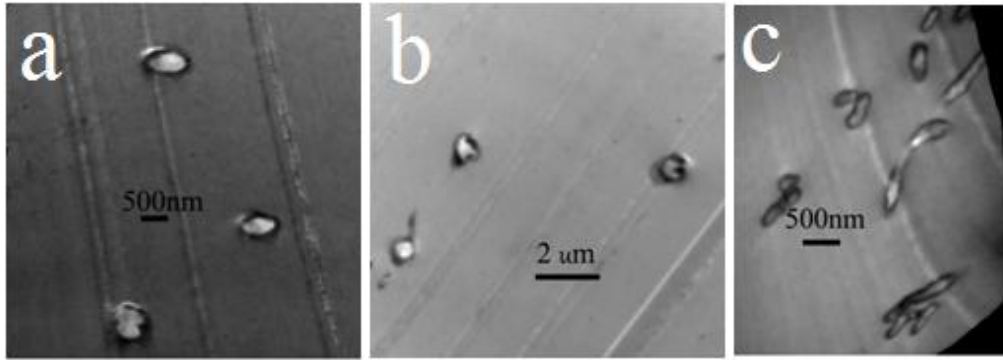


Figure 45: TEM images on the cross-section of the vertical coaxial electrospinning nanofibers

Compared to the cross-section obtained from horizontal electrospinning, vertical coaxial electrospinning resulted in fibers with dark regions at the edge and lighter region in the centre. The light region is the result of poly(ethylene) glycol and the dark region represents collagen protein. Although in some cases, the uneven distribution of core-shell material can still be seen, most of the cross-section remains dark edge and light core. The difference in shape of the cross-section is caused by the random cutting of the randomly deposited nanofibers. If the ultra-microtoming section is at right angle across the fiber, regular round structure can be obtained (Fig 46 a) . If the fibers were cut along the fiber, then elliptical irregular shapes were observed (Fig 46 b).

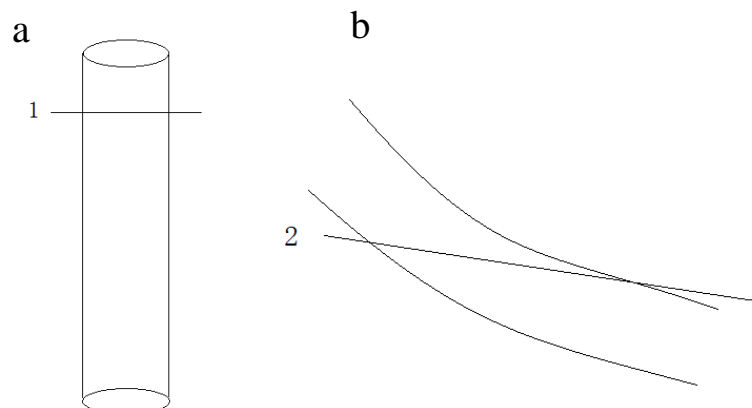


Figure 46: Microtoming directionality determines the resultant cross-section shape. a: round fiber cross-section. b: ellipse shape cross-section

When BSA-PEG was used as the core material, the proteins were not fully dissolve, rather, the proteins were dispersed in the PEG solution, so some of the resultant nanofibers cross-section look similar to the horizontal electrospun nanofibers with both dark regions appear at the edge and the core of the structure (Fig 47).

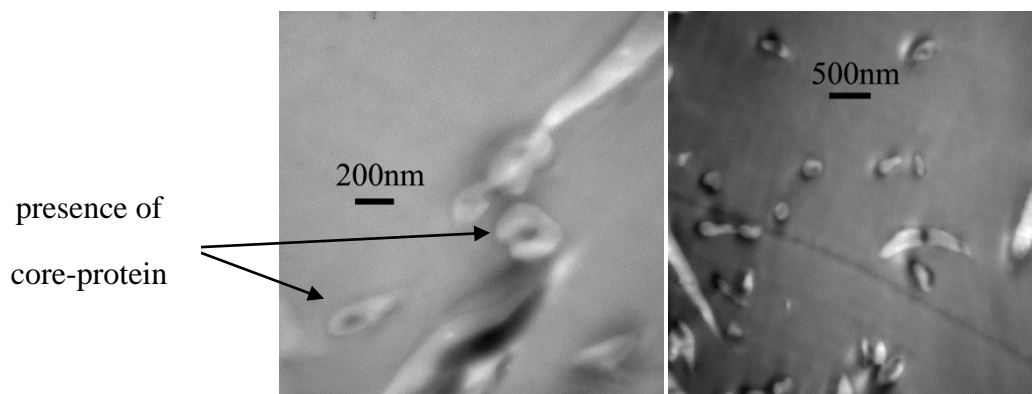


Figure 47: Cross-section of the genipin-crosslinked core-shell nanofibers with BSA encapsulation

To boost the core structure under TEM, the microtomed cross-sections were stained. From Figure 48, the stain did not enhance the contrast between the core-shell region, but the porous structure of the core material can be seen.

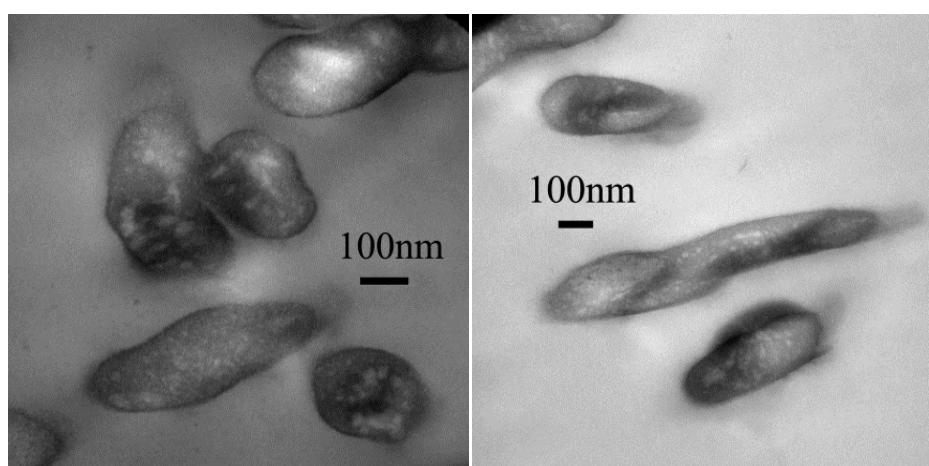


Figure 48: Cross-section of the uranyl acetate stained nanofibers

The formation of this porous structure comprises microcavities within the fiber bulk. This porous structure was mainly contributed by the presence of high molecular

weight PEG in the core material. During electrospinning, the fast evaporation of 80% ethanol allowed rapid precipitation of the PEG around the individual water droplets present in the solution. During crosslinking and ultramicrotoming, PEG dissolved and leached out, result in the formation of microcavities.

4.6 Genipin crosslinking on core-shell collagen nanofibers preparation

The as-spun core-shell BSA-PEG/collagen nanofibers were unstable in water. From Figure 49, by immersing the scaffold in water for 5 seconds, nanofibers disintegrated immediately at room temperature.

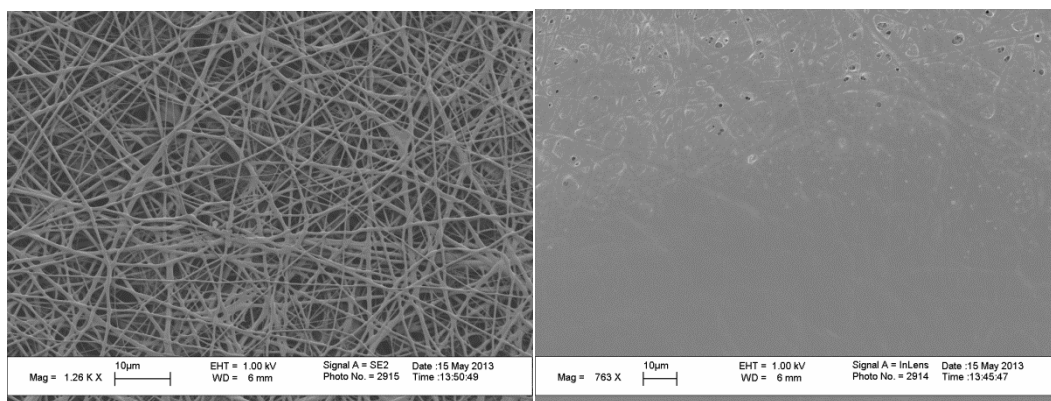


Figure 49: SEM images on Left: The as spun electrospun core-shell BSA-PEG/collagen nanofibers . Right: Electrospun core-shell BSA-PEG/collagen nanofibers immersed in water for 5 seconds.

Thus, for the core-shell BSA-PEG/collagen nanofibers to have any usefulness, they have to be stabilized. The biocompatible genipin crosslinking reagent would crosslink the collagen core-shell nanofibers with relatively low cytotoxicity. This cell-friendly crosslinking reagent is most suitable for tissue engineering applications. As the vertical electrospinning produced core-shell nanofibers with more uniform structure, these samples were used for crosslinking.

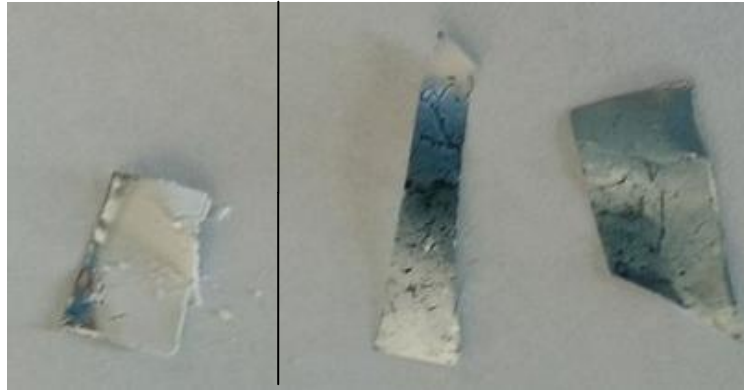


Figure 50: Left: As-spun core-shell core-shell BSA-PEG/collagen nanofibers on aluminum foil. Right: Crosslinked core-shell core-shell BSA-PEG/collagen nanofibers turned blue

The crosslinking conditions were determined previously on the stability of solid collagen fibers [9]. Fibers changed color after crosslinking. As-spun samples were white prior to crosslinking, upon crosslinking, the samples turned deep blue (Fig 50).

The crosslinked samples had an average diameter of $721.3 \pm 270.9\text{nm}$, indicates high degree of fiber swelling during crosslinking reaction. The stability of the crosslinked fibers was tested by placing the samples in distilled water for 7 days. Compared to the as-spun samples where fibers immediately gelled in water, the crosslinked fibers were much more stable in water (Fig 51). The fibers average diameter was reduced to $250.6 \pm 137.3\text{nm}$ over the 7 days stability test, indicates fibers degraded over time.

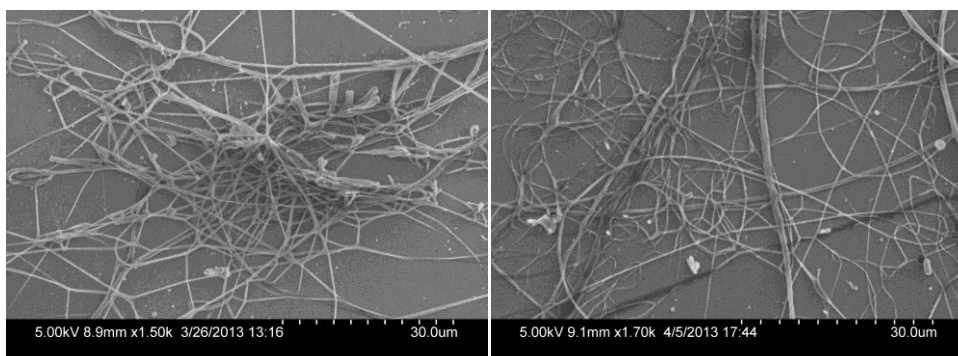


Figure 51: Left: Crosslinked collagen core-shell nanofibers. Right: Crosslinked collagen core-shell nanofibers immersed in water for 7 days

4.7 Change in auto-fluorescent before and after crosslinking (LSCM)

After the core-shell nanofibers were crosslinked, genipin induced strong auto-fluorescence in the fibers (Fig 52). The fluorescence emission maximum of the fluorescent adducts were formed by genipin exhibit a strong dependence on the excitation wavelength [104]. Depends on the excitation wavelength, the emission maximum was at 630nm when the crosslinked samples was excited with 590nm (Fig 52b). The emission maximum shifted to ~520nm when the 488nm laser was used for excitation (Fig 52a). The fluorescence induced by the crosslinking reaction overwhelmed the fluorescence signal of BSA-Alexa Fluoro 594, thus the embedded proteins cannot be differentiated.

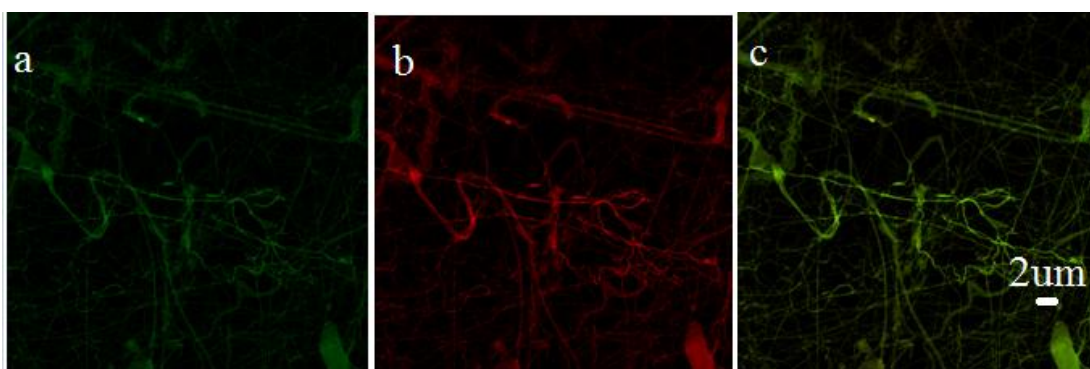


Figure 52: Confocal images of crosslinked electrospun core-shell BSA-PEG/collagen nanofibers: genipin crosslinked nanofibers fluorescence overwhelmed other fluorescence signals

Because genipin generates both color and fluorescence in a single reaction with primary amine groups in the structure, the resultant broad range fluorescence prevents the usefulness of fluorescence-tag protein incorporated in the core-material. Thus, LSCM can only be useful to verify the presence of the core protein in the as-spun nanofibers, but not sufficient for core-shell structure identification before or after the genipin crosslinking. On the other hand, the genipin induced auto-fluorescence of collagen could be served as a natural stain for collagen-contain materials to enhance the signal of the present collagen.

4.8 Cell attachment

Primary human fibroblasts were acquired from the palmar hand fascia of patients that underwent carpal tunnel release surgery. To verify the biocompatibility of the scaffold, fibroblasts were seeded on the genipin-crosslinked BSA-PEG/collagen core-shell nanofibers. As shown in Figure 53, by using different excitation and emission wavelength, the scaffold morphology and cell morphology can be clearly distinguished. Not only the scaffold supported fibroblast attachment (72 hours), the fibrous morphology of the crosslinked nanofibers was also maintained over the cell growth period. It should also be noted that crosslinked fiber scaffolds which were not anchored on the substrate and freely suspended in the culture medium did not have any cell attachment.

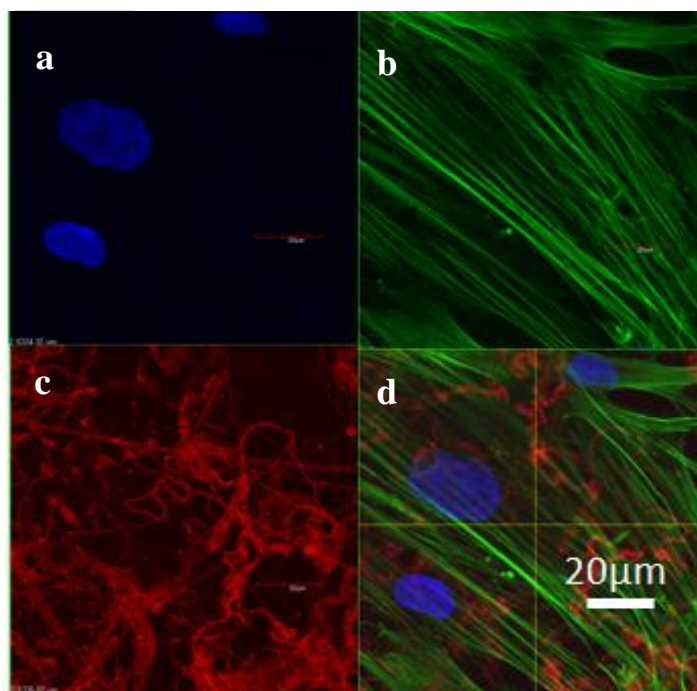


Figure 53: Fluorescence images of primary human fibroblasts cultured on crosslinked BSA-PEG/collagen core-shell nanofibers (3D) a: cell nucleus; b: filamentous actin; c: crosslinked-nanofibers; d: overlaid image (scale bar = 20 μm)

Z-stack fluorescence images were also taken to investigate scaffold thickness and cell population (Fig 54). The overall thickness of this scaffold was about 10 μm and cells

were populated only at the surface of the scaffold with no signs of cell migration.

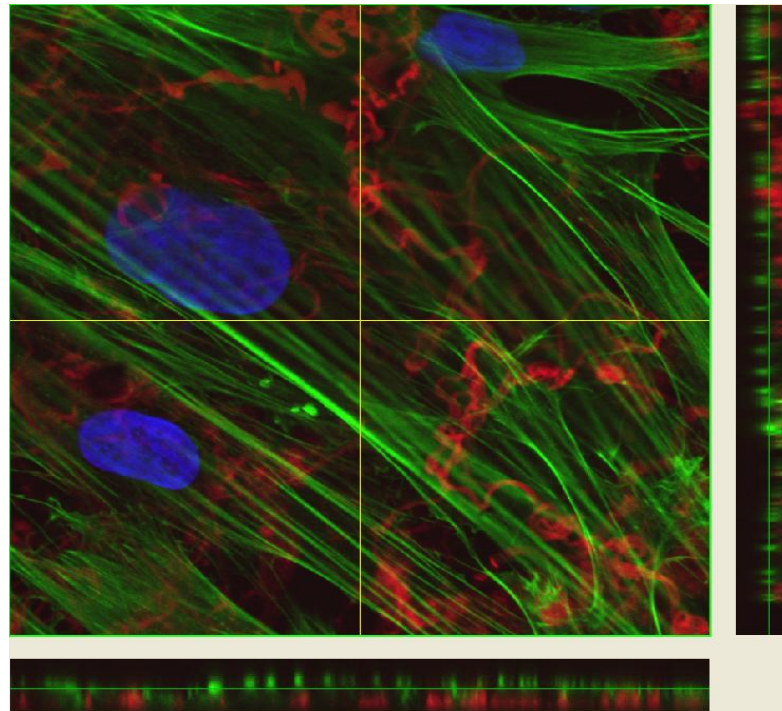


Figure 54: Fluorescence images of primary human fibroblasts cultured on crosslinked BSA-PEG/collagen core-shell nanofibers (3D). Blue: cell nucleus, green: actin filament, red: genipin-crosslinked core-shell collagen nanofibers. Side bars represent the side view of the scaffold.

5 Discussion

In all the published studies, the geometrical arrangements of the spinning needle and collector were always fixed for electrospinning. Very few studies had been done on fiber quality between different electrospinning configurations [40, 41]. Whereas no studies have been done on effect of coaxial electrospinning configuration on fiber quality. Rodoplu and Mutlu [41] even indicated that the gravitational force is negligible with respect to the electric field forces. However, as results collected in this study, summarized in table 6, shows that the effect of gravitational force on Taylor cone stability also determines the resultant fiber quality.

Table 6: Comparison of horizontal and vertical coaxial electrospinning

	Horizontal Coaxial Electrospinning	Vertical Coaxial Electrospinning
Processing Parameters	Although the condition for fiber formation was specific, nanofibers can be formed within a wide range voltage (i.e. 19~24kV)	Despite the specific condition for fiber formation, the voltage requirement is narrow (i.e. 22-23kV)
Taylor cone distortion	Taylor cone distorted extensively due to gravitational force	Taylor cone was less distorted
Fiber diameter distribution	Average fiber diameter at around 500 ~550 nm, largest fiber at~ 1.2 μ m. Most fiber diameter distribution do not fit to Normal function	Average fiber diameters at around 300nm, largest fiber at ~600nm. Fiber diameter distribution fit to Normal function.
Fiber quality	Less than ~10% fibers exhibit core-shell structure while most fibers resemble solid fiber structure	~60% fibers resemble core-shell structure
Cross-section	Non-uniform distribution of core-shell material	The core-shell structure can be distinguished

Horizontal coaxial electrospinning allows fiber formation within a wider voltage range could be attributed to that fact electro spraying and electrospinning can occur simultaneously with stable Taylor cone. For horizontal coaxial electrospinning, gravitational force dominates the droplets deposition path and droplets deposited at other locations rather than the collecting substrate; while a portion of fibers can still

be carried to the collector with fiber whipping and electrostatic force. For vertical coaxial electrospinning, any resultant droplets can only be collected at the substrate surface due to the cooperative effect of electrostatic force and gravitational force, so the resultant samples have both droplets and fibers collected (Fig 38,39). Thus, in order to only collect fiber, vertical coaxial electrospinning requires a more specific condition where only electrospinning takes place.

From Figure 21b, it can be seen that even if the Taylor cone was distorted, fibers could still be formed. This distortion showed that there was extensive solution retention at the tip of the needle which would promote solution mixing. The unstable Taylor cone resulted in non-uniform core-shell material distribution (Fig 31-32,34). The distorted Taylor cone and non-uniform material distribution due to mixing indicate the importance of Taylor cone stability for coaxial electrospinning. The steady state coaxial electrospinning has to be maintained to ensure continuous core-shell nanofiber formation. Without this stable Taylor cone throughout the coaxial electrospinning process, the resultant fibers would not have the desired morphology or structure. In comparison, with vertical coaxial electrospinning where the Taylor cone was much more stable through the experiment, the produced fiber have more uniform core-shell structure (Fig 45).

Although vertical coaxial electrospinning indeed had improved fiber quality in terms of structure uniformity, the resultant fibers were not all core-shell. Other than the fiber structures illustrated in Figure 43, the formation of the core shell nanofibers with reversed contrast cannot be accounted for. Reports on other core-shell systems only focus on the core-shell portion of the nanofibers [57, 105, 58, 53], and even for the TEM images which also showed the presences of both core-shell and solid structures with reverse contrast fibers [106, 107], no discussions or further characterizations were carried out on such structure. Reznik et al. [108] recognized the fact that core-shell droplet at the tip of the needle does not necessarily result in core solution

entrainment and not all fibers possess the core-shell structure with coaxial electrospinning process. They proposed to use protruded inner needle to facilitate core solution entrainment, though no experimental works were done to support such theory.

The reverse contrast observed in the current study could be attributed to the fusion of two core-shell nanofibers or the transition phase during fiber branching or splitting into two core-shell nanofibers. In either case, the fibers should still have core-shell structure with encapsulation of the embedded material.

In general, the results had shown that horizontal coaxial electrospinning would not generate uniform core-shell nanofibers, vertical coaxial electrospinning should be the preferred configuration.

The stability of the crosslinked fibers was tested in distilled water for up to 7 days, and the scaffolds were more stable compared to as-spun fibers (Fig 51). Even after the fibers were immersed in cell growth media for 3 days and PBS washed for more than 20 times for cell staining, the fibrous morphology of the scaffold could still be observed (Fig 54). The current study is only a preliminary study to validate the possibility of crosslinking core-shell collagen nanofibers, a previous study on genipin crosslinked collagen nanofibers determined conditions where the degree of swelling and degree of crosslinking of solid collagen nanofibers can be tuned [9]. The different degrees of swelling and crosslinking can be achieved by varying crosslinking conditions leading to further control fiber properties for tissue engineering purposes. Even though the fibers did degrade over time during the stability test, the degradation rate could be tuned with crosslinking conditions.

Since the crosslinking reaction was starting from the surface of the fiber where the collagen was in contact with the crosslinking solution, to crosslink the material underneath the surface, the crosslinking reagent had to pass through the crosslinked

surface barrier. As a result, this reaction is self-limiting through the thickness of the fiber shell. By adjusting the crosslinking condition, the crosslinking reaction can be tuned so that the genipin penetration depth is comparable to the shell layer thickness and the core material can stay intact from the crosslinking reagent. This consideration is of importance as in tissue engineering applications, bioactives such as growth factors will be in the core of the fiber. These molecules have to be unaffected by genipin to remain active to stimulate and guide cell activities.

However, there are several reports indicated that the incorporation of PEG in the core solution would create porous structure [55, 57]. If this is the case, the core material upon exposure to an aqueous solution such as cell culture media, can diffuse through the porous structure. The core protein and the core component release would be diffusion controlled or depend on a combination mechanism of core diffusion and shell degradation.

The cell compatibility tests showed that fibroblasts populated across the scaffold surface with no cell migration into the scaffold. This result demonstrated cell compatibility of the collagen scaffold in a manner similar to the genipin crosslinked solid collagen fiber reported earlier in our lab [9]. This result suggests that the scaffold support fibroblast attachment, however, the encapsulated BSA does not affect cell behavior. To stimulate cell migration, growth factors should be incorporated into the core. The incorporation of appropriate growth factor should guide and signal cells for migration, adhesion and differentiation.

And with the possibility of controlling crosslinking of the nanofibers, the fiber properties can be interrelated by studying the effect of degree of crosslinking on both mechanical properties and cellular activities. Since cellular behavior also relates to mechanical properties of the substrate, changes in mechanical properties may also tailor the cellular activities of the crosslinked scaffold. Hence a systematic study on correlate degree of crosslinking, mechanical property, and cellular activates of the

core-shell collagen nanofibers would yield important information on how best is use this type of scaffold in tissue engineering applications.

6 Summary and Conclusion

The goal of this work was to develop core-shell nanofibrous scaffolds using collagen as the shell and encapsulate bioactive molecules in the core. To achieve this goal, coaxial electrospinning was utilized. Although, many studies have been published to describe the process and control of core-shell thickness through adjustment of core-shell solution flow rate, the knowledge of how various process parameters influence the preparation and resulting fiber quality and structure is limited. In this project, collagen was selected as the shell polymer and PEG in 80% ethanol was selected as the core carrier solution for model protein. Fluoresce-tag proteins were then added to the core-solution to produce PEG-BSA/collagen nanofibrous scaffold of desired morphologies and structure for tissue engineering applications. As the obtained as-spun scaffolds were unstable in aqueous condition, a natural crosslinking reagent, genipin, derived from the fruits of *Gardenia jasminoides* was employed to stabilize the structure due to its low cytotoxicity and high biocompatibility.

Initial studies were aimed at understanding the spinning process and indentifying factors that produced significant effects on fiber morphology. With the use of high speed photography, the stable Taylor cone can be formed and maintained during the electrospinning process by adjusting processing parameters under ambient conditions. It was observed that the applied voltage played a major role in controlling the core-shell fiber formation. The desired stable Taylor cone was only formed when the voltage was maintained within a specific narrow range. This range primarily depended on the tip to collector distance, shape and size of the Taylor cone and solution flow rate. At the optimum voltage, core-shell fibers with desired morphology were obtained. The effects of vertical and horizontal spinning were then investigated by characterizing the nanofibers with desired morphology under TEM. The obtained fiber structures were identified and vertical coaxial electrospinning did produce fibers with narrower fiber distribution and more uniform core-shell structure. Subsequently,

with encapsulation of fluoresce-tag proteins, LSCM confirmed the presence of proteins in the structure, however, with the low magnification of LSCM system, the definite core-shell structure cannot be verified. With the vertical coaxial electrospun collagen nanofibers, genipin crosslinking was performed followed by cell seeding of primary human skin fibroblasts. Fluorescence microscopy images showed the attachment of cells to the collagen scaffold.

The major conclusions derived from this investigation are as follows:

- 1) For the preparation of uniform nanofibers from collagen/PEG-BSA, a certain minimum conditions were required. The optimum conditions which allow uniform core-shell nanofibers lie in a very narrow range (e.g. voltage above or below the critical voltage would not allow continuous fiber formation).
- 2) The coaxial electrospinning configuration not only affects the shape of the droplet, but also the fiber diameter distribution and core-shell fiber structure. Gravitational force extensively distorted horizontal coaxial electrospinning Taylor cone, led to non-uniform core-shell structure. Vertical coaxial electrospinning allowed better fiber drawing along the direction of gravitational force and gravitational force strengthened the effect of electric field to make the fiber extend sufficiently. Compared to the non-uniform structure obtained with horizontal coaxial electrospinning, vertical coaxial electrospinning resulted in fibers with smaller fiber diameter and more uniform core-shell structure. Therefore vertical coaxial electrospinning is preferred.
- 3) Genipin crosslinking stabilized the core-shell collagen nanofibers and after immersing fibers in water for 7 days, fibers were more stable compared to as-spun fibers.
- 4) Cell compatibility was tested by seeding the crosslinked samples with primary human fibroblasts. Fluorescence microscopy images showed scaffold supported cell attachment.

7 Future Work

The current research demonstrated the improvements in core-shell nanofibrous structure and fiber diameter distribution with vertical coaxial electrospinning. Such core-shell structure shows great potential for various applications.

However, the resultant fibers still showed irregularity in core-shell structure and some degree of material mixing. The process should be further controlled and optimized by considering other aspects such as solution properties including vapor pressure, miscibility, conductivity and difference in surface tension. Ambient temperature, humidity, and air velocity should also be more precisely controlled to eliminate any unnecessary perturbations in the system.

For tissue engineering applications, the mechanical integrity and stability of the scaffold should be investigated and modeled. Previous works on collagen crosslinking showed different degree of fiber swelling and crosslinking due to various crosslinking conditions. The effect of such crosslinking on the mechanical properties and degradation rate of the structure should be investigated. It would be ideal if the degree of crosslinking can be related to the mechanical properties and degradation rate of the structure.

Collagen was chosen in this study with the hypothesis that being a part of the native extracellular matrix (ECM), collagen will improve cell growth behavior on the scaffold. Cell seeding experiment proved the cell compatibility and fiber stability, but the experiment should be repeated independently to obtain statistical reliable results.

The advantage of using core-shell nanofibers rather than solid fibers is the possibility of encapsulating bioactive molecules or drugs in the structure, controlled release studies should be carried out on the core-shell nanofibers to investigate its controlled release mechanism and releasing rate. As BSA do not affect cell behavior, growth

factors should be incorporated to stimulate cell migration and differentiation.

References

1. **T. Dvir, B.P. Timko, D.S. Kohane, R. Langer.** Nanotechnological Strategies for Engineering Complex Tissues. 2011, *Nature Nanotechnology*, Vol. 6, pp. 13-22.
2. **F.J. O'Brien, B.A. Harley, M.A. Waller, I.V. Yannas, L.J. Gibson, P.J. Prendergast.** The effect of pore size on permeability and cell attachment in collagen scaffolds for tissue engineering. 2007, *Technol Health Care*, Vol. 15, pp. 3-17.
3. **F.J. O'Brien, B.A. Harley, I.V. Yannas, L. Gibson.** Influence of freezing rate on pore structure in freeze-dried collagen-GAG scaffolds. 2004, *Biomaterials*, Vol. 25, pp. 1077-1086.
4. **G. Chen, T. Ushida, T. Tateishi.** Scaffold design for Tissue Engineering. 2002, *Macromolecular Bioscience*, Vol. 2, pp. 67-77.
5. **D.S. Katti, K.W. Robinson, F.K. Ko, C.T. Laurencin.** Bioresorbable nanofiber-based systems for wound healing and drug delivery: optimization of fabrication parameters. 2004, *Journal of Biomedical Materials Research*, Vol. 70B, pp. 186-296.
6. **A.K. Moghe, B.S. Gupta.** Co-axial Electrospinning for Nanofiber Structures: Preparation and Applications. 2008, *Polymer Reviews*, Vol. 48, pp. 353-377.
7. **K. Gelse, E. Poschi, T. Aigner.** Collagens - structures, function, and biosynthesis. 2003, *Advanced Drug Delivery Review*, Vol. 55, pp. 1531-1546.
8. **M.W. King, R.L. Ornberg, Y. Marois, G.R. Marinov, R. Cadi, J.H. Southern, S.L. Weinberg, S.W. Shalaby, R. Guidoin.** Partially Bioresorbable bicomponent fibers for tissue engineering: Mechanical stability of core polymers. 2000. 6th World Biomaterials Congress.
9. **M. Mekhail, K.K.H. Wong, D.T. Padavan, Y. Wu, D.B. O'Gorman, W. Wan.** Genipin-cross-linked electrospun collagen fibers. 2011, *Journal of Biomaterials Science*, Vol. 22, pp. 2241-2259.
10. **J. Zeleny.** The electrical discharge from liquid points, and a hydrostatic method of

- measuring the electric intensity at their surfaces. 1914, *Physical Review Letters*, Vol. 3, pp. 69-91.
11. **A. Formhals.** Process and apparatus for preparing artificial threads. 1,975,504 1934.
 12. **G.I. Taylor.** Electrically driven jets. 1969, *Proceedings of the Royal Society A: Mathematical, Physical and Engineering Science*, Vol. 313, pp. 453-475.
 13. **Y.M. Shin, M.M. Hohman, M.P. Brenner, G.C. Rutledge.** Experimental characterization of electrospinning: the electrically forced jet and instabilities. 2001, *Polymer*, Vol. 42, pp. 9955-9967.
 14. **A.L. Yarin, S. Koombhongse, D.H. Reneker.** Taylor cone and jetting from liquid droplets in electrospinning of nanofibers. 2001, *Journal of Applied Physics*, Vol. 90, pp. 4836-4846.
 15. **J. Doshi, D.H. Reneker.** Electrospinning process and applications of electrospun fibers. 1995, *Journal of Electrostatics*, Vol. 35, pp. 151-160.
 16. **L. Rayleigh.** On the equilibrium of liquid conducting masses charged with electricity. 1882, *Philosophical Magazine*, Vol. 14, pp. 184-186.
 17. **J. M. Deitzel, J. Kleinmeyer, D. Harris, N.C.B. Tan.** The effect of processing variables on the morphology of electrospun nanofibers and textiles. 2001, *Polymer*, Vol. 42, pp. 261-272.
 18. **S.B. Warner, A. Buer, S.C. Ugbolue, B.C. Rutledge, M.Y. Shin.** A fundamental investigation of the formation and properties of electrospun fibers. s.l. : Annual Report, National Textile Centre, 1999.
 19. **A.L. Yarin, S. Koombhongse, D.H. Reneker.** Bending instability in electrospinning of nanofibers. 2001, *Journal of Applied Physics*, Vol. 89, pp. 3018-3026.
 20. **P.K. Baumgarten.** Electrostatic spinning of acrylic microfibers. 1971, *Journal of Colloid Interface Science*, Vol. 36, pp. 71-79.
 21. **D.H. Reneker, A.L. Yarin, H. Fong, S. Koombhongse.** Bending instability of

- electrically charged liquid jets of polymer solutions in electrospinning. 2000, *Journal of Applied Physics*, Vol. 87, pp. 4531-4547.
22. **M.M. Hohman, Y.M. Shin, G. Rutledge, M.P. Brenner.** Electrospinning and electrically forced jets. I. Stability theory. 2001, *Physical Fluids*, Vol. 13, pp. 2201-2220.
23. **C.J. Thompson, G.G. Chase, A.Y. Yarin, D.H. Reneker.** Effects of parameters on nanofiber diameter determined from electrospinning model. 2007, *Polymer*, Vol. 48, pp. 6913-6922.
24. **C. Thompson.** An analysis of variable effects on a theoretical model of the electrospin process for making nanofibers, thesis. Akron, Ohio : The University of Akron, 2006.
25. **T. Jarusuwannapoom, W. Hongrojjanawiwat, S. Jitjaicham, L. Wannatong, M. Nithitanakul, C. Pattamaprom.** Effect of solvents on electrospinnability of polystyrene solutions and morphological appearance of resulting electrospun polystyrene fibers. 2005, *European Polymer Journal*, Vol. 41, pp. 409-421.
26. **G.G. Chase, D.H. Reneker.** Nanofibers in filter media. 2004, *Fluid/Particle Separation Journal*, Vol. 16, pp. 105-117.
27. **T.J. Sill, H.A. von Recum.** Electrospinning: Applications in drug delivery and tissue engineering. 2008, *Biomaterials*, Vol. 29, pp. 1989-2006.
28. **M.G. McKee, G.L. Wilkes, R.H. Colby, T.E. Long.** Correlations of solution rheology with electrospun fiber formation of linear and branched polyesters. 2004, *Macromolecules*, Vol. 37, pp. 1760-1767.
29. **S.L. Shenoy, W.D. Bates, H.L. Frisch, G.E. Wnek.** Role of chain entanglements on fiber formation during electrospinning of polymer solutions: good solvent, non-specific polymer-polymer interaction limit. 2005, *Polymer*, Vol. 46, pp. 3372-3384.
30. **H. Fong, I. Chun, D.H. Reneker.** Beaded nanofibers formed during electrospinning. 1999, *Polymer*, Vol. 40, pp. 4585-4592.

31. **J.M. Deitzel, J. D. Kleinmeyer, D. Harris, N.C. Tan.** The effects of solution properties and polyelectrolyte on electrospinning of ultrafine poly(ethylene oxide) fibers. 2004, *Polymer*, Vol. 45, pp. 2959-2966.
32. **T. Zhou.** Bi-component nano-fibrous complexes via coaxial electrospinning. Raleigh, North Carolina : North Carolina State University, 2011.
33. **A.K. Moghe.** Core-sheath differentially biodegradable nanofiber structures for tissue engineering. Raleigh, North Carolina : North Carolina State University, 2008.
34. **J.S. Choi, S.W. Lee, L. Jeong, S. Bae, B.C. Min, J.H. Youk, W.H. Park.** Effect of organosoluble salts on the nanofibrous structure of electrospun poly(3-Hydroxybutyrate-Co-3-Hydroxyvalerate). 2004, *International Journal of Biological Macromolecules*, Vol. 34, pp. 249-256.
35. **L. Wannatong, A. Sirivat, P. Supaphol.** Effects of solvents on electrospun polymeric fibers: preliminary study on polystyrene. 2004, *Polymer International*, Vol. 53, pp. 1851-1859.
36. **K. Arayanarakul, N. Choktaweasap, D. Aht-Ong, C. Meechaisue, P. Supaphol.** Effects of poly (ethylene glycol), inorganic salts, sodium dodecyle sulfate, and solvent system on electrospinning of poly (ethylene oxide). 2006, *Macromolecular Materials and Engineering* , Vol. 291, pp. 581-591.
37. **S. Megelski, J.S. Stephens, D.B. Chase, J.F. Rabolt.** Micro- and nanostructured surface morphology on electrospun polymer fibers. 2002, *Macromolecules*, Vol. 35, pp. 8456-8466.
38. **S.Y. Gu, J. Ren, G.J. Vancso.** Process optimization and empirical modeling for electrospun polyacrylonitrile (PAN) nanofiber precursor of carbon nanofibers. 2005, *European Polymer Journal*, Vol. 41, pp. 2559-2568.
39. **C.L. Casper, J.S. Stephens, N.G. Tassi, D.B. Chase, J.F. Rabolt.** Controlling surface morphology of electrospun polystyrene fibers: effect of humidity and molecular weight in . 2004, *Macromolecules*, Vol. 37, pp. 573-578.

40. **C. Yang, Z. Jia, Z. Xu, K. Wang, Z. Guan, L. Wang.** Comparisons of fibers properties between vertical and horizontal type electrospinning systems. 2009. Annual Report Conference on Electrical Insulation and Dielectric Phenomena.
41. **D. Rodoplu, M. Mutlu.** Effects of electrospinning setup and process parameters on nanofiber morphology intended for the modification of quartz crystal microbalance surfaces. 2012, *Journal of Engineered Fibers and Fabrics*, Vol. 7, pp. 118-123.
42. **D.H. Reneker, A. L. Yarin, H. Fong, S. Koombhongse.** Bending instability of electrically charged liquid jets of polymer solutions in electrospinning. 2000, *Journal of Applied Physics*, Vol. 87, pp. 4531-4547.
43. **T. Han, A. L. Yarin, D. H. Reneker.** Viscoelastic Electrospinning Jets: Initial Stresses and Elongation Rheometry. 2008, *Polymer*, Vol. 49, pp. 1651-1658.
44. **A.L. Yarin.** Coaxial electrospinning and emulsion electrospinning of core-shell fibers. 2011, *Polymers Advanced Technologies*, Vol. 22, pp. 310-317.
45. **I.G. Loscertales, A. Barrero, I. Guerrero, R. Cortijo, M. Marquez, A.M. Ganan-Calvo.** Micro/Nano encapsulation via electrified coaxial liquid jets. 2002, *Science*, Vol. 295, pp. 1695-1698.
46. **Z. Sun, E. Zussman, A.L. Yarin, J.H. Wendorff, A. Greiner.** Compound core-shell polymer nanofibers by co-electrospinning. 2003, *Advanced Materials*, Vol. 15, pp. 1929-1932.
47. **I.G. Loscertales, A. Barrero, M. Marquez, R. Spretz, R. Velarde-Ortiz, G. Larsen.** Electrically forced coaxial nanojets for one-step hollow nanofiber design. 2004, *Journal of the American Chemical Society* , Vol. 126, pp. 5376-5377.
48. **D. Li, A. Babel, S.A. Jenekhe, Y. Xia.** Nanofibers of conjugated polymers prepared by electrospinning with a two-capillary spinneret. 2004, *Advanced Materials*, Vol. 16, pp. 1562-1566.
49. **A. Greiner, J.H. Wendorff, A.L. Yarin, E. Zussman.** Biohybrid nanosystems with polymer nanofibers and nanotubes. 2006, *Applied Microbiology and*

- Biotechnology, Vol. 71, pp. 387-393.
50. **D. Li, Y. Xia.** Direct fabrication of composite and ceramic hollow nanofibers by electrospinning . 2004, Nano Letters, Vol. 4, pp. 933-938.
51. **A.L. Yarin, E. Zussman, J. H. Wendorff, A. Greiner.** Material encapsulation and transport in core-shell micro/nanofibers, polymer and carbon nanotubes and micro/nanochannels. 2007, Journal of Materials Chemistry, Vol. 17, pp. 2585-2599.
52. **D.H. Reneker, A.L. Yarin.** Electrospinning jets and polymer nanofibers. 2008, Polymer, Vol. 49, pp. 2387-2425.
53. **H.T. Zhou, J.L. Hu, S.J. Chen.** Coaxial Electrospun Polyurethane Core-Shell Nanofibers for Shape Memory and Antibacterial Nanomaterials. 2011, eXPRESS Polymer Letters, Vol. 5, pp. 182-187.
54. **Y.Z. Zhang, J. Venugopal, Z. Huang, C.T. Lim, S. Ramakrishna.** Characterization of the Surface Biocompatibility of the Electrospun PCL-Collagen Nanofibers using Fibroblasts. 2005, Biomacromolecules, Vol. 6, pp. 2583-2589.
55. **Y.Z. Zhang, X. Wang, Y. Feng, J. Li, C.T. Lim, S. Ramakrishna.** Coaxial Electrospinning of (Fluorescein Isothiocyanate-Conjugated Bovine Serum Albumin)-Encapsulated Poly(Caprolactone) Nanofibers for Sustained Release. 2006, Biomacromolecules, Vol. 7, pp. 1049-1057.
56. **A.K. Moghe, J.M. Gluck, B.S. Gupta, M.W. King.** Electrospun bicomponent fibers for soft tissue engineering: Book of Abstracts. Newark NJ, USA : s.n., 2005. The Fiber Society Fall 2005 Annual Meeting and Technical Conference.
57. **T.T.T. Nguyena, O.H. Chungb, J.S. Parka.** Coaxial electrospun poly(lactic acid)/chitosan (core/shell) composite nanofibers. 2011, Carbohydrate Polymers , Vol. 86, pp. 1799-1806.
58. **Y. Z. Zhang, X. Wang, Y. Feng, J. Li, C. T. Lim, S. Ramakrishna.** Coaxial Electrospinning of (Fluorescein Isothiocyanate-Conjugated Bovine SerumAlbumin)-Encapsulated Poly(E-caprolactone) Nanofibers for Sustained Release. 2006, Biomacromolecules , Vol. 7, pp. 1049-1057.

59. **J.E. Diaz, A. Barrero, M. Marquez, I.G. Loscertales.** Controlled encapsulation of hydrophobic liquids in hydrophilic polymer nanofibers by co-electrospinning. 2006, *Advanced Functional Materials*, Vol. 16, pp. 2110-2116.
60. **Y. Zhang, Z. Huang, X. Xu, C.T. Lim, S. Ramakrishna.** Preparation of Core-Shell Structured PCL-r-Gelatin Bi-Component Nanofibers by Coaxial Electrospinning. 2004, *Chemistry of Materials*, Vol. 16, pp. 3406-3409.
61. **C. He, Z. Huang, X. Han, L. Liu, H. Zhang, L. Chen.** Coaxial electrospun poly(lactic acid) ultrafine fibers for sustained drug delivery. 2006, *Journal of Macromolecular Science, Part B*, Vol. 45, pp. 515-524.
62. **J. Yu, S. Fridrikh, G. Rutledge.** Production of submicrometer diameter fibers by two-fluid electrospinning. 2004, *Advanced Materials*, Vol. 16, pp. 1562-1566.
63. **Z. Kurban, A. Lovell, S.M. Bennington, D.W.K. Jenkins, K.R. Ryan, M.O. Jones, N.T. Skipper, W.I.F. David.** A Solution Selection Model for Coaxial Electrospinning and its Application to Nanostructured Hydrogen Storage Materials. 2010, *The Journal of Physical Chemistry C*, Vol. 114, pp. 21201-21213.
64. **G. Larsen, R. Spretz, R. Velarde-Ortiz.** Use of coaxial gas jackets to stabilize Taylor cones of volatile solutions and to induce particle-to-fiber transitions. 2004, *Advanced Materials*, Vol. 16, pp. 166-169.
65. **D. Zhang, J. Chang.** Electrospinning of three-dimensional nanofibrous tubes with controllable architectures. 2008, *Nano Letters*, Vol. 8, pp. 3283-3287.
66. **D. Li, Y.L. Wang, Y.N. Xia.** Electrospinning of polymeric and ceramic nanofibers as uniaxially aligned arrays. 2003, *Nano Letters*, Vol. 3, pp. 1167-1171.
67. **D. Li, Y.L. Wang, Y.N. Xia.** Electrospinning nanofibers as uniaxially aligned arrays and layer-by-layer stacked films. 2004, *Advanced Materials*, Vol. 16, pp. 361-366.
68. **D. Li, G. Ouyang, J.T. Maccann, Y.N. Xia.** Collecting electrospun nanofibers with patterned electrodes. 2005, *Nano Letters*, Vol. 5, pp. 913-916.
69. **M. Wei, J. Lee, B.W. Kang, J. Mead.** Preparation of Core-Sheath Nanofibers

- from Conducting Polymer Blends. 2005, *Macromolecular Rapid Communications*, Vol. 26, pp. 1127-1132.
70. **D. Han, A.J. Steckl.** Superhydrophobic and Oleophobic Fibers by Coaxial Electrospinning. 2009, *Langmuir*, Vol. 25, pp. 9454-9462.
71. **H.X. Qu, P. Hu, J. XU, A. Wang.** Encapsulation of drug reservoirs in fibers by emulsion electrospinning: morphology characterization and preliminary release assessment. 2006, *Biomacromolecules*, Vol. 8, pp. 2327-2330.
72. **Y. Dror, W. Salalha, R. Avrahami, E. Zussman, A.L. Yarin, R. Dersch, A. Greiner, J.H. Wendorff.** One-step production of polymeric microtubes by co-electrospinning. 2007, *Small*, Vol. 3, pp. 1064-1073.
73. **H.L. Jiang, Y.Q. Hu, Y.Li, P. Zhao, K. Zhu, W. Chen.** A facile technique to prepare biodegradable coaxial electrospun nanofibers for controlled release of bioactive agents. 2005, *Journal of Controlled Release*, Vol. 108, pp. 237-243.
74. **M. Schindler, E.K.A. Nur, I. Ahmed, J. Kamak, H. Liu, N. Amor, A.S. Ponery, D.P. Crockett, T.H. Grafe, H.Y. Chung.** Living in three dimensions: 3D nanostructured environments for cell culture and regenerative medicine. 2006, *Cell Biochemistry Biophysics*, Vol. 45, p. 215.
75. **M.E. Nimni et. al.** Collagen: Molecular structure and biomaterial properteis. Encyclopedic handbook of biomaterials and bioengineering Part A: Materials. New York : D.W. Wise, 1995, pp. 1229-1243.
76. **P.P. M. van Zuijlen, J.J.B. Ruurda, H.A. van Veen, J. van Marle, A.J. M. van Trier, F. Groenevelt, R.W. Kreis, E. Middelkoop.** Collagen morphology in human skin and scar tissue: no adaptations in response to mechanical loading at joints. 2003, *Burns*, Vol. 29, p. 423.
77. **K.S. Weadock, E.J. Miller, E.L. Keuffel, M.G. Dunn.** Effect of physical crosslinking methods on collagen-fiber durability in proteolytic solutions. 1996, *Journal of Biomedical Materials Research*, Vol. 32, pp. 221-226.
78. **M.G. Haugh, M.J. Jaasma, F.J. O'Brien.** The effect of dehydrothermal

- treatment on the mechanical and structural properties of collagen-GAG scaffolds. 2009, *Journal of Biomedical Materials Research. Part A*, Vol. 89A, pp. 363-369.
79. **K. Weadock, R.M. Olson, F.H. Silver.** Evaluation of collagen crosslinking techniques. 1983, *Biomaterial Medical Devices Artificial Organs*, Vol. 11, pp. 293-318.
80. **M.G. Haugh, C.M. Murphy, R.C. McKiernan, C. Altenbunchner, F.J. O'Brien.** Crosslinking and Mechanical Properties Significantly Influence Cell Attachment, Proliferation, and Migration Within Collagen Glycosaminoglycan Scaffolds. 9/10, 2011, *Tissue Engineering: Part A*, Vol. 17, pp. 1201-1208.
81. **L.P. Yan, Y.W. Wang, L.Ren, G. Wu, S.G. Caridade, J.B. Fan, L.Y. Wang, P.H. Ji, J.M. Oliveira, J.T. Oliveira.** Genipin-cross-linked collagen/chitosan biomimetic scaffolds for articular cartilage tissue engineering applications. 2010, *Journal of Biomedical Materials Research A*, Vol. 95A, pp. 465-475.
82. **A. F.S.A. Habeeb, R. Hiramoto.** Reaction of proteins with glutaraldehyde . 1968, *Archives of Biochemistry and Biophysics*, Vol. 126, pp. 16-26.
83. **B. Xu, M.J. Chow, Y. Zhang.** Experimental and Modeling Study of Collagen Scaffolds with Effects of Crosslinking and Fiber Alignment. 2011, *International Journal of Biomaterials*. 10.1155/2011/172389.
84. **P.B. Van Wachem, M.J.A. Van Luyn, L. Damink, P.J. Dijkstra, J. Feijen, P. Nieuwenhuis.** Biocompatibility and tissue regenerating capacity of crosslinked dermal sheep collagen. 1994, *Journal of Biomedical Materials Research*, Vol. 28, pp. 353-363.
85. **E. Khor.** Methods for the treatment of collagenous tissues for bioprotheses. 1997, *Biomaterials*, Vol. 18, pp. 95-105.
86. **J.M. Lee, H.H.L. Edwards, C.A. Pereira, S.I. Samii.** Crosslinking of tissue-derived biomaterials in 1-ethyl-3-(3-dimethylaminopropyl)-carbodiimide (EDC). 1996, *Journal of Materials Science: Materials in Medicine*, Vol. 7, pp. 531-541.

87. **C.P. Barnes, C.W. Pemble IV, D.D. Brand, D.G. Simpson, G.L. Bowlin.** Cross-linking Electrospun Type II collagen Tissue Engineering Scaffolds with Carbodiimide in Ethanol. 2007, *Tissue Engineering*, Vol. 13, pp. 1593-1605.
88. **M. Kikuchi, H. N. Matsumoto, T. Yamada, Y. Koyama.** Glutaraldehyde cross-linked hydroxyapatite/collagen. 2004, *Biomaterials*, Vol. 25, pp. 63-69.
89. **I. Rault, V. Rei, D. Herbage, N. Abdul-Marak, A. Huc.** Evaluation of different chemical methods for crosslinking collagen gels, films and sponges. 1996, *Journal of Material Science: Materials in Medicine*, Vol. 7, pp. 215-222.
90. **L.H.H. Olde Damink, P.J. Dijkstra, M.J.A. Van Luyn, P.B. Van Wachem, P. Nieuwenhuis, J. Feijen.** Glutaraldehyde as a crosslinking agent for collagen-based biomaterials. 1995, *Journal of Materials Science: Materials in Medicine*, Vol. 6, pp. 460-472.
91. **Y. Wine, N. Cohen-Hadar, A. Freeman, F. Frolow.** Elucidation of the Mechanism and End Products of Glutaraldehyde Crosslinking Reaction by X-Ray Structure Analysis. 2007, *Biotechnology and Bioengineering*, Vol. 98, pp. 711-718.
92. **I. Migneault, C. Dartiguenave, M.J. Bertrand, K. C. Waldron.** Glutaraldehyde: behavior in aqueous solution, reaction with proteins, and application to enzyme crosslinking. 2004, *Biotechniques*, Vol. 37, pp. 190-802.
93. **L. Yang, C.F.C. Fitie, K.O. van der Werf, M.L. Bennink, P.J. Dijkstra, J. Feijen.** Mechanical Properties of single electrospun collagen type I fibers. 2008, *Biomaterials*, Vol. 29, pp. 955-962.
94. **G.M. Cunniffe, F.J. O'Brien.** Collagen scaffolds for orthopedic regenerative medicine. 2011, *Biomaterials for Regenerative Medicine*, Vol. 63, pp. 66-73.
95. **J.E. Park, J.Y. Lee, H.G. Kim, T.R. Hahn, Y.S. Paik.** Isolation and characterization of water-soluble intermediates of blue pigments transformed from geniposide of *Gardenia jasminoides*. 2002, *Journal of Agricultural and Food Chemistry*, Vol. 50, pp. 6511-6514.
96. **M.F. Butler, Y.F. Ng, P.D.A. Pudney.** Mechanism and Kinetics of the

- Crosslinking Reaction between Biopolymers Containing Primary Amine Groups and Genipin. 2003, *Journal of Polymer Science: Part A: Polymer Chemistry*, Vol. 41, pp. 3941-3953.
97. **Y. Chang, C. Tsai, H. Liang, H. Sung.** Reconstruction of the right ventricular outflow tract with a bovine jugular vein graft fixed with a naturally occurring crosslinking agent (genipin) in a canine model. 2001, *The Journal of Thoracic and Cardiovascular Surgery*, Vol. 122, pp. 1208-1217.
98. **R. Touyama, Y. Takeda, K. Inoue, I. Kawamura, M. Yatsuzuka, T. Ikumoto.** Studies on the blue pigments produced from genipin and methylamine. I. Structures of the brownish-red pigments, intermediates leading to the blue pigments. 1994, *Chemical & Pharmaceutical Bulletin*, Vol. 42, pp. 667-673.
99. **J. Qu, Y. Hu, R. You, M. Li.** The Cytocompatibility of Genipin-Crosslinked Silk Fibroin Films. L. Wang, Y. Wang, 2013, *Journal of Biomaterials and Nanobiotechnology*, Vol. 4, pp. 213-221.
100. **Y. Zhu, M. Chan-Park.** Density quantification of collagen grafted on biodegradable polyester. Its application to esophageal smooth muscle cell. 2007, *Analytical Biochemistry*, Vol. 363, pp. 119-127.
101. **R.A.A. Muzzarelli.** Genipin-crosslinked chitosan hydrogels as biomedical and pharmaceutical aids. 2009, *Carbohydrate Polymers*, Vol. 77, pp. 1-9.
102. **H.W. Sung, W.H. Chang, C.Y. Ma, M.H. Lee.** Crosslinking of biological tissues using genipin and/or carbodiimide. 2003, *Journal of Biomedical Materials Research Part A*, Vol. 64A, pp. 427-438.
103. **E.M. Lee.** Master's Thesis: Core-shell Nanofibres for Heart Valve Leaflet Tissue Engineering. London, Ontario, Canada : The University of Western Ontario, 2011.
104. **Y.J. Hwang, J.Larsen, T.B. Krasieva, J. G. Lyubovitsky.** Effect of Genipin Crosslinking on the Optical Spectral Properties and Structures of Collagen Hydrogels. 2011, *ACS Applied Materials and Interfaces*, Vol. 3, pp. 2579-2584.
105. **T. Nguyen, J.S. Park.** Fabrication of polyethylene glycol/polyvinylidene

- fluoride core/shell nanofibers via melt electrospinning and their characteristics. C. V. Do, 2012, Solar Energy Materials & solar cells, Vol. 104, pp. 131-139 .
106. **D. Han, S. T. Boyce, A.J. Steckl.** Versatile core-sheath biofibers using coaxial electrospinning. 2008, Materials Research Society Symposium Proceedings, Vol. 1094. 1094-DD06-02.
107. **Y. Srivastava, I. Loscertales, M. Marquez, T. Thorsen.** Electrospinning of hollow and core/sheath nanofibers using a microfluidic manifold. 2007, Microfluid Nanofluid. s10404-007-0177-0.
108. **S.N. Reznik, A.L. Yarin, E. Zussman, L. Bercovici.** Evolution of a compound droplet attached to a core-shell nozzle under the action of a strong electric field. 2006, Physics of Fluids, Vol. 18. 062101.

Appendix A Isolation of Type I Collagen from Rat Tails

- 1) Thaw frozen rats tails in 70% ethanol for 1 hour
- 2) Use scalpel to cut off skin of tail and expose white collagen fibres. Using forceps pull out collagen fibres from tail and place in separate sterile dish.
- 3) Continue cutting rat tail in segments, exposing and pulling out fibres, ensuring to clean fibres of contaminating tissue.
- 4) At this point, fibres can be stored at -20 °C or proceed to collagen solution.
- 5) Weigh out 4 g/L of fibres (approximately 5 tails) and soak in 200 mL of 70% ethanol for 30 minutes with forceps.
- 6) Place fibres in sterile Petri dish and leave overnight in a tissue culture hood with UV light on to sterilize fibres.
- 7) Prepare acetic acid solution (1 mL of concentrated acetic acid in 1 L of distilled water) and filter sterilize.
- 8) Add 900 mL of acetic acid solution to collagen fibres in an autoclaved 1 litre flask with sterile stir bar. Place on stirrer in cold room (at 4 °C) for 4-7 days to dissolve collagen.
- 9) Centrifuge the solution at 11, 000 rpm (10, 000 g) for 2 hours at 4 °C with brakes on.
- 10) Collect supernatant in a sterile bottle and measure protein concentration using Sircol Collagen Assay (should be 1-3 mg/mL)
- 11) Collagen solution can be stored at this point at 4 °C.
- 12) To obtain collagen protein powder, freeze small samples (~10-15 ml) overnight in a -20 °C freezer and lyophilize for 1-2 days.

Appendix B Low Viscosity Embedding Media (Spurr's Kit)

Spurr's Low Viscosity embedding mixture is recommended because of its excellent penetration qualities, which provide good and rapid infiltration of tissues. It is easy to prepare, and mixes rapidly by shaking and swirling. The hardness is adjusted by changing the amount of the flexibilizer, DER 736; the blocks have good trimming and sectioning qualities and the sections are tough under the electron beam. (Grids, without supporting membranes can be used.)

Ingredients

ERL 4206 - vinyl cyclohexene dioxide (VCHD) is a cycloaliphatic diepoxide, with a M.W. of 140.18 and epoxies equivalent of 74-78. Its viscosity is 7.8 cP, lower than other epoxy resin embedding media such as Epon 812, maraglas and Araldite.

NOTE: ERL - 4206 is a proven carcinogen and is toxic. extreme care must be employed-Do all work under a fume hood.

DER 736 - diglycidyl ether of polypropylene glycol, a flexibilizer to control the hardness of the polymerized block. It was selected because of its low viscosity: 30-60 cP 25 C.

It has a M.W of 380 and an epoxy equivalent of 175-205.

NSA - nonenyl succinic anhydride, a hardener with a relatively low viscosity of 102.8 cP at 25C and a M.W. of 227. A minimum exposure to air is recommended to avoid hydrolysis.

DMAE - dimethylaminoethanol (S-1) an accelerator, used because of its low viscosity and results in blocks with less color. In addition, it induces rapid cure when the temperature is elevated to 70C. It is effective in a very low concentration. (less than 1.0%) The optimum concentration for color transparency is 0.7-0.75%.

	A	B	C	D
	Firm standard	Hard	Soft	Longer pot life Lower viscosity
ERL 4206	10.0g	10.0g	10.0g	10.0g
DER 736	6.0g	4.0g	8.0g	6.0g
NSA	26.0g	26.0g	26.0g	26.0g
DMAE	0.3g	0.3g	0.3g	0.2g
Cure Time at 70° C (hours)	8	8	8	16
Pot Life (Days)	3-4	3-4	3-4	7

Mixing Instructions

Add each component in turn to a disposable plastic beaker. An exact weight is recommended, and care must be used in dispensing the final amounts of each component so that no excess is added.

The catalyst (DMAE) should be added last, after gently mixing the three other components.

The complete formula should be mixed thoroughly.

The complete mixture with the hardener can be used immediately for infiltration, and then for embedding. Although the mixture can be stored in a disposable syringe, well capped and with no air, in a freezer for several months it is highly recommended that freshly prepared embedding medium always be used. If you choose to store the mixture it is imperative that you warm it thoroughly prior to use.

Dehydration-Infiltration and Polymerization

This embedding media is compatible with all dehydrating agents: acetone, dioxane, ethanol, hexyleneglycol, isopropyl alcohol, propylene oxide tert-butyl alcohol. the

schedule and concentration can be established by the investigator. Dehydration is generally done at room temperature. All dehydrating agent must totally be removed during infiltration due to the fact that it will effect curing.

The embedding media is completely compatible with ethanol. Thus, it is not mandatory to have a change to propylene oxide prior to infiltration as is true for other epoxy resin mixtures. If working with plant cells it is recommended to use propylene oxide.

The infiltration (one should employ a specimen rotator) can be started by adding the embedding media to an equal quantity (1:1) of the dehydrating fluid left in the vial with the tissue. Swirl the mixture and allow it to stand for 30 minutes for 2 hours. Replace with a 1:3 dehydrating agent/embedding medium, swirl, and allow it to stand for another 30 minutes to 2 hours. Pour and drain the mixture and add fresh embedding media. For small specimens, 4-6 hours; for large specimens, 4-6 hours followed by overnight. Curing takes 16-24 hours at 60 °C. (The mixture can be left in an oven overnight).

CATALOG # 14300 Low Viscosity Embedding Media Kit Consists of:

CAT# 15000 ERL 4206 -vinyl cyclohexene dioxide - 225ml

CAT# 13000 DER 736 - diglycidyl ether polypropylene glycol - 225ml

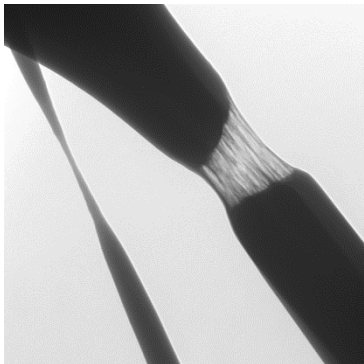
CAT# 19050 NSA - nonenyl succinic anhydride - 450m;

CAT# 13300 DMAE - dimethylamino ethanol - 25ml

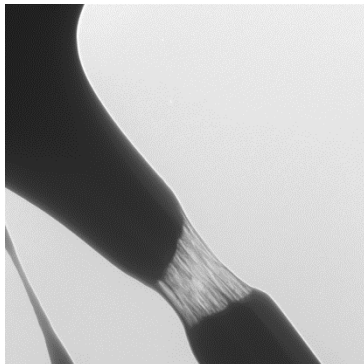
Reference:

Spurr, A.R. (1969), J. Ultrastruct. Res. 26, 31

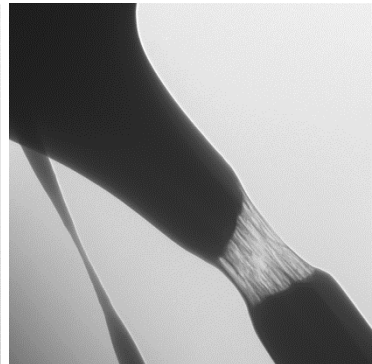
Appendix C TEM on Fiber Breakage



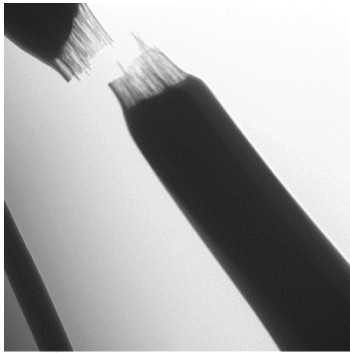
Betty.129.111
collagen BGA
Print Mag: 19700x @ 51 mm
11:48 03/18/13
TEM Mode: Imaging
500 nm
HV: 80kV
Direct Mag: 34000x
X: -924.261 Y: 316.862
Biotron LMD



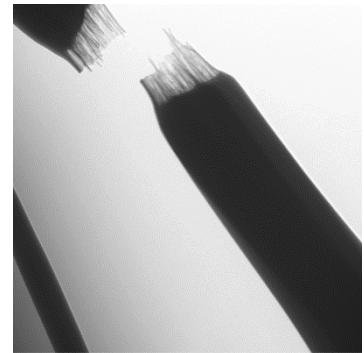
Betty.130.111
collagen BGA
Print Mag: 19700x @ 51 mm
11:49 03/18/13
TEM Mode: Imaging
500 nm
HV: 80kV
Direct Mag: 34000x
X: -923.756 Y: 316.624
Biotron LMD



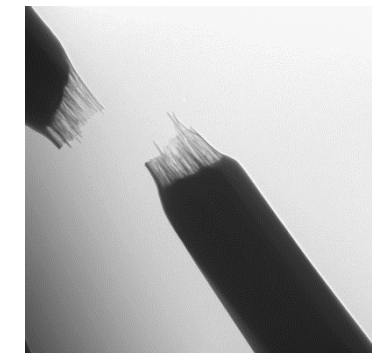
Betty.131.111
collagen BGA
Print Mag: 19700x @ 51 mm
11:49 03/18/13
TEM Mode: Imaging
500 nm
HV: 80kV
Direct Mag: 34000x
X: -924.948 Y: 316.776
Biotron LMD



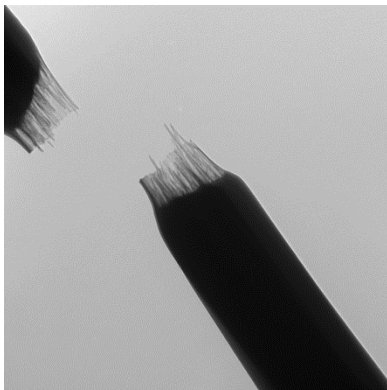
Betty.132.111
collagen BGA
Print Mag: 19700x @ 51 mm
11:50 03/18/13
TEM Mode: Imaging
500 nm
HV: 80kV
Direct Mag: 34000x
X: -924.209 Y: 319.247
Biotron LMD



Betty.133.111
collagen BGA
Print Mag: 19700x @ 51 mm
11:50 03/18/13
TEM Mode: Imaging
500 nm
HV: 80kV
Direct Mag: 34000x
X: -924.209 Y: 319.247
Biotron LMD



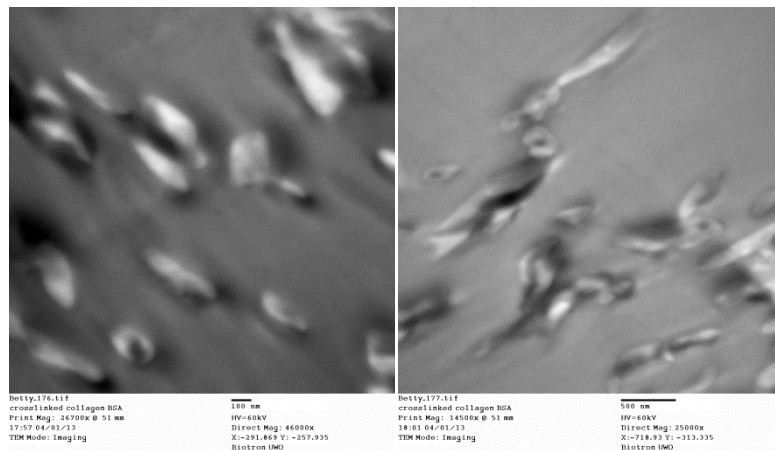
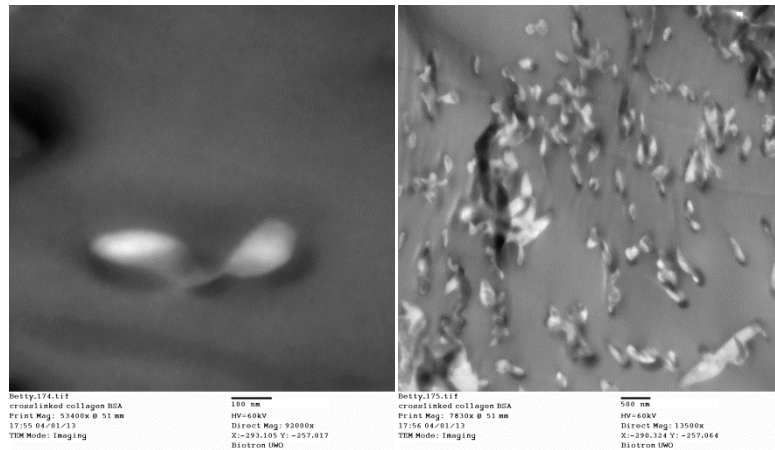
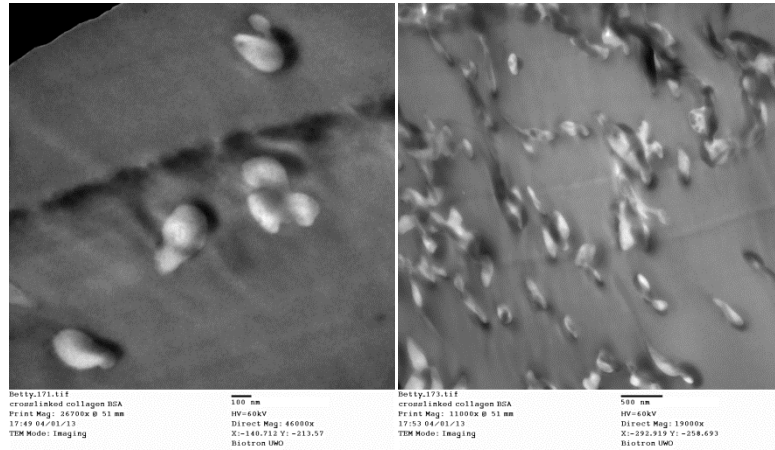
Betty.134.111
collagen BGA
Print Mag: 19700x @ 51 mm
11:51 03/18/13
TEM Mode: Imaging
500 nm
HV: 80kV
Direct Mag: 34000x
X: -925.636 Y: 318.468
Biotron LMD

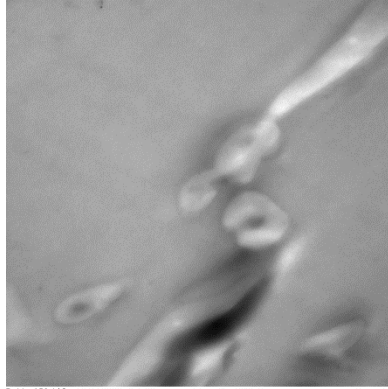


Betty.135.111
collagen BGA
Print Mag: 19700x @ 51 mm
11:51 03/18/13
TEM Mode: Imaging
500 nm
HV: 80kV
Direct Mag: 34000x
X: -925.76 Y: 318.694
Biotron LMD

Appendix D TEM images on fiber cross-section

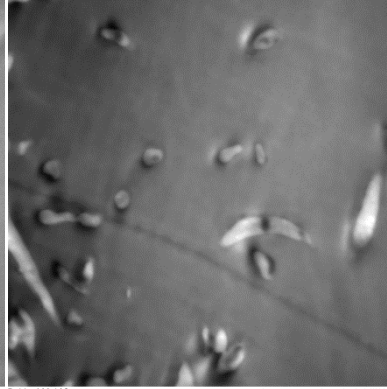
Vertical Coaxial Electrospun Nanofibers





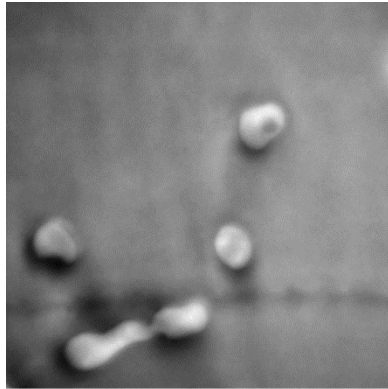
Betty_179.tif
crosslinked collagen BSA
Print Mag: 26700x @ 51 nm
18.04.04/01/13
TEM Mode: Imaging

100 nm
HV=60kV
Direct Mag: 46000x
X=-719.116 Y=-214.633
Biotron IWO



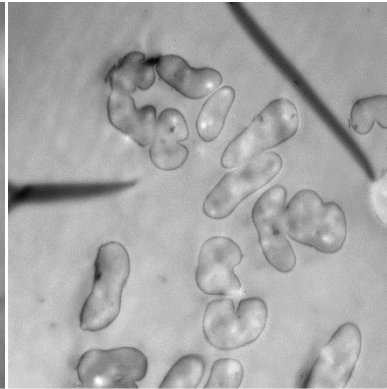
Betty_180.tif
crosslinked collagen BSA
Print Mag: 11000x @ 51 nm
18.08.04/01/13
TEM Mode: Imaging

500 nm
HV=60kV
Direct Mag: 19000x
X=-836.661 Y: 428.234
Biotron IWO

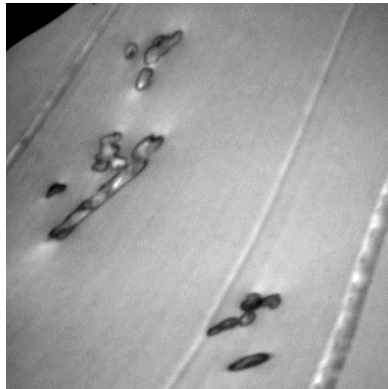


Betty_181.tif
crosslinked collagen BSA
Print Mag: 26700x @ 51 nm
18.10.04/01/13
TEM Mode: Imaging

100 nm
HV=60kV
Direct Mag: 46000x
X=-836.662 Y: 418.569
Biotron IWO

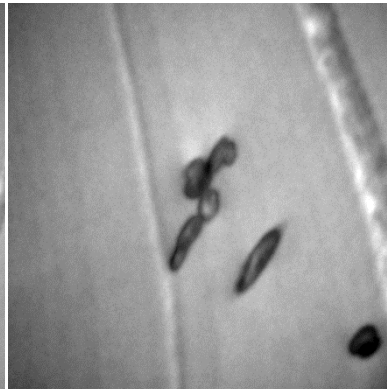


Betty_305.tif



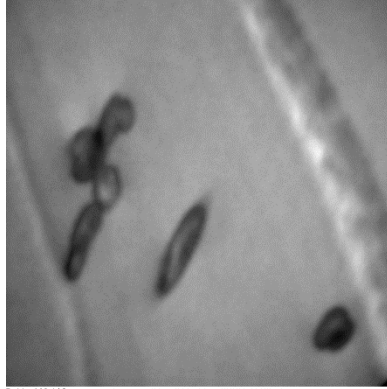
Betty_190.tif
crosslinked collagen BSA
Print Mag: 7800x @ 51 nm
13.12.04/02/13
TEM Mode: Imaging

500 nm
HV=60kV
Direct Mag: 13580x
X=-49.37 Y: 825.426
Biotron IWO

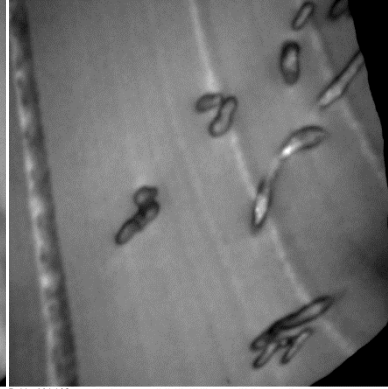


Betty_191.tif
crosslinked collagen BSA
Print Mag: 14500x @ 51 nm
13.12.04/02/13
TEM Mode: Imaging

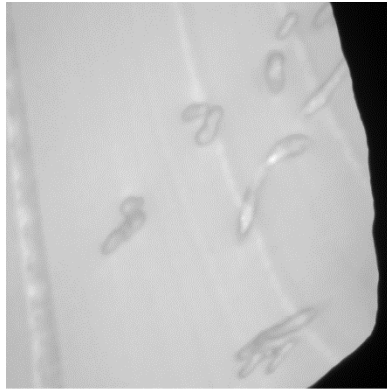
500 nm
HV=60kV
Direct Mag: 25090x
X=-50.741 Y: 827.393
Biotron IWO



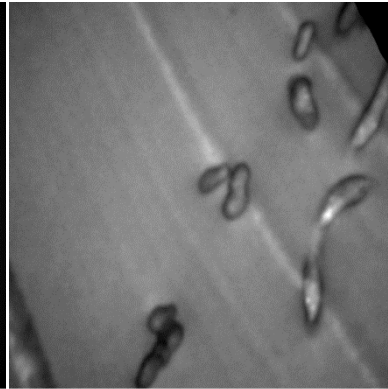
Betty.193.tif
crosslinked collagen BSA
Print Mag: 19700x @ 51 nm
13:14:04/02/13
TEM Mode: Imaging
500 nm
HV=60kV
Direct Mag: 34000x
X=-56.826 Y: 828.731
Biotron UMO



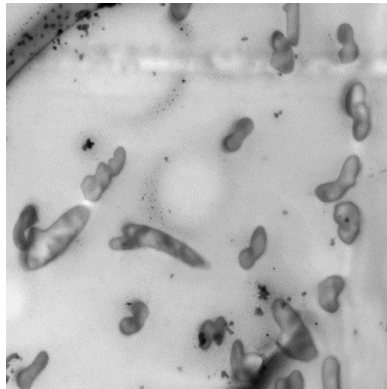
Betty.194.tif
crosslinked collagen BSA
Print Mag: 11000x @ 51 nm
13:15:04/02/13
TEM Mode: Imaging
500 nm
HV=60kV
Direct Mag: 19000x
X=-54.657 Y: 826.711
Biotron UMO



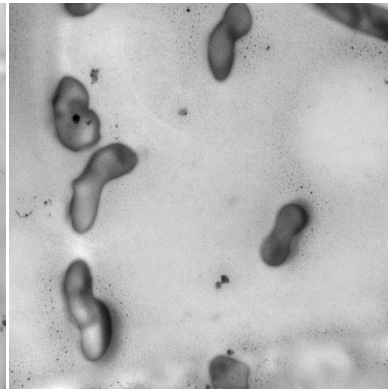
Betty.195.tif
crosslinked collagen BSA
Print Mag: 11000x @ 51 nm
13:16:04/02/13
TEM Mode: Imaging
500 nm
HV=60kV
Direct Mag: 19000x
X=-54.653 Y: 826.708
Biotron UMO



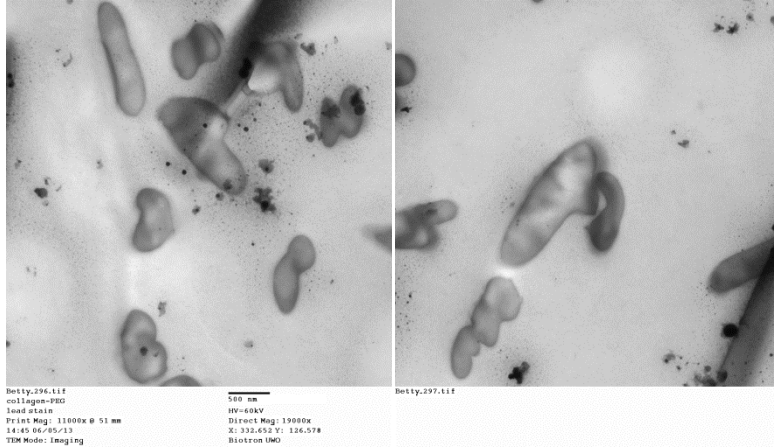
Betty.196.tif
crosslinked collagen BSA
Print Mag: 14500x @ 51 nm
13:16:04/02/13
TEM Mode: Imaging
500 nm
HV=60kV
Direct Mag: 15000x
X=-55.148 Y: 825.267
Biotron UMO



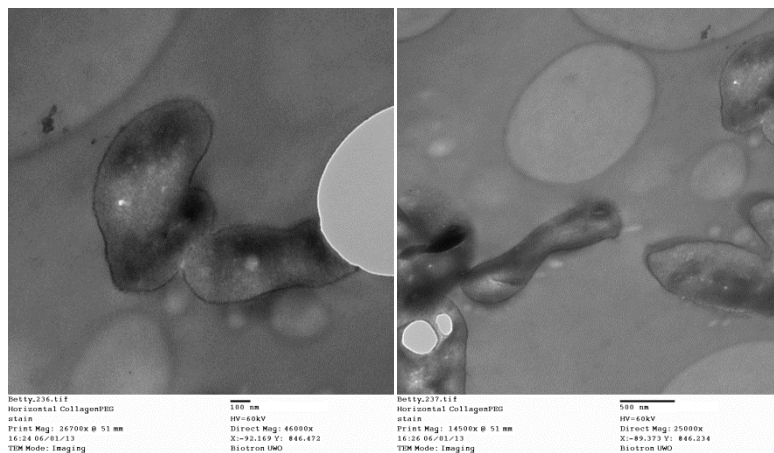
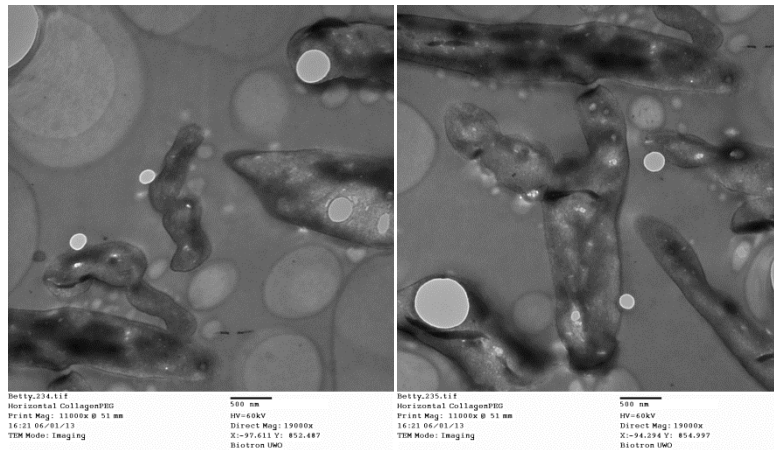
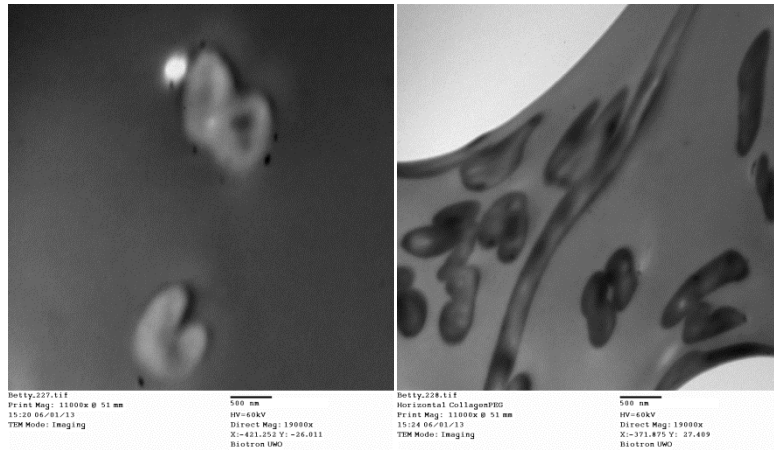
Betty.294.tif
collagen-PEG
lead stain
Print Mag: 6990x @ 51 nm
14:43:06/05/13
TEM Mode: Imaging
500 nm
HV=60kV
Direct Mag: 10580x
X: 329.728 Y: 129.86
Biotron UMO

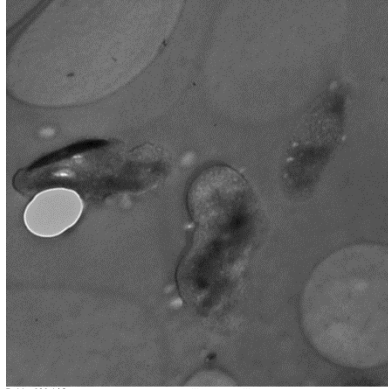


Betty.295.tif
collagen-PEG
lead stain
Print Mag: 11000x @ 51 nm
14:44:06/05/13
TEM Mode: Imaging
500 nm
HV=60kV
Direct Mag: 19090x
X: 333.239 Y: 129.469
Biotron UMO

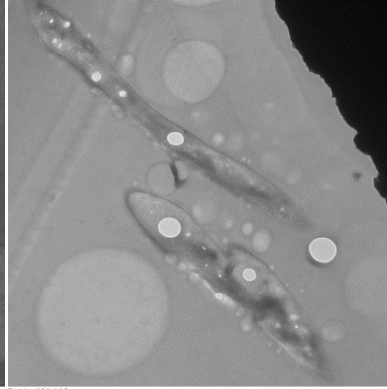


Horizontal Coaxial Electrospun nanofibers

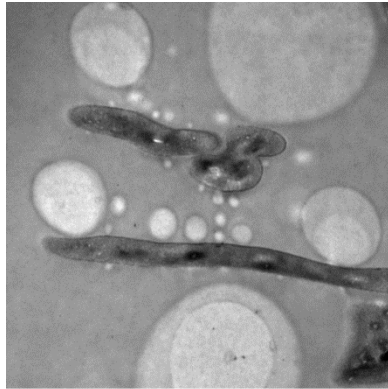




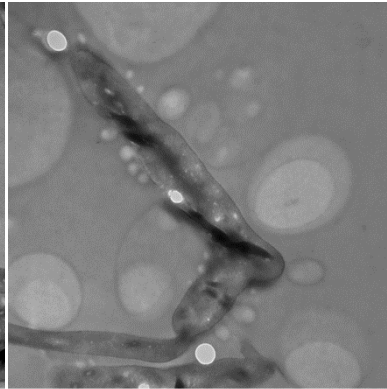
Betty.238.tif
Horizontal CollagenPDS
stain
Print Mag: 14500x @ 51 mm
16:28 06/01/13
TEM Mode: Imaging
500 nm
HV=60kV
Direct Mag: 25000x
X=96.993 Y: 846.552
Biotron IWO



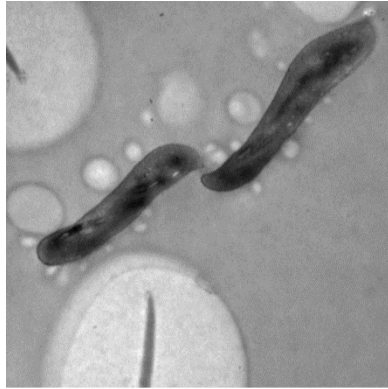
Betty.239.tif
Horizontal CollagenPDS
stain
Print Mag: 7430x @ 51 mm
16:30 06/01/13
TEM Mode: Imaging
500 nm
HV=60kV
Direct Mag: 13500x
X=111.006 Y: 847.585
Biotron IWO



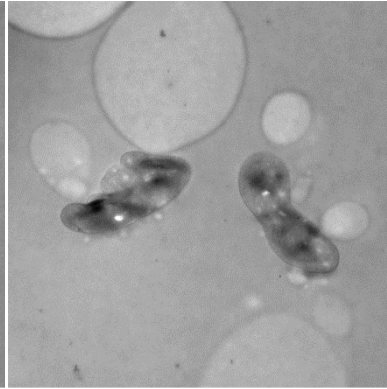
Betty.240.tif
Horizontal CollagenPDS
stain
Print Mag: 11000x @ 51 mm
16:32 06/01/13
TEM Mode: Imaging
500 nm
HV=60kV
Direct Mag: 19000x
X=133.196 Y: 811.692
Biotron IWO



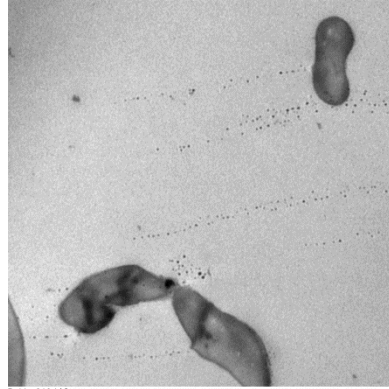
Betty.241.tif
Horizontal CollagenPDS
stain
Print Mag: 11000x @ 51 mm
16:34 06/01/13
TEM Mode: Imaging
500 nm
HV=60kV
Direct Mag: 19000x
X=137.004 Y: 812.768
Biotron IWO



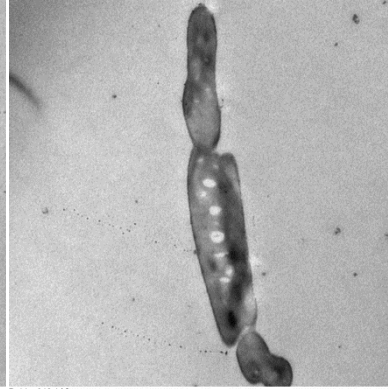
Betty.242.tif
Horizontal CollagenPDS
stain
Print Mag: 14500x @ 51 mm
16:35 06/01/13
TEM Mode: Imaging
500 nm
HV=60kV
Direct Mag: 25000x
X=144.061 Y: 802.697
Biotron IWO



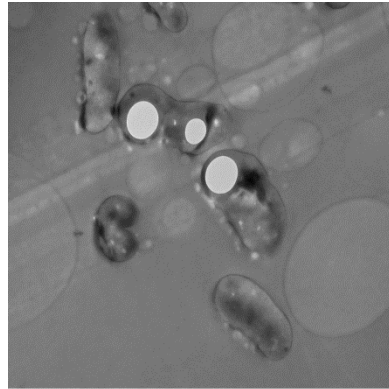
Betty.243.tif
Horizontal CollagenPDS
stain
Print Mag: 11000x @ 51 mm
16:39 06/01/13
TEM Mode: Imaging
500 nm
HV=60kV
Direct Mag: 19000x
X=138.654 Y: 805.634
Biotron IWO



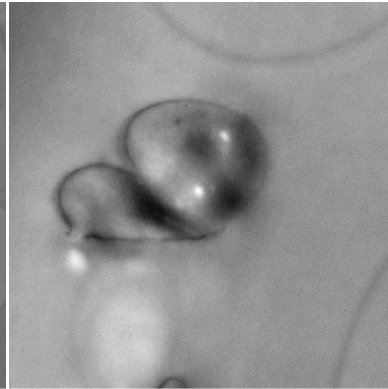
Betty.246.tif
Horizontal CollagenFIB
Print Mag: 11000x @ 51 mm
16:56:06/01/13
TEM Mode: Imaging
500 nm
HV=60KV
Direct Mag: 10000x
X: 463.683 Y: -429.667
Biotron UMO



Betty.248.tif



Betty.284.tif
collagen-FIB
stain
Print Mag: 7830x @ 51 mm
14:33:06/04/13
TEM Mode: Imaging
500 nm
HV=60KV
Direct Mag: 13580x
X: 278.782 Y: 231.414
Biotron UMO



Betty.286.tif
collagen-FIB
stain
Print Mag: 26700x @ 51 mm
14:35:06/04/13
TEM Mode: Imaging
100 nm
HV=60KV
Direct Mag: 46000x
X: 296.21 Y: 228.236
Biotron UMO

CURRICULAM VITAE

Name	Ying (Betty) Li
Post-secondary Education and Degrees:	University of Toronto Toronto, Ontario, Canada 2007-2011, BAsC in Engineering Science Major in NanoEngineering University of Western Ontario London, Ontario, Canada 2011-2013, MESc in Chemical and Biochemical Engineering
Honors and Awards:	Engineering Design Award, Institute for Aerospace Study and Division of Engineering Science University of Toronto 2009 NSERC Undergraduate Student Research Award (USRA) University of Toronto 2010
Related Work Experience:	Teaching Assistant University of Western Ontario 2011-2013
Conference Proceedings:	S. Makaremi, Y. Li , W. Wan. Nanomechanics of Electrospun Poly(Caprolactone) Nanofibres. Proceedings of the 3rd International Conference on Nanotechnology: Fundamentals and Applications, Montreal, Canada, 2012 Y. Li , J. Liu, W. Wan. Genipin Cross-Linked Electrospun Core-Shell Nanofibrous Scaffolds for Tissue Regeneration and Drug Delivery Applications. Proceedings of the 4rd International Conference on Nanotechnology: Fundamentals and Applications, Toronto, Canada, 2013